Theses and Dissertations

12-15-2014

# Application of Various Adsorbents to Remove Micro-Pollutants in Aquatic System

Chanil Jung
*University of South Carolina - Columbia*

Follow this and additional works at: http://scholarcommons.sc.edu/etd

www.manaraa.com

# APPLICATION OF VARIOUS ADSORBENTS TO REMOVE MICRO-POLLUTANTS IN AQUATIC SYSTEM

by

Chanil Jung

Bachelor of Science and Engineering
Hanyang University, 2006

Master of Science and Engineering
Hanyang University, 2008

Master of Science and Engineering
Carnegie Mellon University, 2010

Submitted in Partial Fulfillment of the Requirements

For the Degree of Doctor of Philosophy in

Civil and Environmental Engineering

School of Engineering and Computing

University of South Carolina

2014

Accepted by:

Yeomin Yoon, Major Professor

Nicole Berge, Committee Member

Joseph R.V. Flora, Committee Member

Ahjeong Son, Committee Member

Lacy Ford, Vice Provost and Dean of Graduate Studies

Foremost, I am highly grateful to *God* for His blessing that continue to flow into my life, and because of *You*, I made this through against all odds.

I dedicate my dissertation work to my family and many friends. First of all, a special feeling of gratitude to my loving parents, *Youngchae Jung* and *Younglee Kim* and in law, *Kyougjong Hong* and *Jeongwon Lee*, whose words of encouragement and push for tenacity ring in my ear. My sister, *Seunghee Jung* has never left my side and is very special. I thank you for constant support, encouragement, and interest in what I am doing.

To my many friends and church family who have supported me throughout the process, I always appreciate all they have done, especially *Linkel Boateng* for helping me develop my technology skills and spending the many hours of proofreading.

Special thanks to my daughter and son, *Dami Jung* and *Haim Jung*. You are the light of my life. I still feel sorry for spending less time with you due to living separately. Nevertheless, your big smiles, hugs and kisses, and love have been encouraging and motivating me to complete this work; both of you have been my best cheerleaders.

For the last, to my lovely wife, *Eunkyoung Hong*, you are my rock in everything and certainly through this four year experience. Without your faith, belief, smiles, hugs, and love, I would not have overcome trials and submitted this dissertation. Thank you for understanding how important this was to me and for supporting me every step of the way. I love you with all that I have.

My love and gratitude goes out to you all.

ACKNOWLEDGEMENTS

With a great pleasure I would like to acknowledge the support, assistances and contribution made by individuals from the beginning of the fieldwork, providing me access, data and information, to the writing process until the completion of this thesis. It would not have been possible to write this doctoral thesis without the guidance of my committee members and their assistance and support of the kind people around me, to only some of whom it is possible to give particular mention here.

I would like to express my deepest gratitude to my advisor, Dr. *Yeomin Yoon*, for his excellent guidance, caring, patience, and for providing me with an excellent atmosphere for doing research. I would like to thank Dr. *Flora*, who gently advised my research and guided me to experience the research of adsorption with molecular modeling in the field and practical issues beyond the textbooks. I would also like to thank Dr. *Berge*, and Dr. *Saleh* for guiding my research for the past several years and helping me to develop my background in physiology and water chemistry. Special thank goes to Dr. Son, who was willing to participate in my final defense committee.

I would like to thank *Linkel Boateng*, who as a good friend was always willing to help and give his best suggestions. It would have been a lonely lab without him. Many thanks to *Jiyong Heo*, *Jongkwon Im*, *Yasir Alhamadani*, *Liang Li*, *Caleb Braswell*, *Seungwoo Nam* for their encouragements which help me to focus on my work. My research would not have been possible without their help.

iv

I would also like to thank my parents, and sister, they were always supporting me and encouraging me with their best wishes.

Finally, I would like to thank my wife, *Eunkyoung Hong*, and lovely daughter, *Dami Jung* and son, *Haim Jung*. They were always there cheering me up and stood by me through the good times and bad.

ABSTRACT

Untreated or insufficiently treated pharmaceuticals and endocrine disrupting compounds (EDCs) as well as heavy metals have influenced the ecosystem and their exposures in the water system have threatened human health; causing cancers and adverse health effect to immune system. While various water treatment techniques have been applied to solve this problem, adsorption has been considered as one of the most efficient and manageable water purification techniques. Advanced analysis methods for aqueous contaminants have improved comprehension, allowing proficiency about the fate of trace leveled emerging contaminants, thus allowed to reveal the adsorption mechanisms of each pollutant. This dissertation focuses on the investigation of adsorption for micro-pollutants in aquatic environment via the application of different types of carbonaceous (powdered activated carbon, carbon nanotubes, and biochars) and biodegradable (chitosan) adsorbent. The effect of water chemistry conditions such as pH, concentration of ionic strength induced species and natural organic matters were considered as significant factors to increase or decrease the adsorption capacity of each adsorbent. This study also illuminates the use of biochar, byproduct of bio-oil, with simple chemical activation as an efficient adsorbent for pharmaceutical and EDCs removal. In-depth analysis about adsorption between these micro-pollutants and biochars was performed by characterization of physicochemical properties by nuclear magnetic resonance analysis in conjunction with molecular modeling subsequently interpreting the binding energy. Aromaticity and composition of

vi

carbonaceous structure of adsorbent controlled the adsorption capacity, while hydrophobicity of adsorbates influenced the adsorption affinity toward the adsorbents. More specifically, the presence of adsorption competitors resulted in less effective binding due to a combination of less favorable binding energy, polarity, and $\pi$-energy with the adsorbent and electrostatic repulsion from the cosolutes that occupied adsorption sites.

# TABLE OF CONTENTS

# LIST OF TABLES

# LIST OF FIGURES

## LIST OF ABBREVIATIONS

AC ................................................................................................ Activated Carbon

ATR ...................................................................................................... Atrazine

BPA .................................................................................................... Bisphenol A

BTE ................................................................................... Brunauer–Emmett–Teller

CBM ............................................................................................ Carbamazepine

CNT .................................................................................................. Carbon Nanotube

CP ................................................................................................. Cross Polarization

Cr(III) ......................................................................................... Trivalent Chromium

Cr(VI) ........................................................................................ Hexavalent Chromium

DCF .................................................................................................... Diclofenac

DFT ..................................................................................... Density Functional Theory

DP .......................................................................................... Direct Polarization

EDA ......................................................................................... Electron Donor Acceptor

EDC ................................................................................ Endocrine Disrupting Compound

E1 ........................................................................................................... Estrone

E2 ...................................................................................................... 17 β-Estradiol

EE2 ............................................................................................... 17α-ethinylestradiol

EPA ........................................................................... Environmental Protection Agency

EWG ............................................................................... Environmental Working Group

FTIR ...................................................................................... Fourier Transform Infrared

GAMESS ............................... General Atomic and Molecular Electronic Structure System

IARC ........................................................International Agency for Research on Cancer

IBP ........................................................................................................................Ibuprofen

ICP-MS ...................................................Inductively Coupled Plasma Mass Spectrometry

IR............................................................................................................................Infrared

MAS........................................................................................... Magic Angle Spinning

MWNT......................................................................... Single-Walled Carbon Nanotube

NMR ...................................................................................... Nuclear Magnetic Resonance

NOM .......................................................................................Natural Organic Matter

NPX.........................................................................................................................Naproxen

NSAID ................................................................... Nonsteroidal Anti-Inflammatory Drug

PAC...................................................................................... Powdered Activated Carbon

PhAC..........................................................................Pharmaceutical Active Compounds

PPCP ............................................................... Pharmaceutical and Personal Care Product

ROS...............................................................................................Reactive Oxygen Species

SA ......................................................................................................................Surface Area

SMD........................Solvation Model Based on the Quantum Mechanical Charge Density

SMX...............................................................................................Sulfamethoxazole

SP ..................................................................................................................Single Pulse

SWNT .......................................................................... Single-Walled Carbon Nanotube

TCEP..........................................................................Tris (2-Carboxyethyl) Phosphine

WWTP ............................................................................. Wastewater Treatment Plant

XRD ................................................................................................ X-Ray Diffraction

XPS ............................................................................. X-Ray Photoelectron Spectroscopy

# CHAPTER 1

## INTRODUCTION AND MOTIVATION

The advanced state of civilization and growth of science enable living to be better, simple, convenient, or more complicated. With the rapid development of industries, heavy metal wastewaters are discharged directly or indirectly into the environment. Unlike organic contaminants, heavy metals are hardly biodegradable and lead to deleterious health effects on aquatic life due to their tendency to be accumulated in living organisms (Kromhout, Bosschieter, and Coulander 1985; Gorell et al. 1997). This leads to more stringent regulations about heavy metal treatment, and toxic and carcinogenic heavy metals are regarded as priority water contaminant. Another emerging water contaminant is endocrine disrupting compounds (EDCs) and pharmaceuticals, and trace-level organic contaminants that have been detected in aquatic environments such as surface waters, wastewater, runoff, and landfill leachates (Kolpin et al. 2002; Benotti et al. 2008a; Yoon et al. 2010). The widespread occurrence of these dissolved chemicals in water sources is of concern due to their adverse effects, such as mimicking or antagonizing natural hormones, hindering metabolic processes, occupying hormone receptors, and causing reproductive and development problems when consumed by humans and aquatic species (Rudder et al. 2004; Comerton, Andrews, and Bagley 2009).

The above water pollutants' common characteristics are their sensitivity to pH, and their moieties vary depending on pH. pH controls a pollutant's net charge and hydrophobicity, and these properties have been considered in water treatment. With this

1

knowledge, one of the well-considered pH effects in water treatment is an adsorption. Adsorption is widely used to remove aqueous micro-pollutants from various contaminated waters. Detailed micro-pollutant adsorption studies involving equilibrium and kinetic data, as well as the effects of water chemistries, characteristics of adsorbents, and other relevant conditions over the adsorption process have been undertaken. When compared to conventional methods, adsorption offers significant economic and environmental advantages such as low cost, availability, profitability, ease of operation, and high removal efficiency. Various synthetic and natural materials have been used as micro-pollutants sorbents including activated carbon, carbon nanotubes, biological materials, zeolites, chitosan, and industrial wastes. The property of each adsorbent performs differently depending on adsorbates; therefore, investigation of the adsorption in the aqueous system is required to improve water treatment. Adsorption with a high-binding adsorbent has been used to eliminate various contaminants in the aqueous phase (Jung, Heo, et al. 2013). The well-established manufacturing process and relatively low cost of activated carbon has led to it becoming a famous adsorbent for water treatment due to its strong interaction with hydrophobic organic contaminants. However, the physical properties of activated carbon, including the irregular and closed pore structure with small micropore sizes (< 2 nm), precludes the adsorption of large molecules, leading to a size-exclusion effect (Kilduff et al. 1996). The crucial role of pore size for the adsorption of dyes and pharmaceuticals has been investigated (Nakagawa et al. 2004; Ji, Shao, et al. 2010), and these studies have concluded that accessible adsorptive spaces are required for effective adsorption to minimize the size-exclusion effect.

Despite exponential growth in activated carbon manufacturing, more eco-friendly or biodegradable adsorbents are required to achieve the optimum water treatment. Next-generation adsorbents must overcome not only the environmental demands, but also customized treatment for specific contaminants.

# CHAPTER 2

## OBJECTIVES AND SCOPE

Heavy metals have been considered as primary water contaminants, and concerns of their negative health effects encourage improvement and development of removal methods. While water treatment has been developed to treat the primary contaminants, another group of contaminants, not historically considered as contaminants and called "emerging contaminant", is a growing concern in the environment on a global scale (Richardson 2008). Although the fate and environmental impacts have been determined for primary contaminants, those of the newly recognized contaminants are not fully understood.

In the point of efficiency and economical view, adsorption with various adsorbents has been applied to remove the primary contaminants (Wang et al. 2007; Wan Ngah and Hanafiah 2008; Rengaraj et al. 2002). Diverse characteristics of different adsorbents are suitable to be applied to water treatment in terms of covering customized removal between complex properties of each contaminant and adsorbent. Furthermore, determination of optimum adsorption condition is able to minimize the scale and cost and maximize the removal efficiency. For this reason, well-manufactured granular or powdered activated carbon has been used in many water treatment facilities (Nowotny et al. 2007). Although activated carbons perform enough to be acceptable to treat water contaminants, it is hard to be applied all contaminants. Therefore, the proposed research applies to investigate the removal mechanism and efficiency with comparison among different adsorbents for

4

specific contaminants. The first objective of our research is to investigate the adsorption characteristics of one of the heavy metals, hexavalent chromium (Cr(VI)), under four different adsorbents: Powdered activated carbon (PAC), chitosan, and single/multi-walled carbon nanotubes (SWNTs/MWNTs). Expected adsorption between dominant chromium species, $CrO_4^{2-}$ and $HCrO_4^{-}$, in acidic condition and positive charged adsorbent might be the main removal mechanism, and this electrostatic interaction will affect the adsorption capacity of different adsorbents. Different from well-known adsorbents, activated carbon, biodegradable chitosan will be applied in hexavalent chromium removal, and nano-sized rolled graphene material, carbon nanotube also will be used investigate its adsorption affinity. Functional groups on each adsorbent analyzed by Fourier transform infrared (FTIR) will be correlated to hexavalent chromium adsorption capacity and size of adsorbent and its surface area will affect adsorption site, providing more opportunities to be contacted.

The second objective in this research is to evaluate adsorption characteristics of biochar for endocrine disrupting compounds and pharmaceuticals. Numerous EDCs and pharmaceuticals are hydrophobic, and their properties are a pH dependent. Therefore, the hypothesis that hydrophobic interaction between those emerging contaminants and biochar is able to be determined through characterization of both adsorbate and adsorbent. Not only element composition analysis, but also chemical structure analysis under $^{13}C$ solid-state nuclear magnetic resonance (NMR) will reveal the adsorption characteristics.

The third component of the research is to determine competitive or non-competitive adsorption of nonsteroidal anti-inflammatory drugs (NSAIDs) onto biochar. NSAIDs; naproxen (NPX), diclofenac (DCF), and ibuprofen (IBP), considering pH

5

depending hydrophobicity of each chemical. General interpretations of NSAID adsorption are performed by both consideration of values of p$K_a$, and exclusive characteristics of biochar. Slight different properties of NSAID might result in significant difference in adsorption. Moreover, the dispersion-corrected density functional theory in single or competitive adsorptive conditions under consideration of conformation and chemical properties of both solute and adsorbent was considered to verify the characteristics of NSAIDs adsorption. Interaction energies between the NSAIDs and the biochar were also calculated to characterize the strength of adsorption and the effect of the various surface functional groups on the adsorption capacity of the char.

6

# CHAPTER 3

## LITERATURE REVIEW AND BACKGROUND

**3.1 Occurrence and exposure of micro-pollutants in the aquatic environment**

**3.1.1 Exposure of hexavalent chromium in aquatic system and its conventional treatments**

The release of chromium compounds having a large variety of valence states (range: –IV to +VI) to water systems may deleteriously affect aquatic life (Fukai 1967). The reason why many people have concerned the exposure of Cr(VI) is its well-established carcinogenic property. In 1989, international agency for research on cancer (IARC) announced that hexavalent chromium was classified as a chemical acts as a carcinogenic compound as well as genotoxic, mutagenic compound (IARC 1989). Like many toxicologists have been focused on the ability of metal to penetrate the cell membrane as a cell disruptor, Cr(VI) deforms the cell due to its toxicological activity and carcinogenicity, performing as a strong oxidant (Cerulli et al. 1998). To comply with the legal limits of 50 μg/L of total chromium concentration for drinking water (Khezami and Capart 2005) and 100 μg/L for discharges to surface water (US Environmental Protection Agency standards) (EPA 1990), chromium must be removed or alternatively converted into a less toxic soluble species (Pandey and Mishra 2011) through electron transfer between hexavalent and trivalent chromium. However, industrial wastewater typically contains high concentrations of total chromium, ranging from 500 to 270,000 μg/L (Patterson 1985), and levels can reach 50–

700 μg/L in groundwater (Oze, Bird, and Fendorf 2007). Recently, the Environmental Working Group (EWG) in California published a report in 2013 revealing the detection of hexavalent chromium in drinking water from selected cities in US. The cities with the highest levels were Norman, Oklahoma, which was detected 12 ng/L, and the average concentration of Cr(VI) in the tap water of the sampled cities was above 0.2 ng/L, which exceeded the state's proposed limit of Cr(VI), 0.06 ng/L to protect public health (Formuzis 2013). In other major cities such as Los Angeles, Atlanta, and New York had the levels of Cr (VI) as 0.2 ng/L, 0.06 ng/L, and 0.03 ng/L, respectively (Michael Hawthorne 2010). Moreover, Table 3.1 shows the result of contamination of Cr(VI) in tap water throughout the most populous counties in California analyzed by EWG.

**Table 3.1** Ten of California's most populous counties impacted by the State's proposed standard (0.06 ng/L) (Formuzis 2013).

| County | Population affected | No. of water systems with Cr(VI) detections ($\leq 10$ ng/L) |
|---|---|---|
| Los Angeles | 7,492,045 | 109 |
| Riverside | 1,978,938 | 38 |
| San Bernardino | 1,948,006 | 57 |
| Orange | 1,878,119 | 19 |
| Santa Clara | 1,707,277 | 23 |
| Sacramento | 1,371,635 | 25 |
| Fresno | 779,198 | 55 |
| Kern | 698,839 | 70 |
| San Joaquin | 634,623 | 76 |
| Ventura | 566,445 | 18 |

Detoxification of chromium is achieved by either conventional or biological treatment processes (Agrawal 2006). A range of approaches is taken in conventional and advanced chromium removal from water including the addition of alkaline solutions (e.g., increasing pH) and subsequent chemical precipitation, reduction of Cr(VI) to Cr(III) prior to precipitation using reducing agents, adsorption on synthetic or natural adsorbents, chelating, ion exchange, filtration (Basu 1989), solvent extraction (Beneitez and Ayllon 1987), membrane separation (Fraser, Pritzker, and Legge 1994), evaporation (Morisset et al. 1955), and electrolysis (Jacukowicz-Sobala 2009). In general, these processes require high levels of expertise and often generate toxic by-products or combine low removal efficiencies with high operation and maintenance costs (Vaiopoulou and Gikas 2012).

### 3.1.2 Exposure of EDCs and pharmaceuticals in aquatic system

A variety of EDCs exist, including pesticides, natural hormones, and industrial chemicals. Atrazine is one of the most widely used herbicides and its continuous exposure into water causes its concentration to accumulate due to its poor degradability compared to other herbicides (Wackett et al. 2002). Recently, 17α-ethinylestradiol (EE2), an oral contraceptive, has been studied extensively due to its higher toxicity compared to other hormones such as estrone or 17 β-estradiol (Segner et al. 2003). Similarly, bisphenol A (BPA), a main monomer in epoxy resin and polycarbonate plastic, has been studied due to the ubiquitous use of plastic in everyday living.

In addition, because of the increasing demand for pharmaceuticals, the level of exposure has increased, paradoxically causing a threat to health. Certain pharmaceuticals have been studied widely, such as nonsteroidal anti-inflammatory drugs such as diclofenac and ibuprofen as well as antibiotics, sulfamethoxazole, and antiseizure medicine,

9

carbamazepine. EDCs and pharmaceuticals are metabolized and adsorbed by organisms at low levels, resulting in exposure to the residues of these compounds or their transformed products when they enter the aquatic environment (Halling-Sørensen et al. 1998; Kolpin et al. 2002). Although these exposures have been issued and considered, lack of detection method and expensive analysis expense due to their trace level in the aquatic system, these compounds are still classified as emerging contaminants, not primary contaminants. Here are selected chemicals which have been exposed and detected in both surface and drinking waters (Table 3.2).

### 3.1.3 Exposure NSAIDs in aquatic system

Nonsteroidal anti-inflammatory drugs (NSAIDs) are inflammatory reducer and pain relief drugs that have analgesic, antipyretic and anti-inflammatory properties. NSAIDs are designed to be retained in human and animal body long enough with an acidic moiety attached to a planar, aromatic functionality (Babbar 2003). Although common form of released NSAIDs is their original form, it is hardly degradable and removed in conventional treatment. In 2011, the World Health Organization announced that slighting or intentional discharged trace level of untreated pharmaceuticals in water raising the concern that the continuous input of pharmaceuticals may pose potential deleterious effects for the organisms living in terrestrial and aquatic environment (Molinari et al. 2006). Especially, these exposure of NSAIDs in aquatic environment as various forms have affected reproduction and development as well as hepatotoxicity and nephrotoxicity (Schwaiger et al. 2004; Mehinto, Hill, and Tyler 2010; Hoeger et al. 2005) in organism. The damage induced by NSAIDs may different depend on their history of usage and persistent ability, resulting negative biological activity and toxicity (Bilotta et al. 2004).

10

**Table 3.2** Occurrence of pharmaceutical and personal care products (PPCPs) and endocrine disrupting compounds (EDCs) in the surface water and drinking water (Padhye et al. 2014; Li et al. 2012; Benotti et al. 2008a).

| Compound | Class | M.W. (g/mol) | Surface water | | | | Drinking water | | | |
|---|---|---|---|---|---|---|---|---|---|---|
| | | | F. D. | Max. conc. (ng/L) | Min. conc (ng/L) | Median conc. (ng/L) | F.D. | Max. conc. (ng/L) | Min. conc. (ng/L) | Median conc. (ng/L) |
| Acetaminophen | Analgesic/Anti-inflammatory | 150.9 | 13 % | $19.2 \pm 1.2$ | 0.0 | 0.0 | 0 % | 0.0 | 0.0 | 0.0 |
| Atenolol | β -Blocker | 266.3 | 0 % | 0.0 | 0.0 | 0.0 | 13 % | $34.1 \pm 0.0$ | 0.0 | 0.0 |
| Atrazine | Herbicide | 215.7 | 100 % | $75.1 \pm 1.2$ | $3.4 \pm 0.2$ | 5.4 | 100 % | $14.8 \pm 4.0$ | $0.6 \pm 0.1$ | 3.7 |
| Bisphenol A | Plasticizer | 228.3 | 75 % | $21.9 \pm 1.6$ | 0.0 | 12.7 | 50 % | $4.3 \pm 10.1$ | 0.0 | 2.7 |
| Caffeine | Stimulant | 194.0 | 50 % | $15.9 \pm 0.6$ | 0.0 | 2.7 | 38 % | $11.6 \pm 0.7$ | 0.0 | 0.0 |
| Carbamazepine | Antiepileptic | 236.0 | 100 % | $4.1 \pm 1.2$ | $0.5 \pm 0.1$ | 0.9 | 13 % | $25.0 \pm 8.8$ | 0.0 | 0.0 |
| Clarithromycin | Antibiotic | 747.9 | 100 % | $1.7 \pm 0.1$ | $0.2 \pm 0.1$ | 0.6 | 75 % | $0.2 \pm 0.1$ | 0.0 | 0.1 |
| Cotinine | Nicotine metabolite | 176.2 | 25 % | $2.7 \pm 0.4$ | 0.0 | 0.0 | 13 % | $0.4 \pm 0.4$ | 0.0 | 0.0 |
| DEET | Insect repellent | 191.2 | 100 % | $256 \pm 62.5$ | $23.3 \pm 3.0$ | 122.4 | 100 % | $24.0 \pm 8.2$ | $0.5 \pm 0.1$ | 11.9 |
| Diclofenac | Analgesic/Anti-inflammatory | 295.0 | 50 % | $24.0 \pm 8.4$ | 0.0 | 1.91 | 25 % | $9.4 \pm 0.1$ | 0.0 | 0.0 |
| Erythromycin-$H_2$O | Antibiotic | 715.9 | 100 % | $2.7 \pm 1.2$ | $0.3 \pm 0.3$ | 2.2 | 100 % | $13.8 \pm 2.6$ | $1.0 \pm 0.1$ | 1.5 |

M.W. is a mole weight (g/mol) and F.D. is a frequency of detection.

**Table 3.2** Occurrence of pharmaceutical and personal care products (PPCPs) and endocrine disrupting compounds (EDCs) in the surface water and drinking water (Padhye et al. 2014; Li et al. 2012; Benotti et al. 2008a) (continued).

| Compound | Class | M.W. (g/mol) | Surface water | | | | Drinking water | | | |
|---|---|---|---|---|---|---|---|---|---|---|
| | | | F. D | Max. conc. (ng/L) | Min. conc. (ng/L) | Median conc. (ng/L) | F.D | Max. conc. (ng/L) | Min. conc. (ng/L) | Median conc. (ng/L) |
| E1 (Estrone) | Steroid hormone | 270.4 | | 197 | 7.3 | - | | 0.9 | 0.3 | 0.7 |
| E2 (17 β-Estradiol) | Steroid hormone | 272.4 | | 48 | 4.9 | - | | 17 | 0.0 | 17 |
| EE2 (17 α-Ethinylestradiol) | Synthetic steroid hormone | 296.4 | | 11 | 0.2 | - | | 1.4 | 0.0 | 1.4 |
| Fluoxetine | Antidepressant | 309.0 | 38 % | $0.9 \pm 0.1$ | 0.0 | 0.0 | 13 % | $19.2 \pm 0.7$ | 0.0 | 0.0 |
| Ibuprofen | Analgesic/Anti-inflammatory | 206.0 | 38 % | $133 \pm 106$ | 0.0 | 0.0 | 13 % | $10.2 \pm 0.0$ | 0.0 | 0.0 |
| Levofloxacin | Antibiotic | 361.4 | 38 % | $1.3 \pm 2.0$ | 0.0 | 0.0 | 0 % | 0.0 | 0.0 | 0.0 |
| Metoprolol | β-Blocker | 267.4 | 100 % | $0.3 \pm 0.1$ | $0.1 \pm 0.0$ | 0.1 | 13% | $1.0 \pm 0.1$ | 0.0 | 0.0 |
| Naproxen | Analgesic/Anti-inflammatory | 230.3 | 13 % | $9.2 \pm 3.9$ | 0.0 | 0.0 | 13% | $5.1 \pm 5.1$ | 0.0 | 0.0 |
| Nonylphenol | Detergent degradate | 220.4 | 100 % | $186 \pm 20.0$ | $53.4 \pm 4.8$ | 83.2 | 100 % | $60.6 \pm 19.2$ | $12.4 \pm 5.3$ | 19.5 |
| Sulfamethoxazole | Antibiotic | 253.0 | 88 % | $7.4 \pm 0.8$ | 0.0 | 2.4 | 13 % | $12.7 \pm 3.6$ | 0.0 | 0.0 |
| TCEP | Flame retardant | 283.9 | 88 % | $51.7 \pm 1.9$ | 0.0 | 5.6 | 88 % | $20.4 \pm 5.8$ | 0.0 | 3.7 |
| Triclosan | Antimicrobial | 287.9 | 63 % | $106 \pm 63.1$ | 0.0 | 3.3 | 63 % | $59.6 \pm 25.7$ | 0.0 | 1.4 |
| Trimethoprim | Anitibiotic | 290.1 | 100 % | $10.9 \pm 0.8$ | $2.2 \pm 0.2$ | 5.8 | 88 % | $19.8 \pm 4.5$ | 0.0 | 1.5 |

Studies about ability to stimulate the sequestration of reactive oxygen species (ROS), which is dexterous to cellular homeostasis, have warned the side effects of exposure of NSAIDs. Therefore, it is required to remove the trace level of NSAIDs in aquatic system (Ruas et al. 2008; SanJuan-Reyes et al. 2013). The most common detected NSAIDs are propionic acids (ibuprofen, naproxen), heteroarylacetic acid (diclofenac) and aspirin, and their detected concentration in wastewater treatment plant (WWTP) and toxicity data are given in Table 3.3.

The regulation of NSAIDs released into water resources has been proposed by the US Environmental Protection Agency and World Health Organization, while the proposed compounds have been limited to readily detectable hydrophobic compounds, such as diclofenac and ibuprofen (Richardson and Ternes 2005). A proposed regulation for dissociated and relatively hydrophilic NSAIDs, such as acetaminophen and naproxen, in the aquatic environment is also desirable to protect against their potential adverse effects.

## 3.2 Various adsorbent for micro-pollutant removal

### 3.2.1 Chitosan as a water treatment material

Chitosan is commercially produced by the deacetylation of chitin, the main structural component of the exoskeleton of crustaceans (e.g., crabs, shrimp) and the cell walls of fungi (Figure 3.1).

Since chitosan contains amino groups (p$K_a$ ~6.5), it is protonated in acidic to neutral solutions, generating a charge density that is pH-dependent (Ko et al. 2002). Chitosan has been widely used as a cationic coagulant supplier for water treatment (Huang, Chen, and Ruhsing Pan 2000). By taking advantage of this characteristic of chitosan, bound fine flocs can be subsequently removed during sand filtration. This process also allows inexpensive, abundant, and is a good adsorbent for heavy metals including

13

**Table 3.3** The detected concentration and frequency of NSAIDs in WWTP influent/effluent, surface water and their acute toxicity data (Cleuvers 2004; Feng et al. 2013).

| Drug | Formula | Solubility (mg/L) | WWTP influent (μg/L) | WWTP effluent (μg/L) | Surface water (μg/L) | Acute toxicity (EC$_{50}$ mg/L) | | | Acute toxicity (LC$_{50}$ mg/L) | | |
|------|---------|-------------------|----------------------|----------------------|----------------------|---------|-------|------|---------|-------|------|
| | | | | | | Daphnia | Algae | Fish | Daphnia | Algae | Fish |
| Aspirin | $C_9H_8O_4$ | 4600 | 100 | 0.05 -1.51 | < 0.05 | 88 | 107 | - | 141 | - | 178 |
| Diclofenac | $C_{14}H_{11}Cl_2NO_2$ | 2 | 0.10-4.11 | 0.04 -1.95 | 0.001 -0.07 | 5057 | 2911 | 532 | 22.4 | 14.5 | - |
| Ibuprofen | $C_{13}H_{18}O_2$ | 21 | 0.17-83.5 | < 95 | n/d -0.20 | 38 | 26 | 5 | 9.1 | 7.1 | 173 |
| Naproxen | $C_{14}H_{14}O_3$ | 144 | 1.79 -611 | 0.17-33 | n.d -0.04 | 15 | 22 | 35 | 43.5 | 320 | 560 |
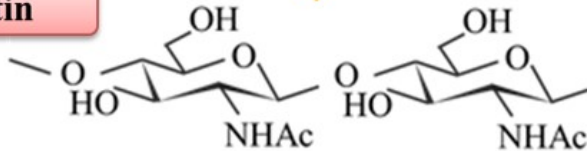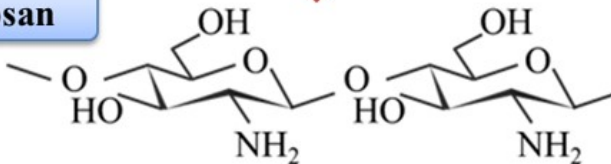
**Figure 3.1** Chitin and chitosan manufacturing process (figure sources: (Ilium 1998); visualdictionaryonlin.com).

chromium. Because of the free amino groups exposed during deacetylation, chitosan presents a high metal-chelating ability (more than five times greater than chitin (Yang and

Zall 1984). In addition, the high hydrophilicity of chitosan makes this material suitable for heavy metal adsorption (Owlad et al. 2009).

### 3.2.2 Carbon nanotubes (CNTs) considered as an attractive adsorbent

CNTs are a relatively new form of carbon materials discovered by Iijima (Iijima 1991). Because of their outstanding properties, CNTs have been widely applied in various fields such as the fabrication of superconductors, optical devices, sensors, energy storage devices, fuel cells, and catalysts (Balasubramanian and Burghard 2005). With regard to water treatment applications, CNTs have also been used as carbonaceous adsorbents for the removal of heavy metals (Dennington et al. 2003), natural organic matter (NOM) (Hyung and Kim 2008), pharmaceuticals and personal care products (Ji, Liu, et al. 2010), and endocrine disrupting chemicals (Joseph et al. 2011; Kiran Kumar and Venkata Mohan 2012). CNTs can be manufactured in the form of SWNTs or MWNTs, distinguished by their number of graphite layers (Figure 3.2). The nano size of CNTs provides a high surface area, thereby leading to higher adsorption capacities and unique electrical properties. These characteristics have allowed CNTs to become attractive as adsorbents (Dennington et al. 2003).
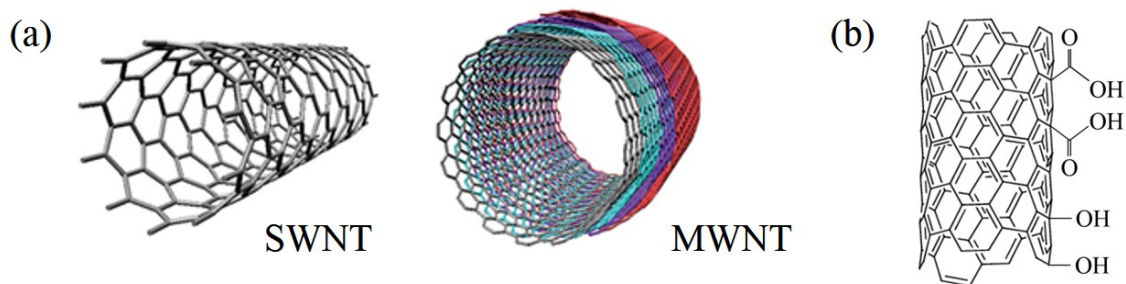


**Figure 3.2** Schematics of (a) SWNT and MWNT (Karthikeyan and Mahalingam 2013), and (b) functionalized SWNT (Mohamed et al., 2013).

16

### 3.2.3 Biochar as a promising water treatment adsorbent

With an advance of biorefinery in the near future, it is expected that biochar will be available for precursors for value-added products. Biochar is the byproduct of the pyrolytic processing of biomass to obtain biofuel such as fast pyrolysis and gasification, and has a potential as a promising adsorbent for the elimination of micro-pollutants due to its superior properties including a highly condensed structure and surface density of functional groups, although its activated product provides a lower surface area and volume than commercialized activated carbon (Ji, Liu, et al. 2010; Chen, Zhou, and Zhu 2008). These properties are controlled by the pyrolysis conditions (residence time, oxygen and hydrogen ratio, and temperature), activation, and type of feedstock; biochar pyrolyzed at a high temperature consists mainly of polyaromatic carbons and has a higher microporosity, which enhances the adsorption of organic compounds, while higher proportions of aliphatic carbons and functional groups are typical of biochars pyrolyzed at a low temperature (Chen, Zhou, and Zhu 2008; Chun et al. 2004). A separate study has shown that chemically activated biochar resulted in higher porous structure, surface area, and lower ash content than commercialized activated carbon (Azargohar and Dalai 2006). Since most organic forms such as any kind of plants, domestic waters, industrial wastes, sewage sludge, and animal manures have used as a pyrolyzer, their composition of elements and ratio of inorganic compounds in biomass varies the both product yield and quality of bio-oil and biochar (Laird et al. 2009). Figure 3.3 shows an example of biochar manufacturing process and its potential applications.
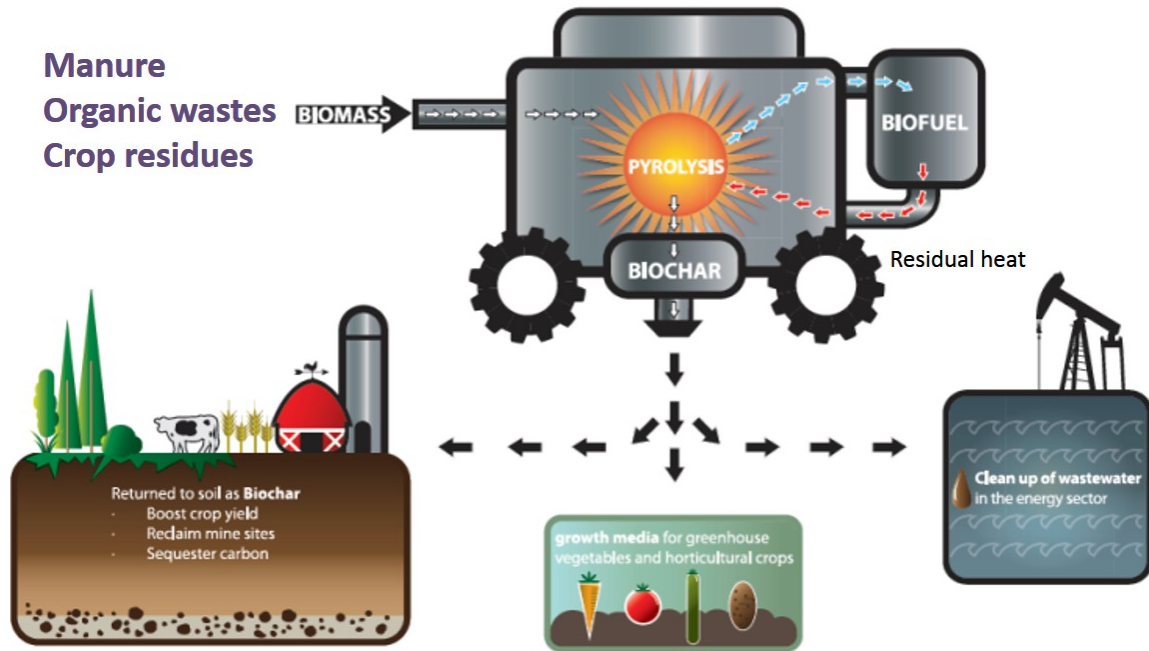
**Figure 3.3** Biochar manufacturing process and its potential applications (source: http://www.lakelandcollege.ca/applied-research/projects/agricultural-science).

## 3.3 Characterization of adsorbent and adsorbate

### 3.3.1 Techniques for adsorbent characterization

To use the material for application in adsorbent, satisfactory knowledge about both water chemistry behind the adsorption and structure of adsorbent are of primary importance. Recent rediscovery of carbonaceous material (i.e., activated carbons (granular or powdered activated carbon)) in water purification enables competent wastewater treatment as well as chitosan, biodegradable materials considered in this field. Unfortunately, some basic information about structure of the materials are still lacking as far as removal mechanism.

Many researchers have been working on the reaction mechanisms in the adsorption process in water purification field; however, precise descriptions of the structure of the

18

reaction path leading to the carbonaceous adsorbents are still not clear (Yao et al. 2007; Baccile et al. 2009). The intrinsic and complex water chemistry and structure of the adsorbent are the main shortcomings, resulting in hard and difficult understanding structural study using common techniques, such as X-ray diffraction (XRD) or infrared (IR) spectroscopy. Nonetheless, Fourier transform infrared (FTIR) and FT-Raman spectroscopies have been used to identify various functional groups on the material due to their easy accessibility (Titirici et al. 2007). X-ray photoelectron spectroscopy (XPS) was also used to determine the main carbonaceous surfaces, and better spectral resolution was allowed with vibrational spectroscopies (Titirici, Thomas, and Antonietti 2007). Moreover, scanning electronic microscopy, optical microscopy, and pyrolysis-gas chromatography-mass spectroscopy, have been employed to characterize the complex structures and properties of functionalized carbonaceous material (Simpson and Hatcher 2004; Fernandes et al. 2003; Song, Peng, and Huang 2002; Song and Peng 2010). Few studies attempted ^{13}C solid state NMR (Budarin et al. 2006; Sun et al. 2011) as complementing and supporting other techniques, resulting spectra only helped in the identification of the selected organic functions like IR did. Nevertheless deeper investigation with more advanced ^{13}C solid state NMR technique rather good spectral resolution obtained on black carbons was deserved (Novotny, Hayes, and Bonagamba 2006).

**3.3.2 Technique of solid state nuclear magnetic resonance (NMR) and its use for adsorbent characterization**

Magnetic interactions in the solid state are described by a sum of four parts (Hamiltonian H); magnetic shielding (producing chemical shifts), dipole-dipole interaction

19

(the direct magnetic coupling of two nuclei through space), scalar spin-spin coupling to other nuclei and quadrupolar interactions (for nuclei with I > 0.5), and Zeeman interaction. According to the detail consideration about this basic nuclear spin interactions, the most important contribution in magnetic interaction is a dipole-dipole interaction (Mehring 1976). This dipole-dipole interaction depends upon inter nuclear distance and orientation of the molecule, described by a $1-3\cos^2\theta$ term; $\theta$ is an angle between molecules. In solution, this term is averaged over all angles $\theta$ and disappears because all molecules rotate rapidly and immediately.

Whereas, the molecules are fixed with respect to the direction of magnetic field in the solid state, resulting production of broad resonance lines (Wawer and Witkowski 2001). This broad resonance lines are contributed by the dipolar interactions between $^1H$ and $^{13}C$, and can not only be removed by high power proton decoupling but also be narrowed further with rapid sample rotationat $\theta = 54°44$, called "magic angle". In the case of polycrystalline sample, applying a random distribution of orientations to the magnetic field, the chemical shift anisotropy increases which may range between 0 to 20 kHz. Although the spinning rates of up to 40 kHz are technically accessible in recent high field spectrometers, the side-band free $^{13}C$ spectra can be obtained by the rotation speed of 6 to 10 kHz. Furthermore, both method of rapidly changed spinning axis in dynamic axis spinning methods (MAS), yielding the solid state spectra with the line range of 5 to 10 Hz (Wu, Rovnyak, and Griffin 1996) and applying rotors spinning one inside another at different angles (double rotation experiments) in the field also have been reported (Schaefer, Stejskal, and Buchdahl 1977).

20

Magic angle spinning (MAS) experiment is more sensitive in comparison to the solution phase because the whole space of the rotor is filled with sampled compound. Higher value of sensitivity in NMR analysis causes further enhancement due to the 1% natural abundancy of $^{13}C$. The cross polarization (CP) pulse sequence is applied to achieve the best result. However, quantificational analysis with CP sequence is more complicated and challenged spin dynamics than single pulse (SP) sequence. Although SP sequence is preferred for quantification due to time consumption, the advantage of obtaining signal enhancements and broadening with CP allows fast information about the chemical composition of samples (Baccile et al. 2009).

The transfer of magnetization from the $^{1}H$ to $^{13}C$ spin reservoir under the Hartmann-Hahn condition results in increase of $^{13}C$ signal magnitude as well as reduction of the delay time between successive pulse sequences due to shorter relaxation time of $^{13}C$ than that of proton spin lattice. Therefore more number of scans per unit time is required to yield better signal to noise ratio. To achieve better outcomes in NMR analysis, applying modified CP condition and two-dimensional $^{13}C$ homonuclear magnetization exchange (Sullivan and Maciel 1982), attempt $^{1}H$ longitudinal relaxation times in the laboratory and rotating time frames (Dela Rosa et al. 1992), and employing the $^{13}C$ transverse dephasing times were performance (Tekely et al. 1986).

**3.3.3 Influence of physicochemical properties of the adsorbates on adsorption: Ionization and p$K_a$**

The aforementioned EDCs (atrazine, EE2, and BPA) and four pharmaceuticals (diclofenac, ibuprofen, sulfamethoxazole, and carbamazepine) are amphoteric species and consist of single or multiple charged groups, as well as polar groups (hydroxyl, carbonyl,

21

carboxyl, amine, sulfonyl) with aromatic rings (benzene, isoxazole, 1,3,5-triazine, azepine). Under acidic conditions, all of these EDCs/ pharmaceuticals are predominantly neutral species ($<$p$K_a$). Increasing the pH varied the content of their ionic forms depending on each p$K_a$ value while basic compounds lose their proton, especially for sulfamethoxazole, diclofenac, and ibuprofen whose p$K_a$ is relatively lower than those of other compounds. At pH values below their p$K_a$, the adsorption capacity increased significantly in this condition; whereas at pH values greater than the p$K_a$, the adsorption capacity dropped sharply (Hong et al. 2008). This difference occurs because the electronic coupling influences the adsorptive interaction with each adsorbent. The strong electron-withdrawing sulfonamide group, carboxyl group and hydroxyl group on sulfamethoxazole, diclofenac and ibuprofen, and bisphenol A, respectively, allow π–π electron donor–acceptor (EDA) interaction with π–electron–acceptor-rich aromatic ring(s) (Ji, Liu, et al. 2010), whereas less variation of adsorption capacity due to their higher p$K_a$ values (less variation in the ionic state) allow carbamazepine, atrazine, and EE2 to show strong hydrophobic interactions throughout a wide pH range.

**3.4 Molecular modeling for structure configuration in adsorption study**

In experimental works, the adsorbate and adsorbent, which were medium to perform the adsorption activity in the system, are also characterized by measuring its physical and chemical properties because decision of suitable adsorbent for target compounds to be removed in the aquatic environment is variables affect the adsorptive activity through the physical and chemical properties of the adsorbent. In principle, if the effects of selection variables on physical-chemical properties, and the effects of physical-chemical properties on the adsorptive activity are identified or understood, then

22

study of adsorption would be improved since better assumption of mechanisms and selection of experimental condition in the adsorption study might be provided. However, this is not an easy task for the actual systems due to existence of the large number of unknown factors and complex interactions among them. Fortunately, the computational resources have been developing in the recent years, and then quantum computational studies have relieved and simplified this complicate molecular modeling for structure configuration, and revealed the actual adsorption system.

### 3.4.1 Application of density functional theory (DFT) in the adsorption study

For prediction of molecular properties such as molecular structures, vibrational frequencies, atomization energy, ionization energies, electric and magnetic properties, and reaction paths, DFT has been used as the most successful and promising approach in the field of chemistry. DFT usually covers computations of the electronic structure of matter with an applicability ranges (Becke, Matta, and Boyd 2007). The key role in DFT is the electron density, and the cluster model of adsorbent is estimated via employment of DFT with information of the ground state properties of specific adsorptive system although the model may be cause some drawbacks of stemming due to the incomplete representation of the electronic system (Neurock 2002). Here are main chemical situations handled by generalized original DCF.

- Spin polarized system
- Multicomponent systems (nuclei and electron hole droplets)
- Free energy at finite temperatures
- Superconductors with electronic pairing mechanisms
- Relativistic electrons

23

- Time dependent phenomena and excited states

- Bosons

- Molecular dynamics

# CHAPTER 4

## Hexavalent chromium removal by various adsorbents: powdered activated carbon, chitosan, and single/multi-walled carbon nanotubes[1]

**Abstract**

The adsorption behavior of ppb-level aqueous solutions of hexavalent chromium [Cr(VI)] on four different adsorbents was investigated as a function of pH, contact time, initial Cr(VI) concentration, adsorbent dose, and the copresence of competing anions. The adsorbents selected were powered activated carbon (PAC), chitosan, single-walled carbon nanotubes (SWNTs), and multi-walled carbon nanotubes (MWNTs). Each adsorbent was characterized by Fourier transform infrared spectroscopy and measurements of zeta potential to determine its suitability for Cr(VI) adsorption. The adsorption of Cr(VI) was found to be favored at low pH because all adsorbents were positively charged under acidic conditions (pH 4), while a dosage of 100 mg/L resulted in efficient adsorption behavior. PAC and chitosan provided the best removal performance. The highly functionalized and

---

porous PAC and the protonated amines on chitosan enabled a better performance and resulted in high Cr(VI) removal efficiencies of 99.4% and 94.7%, respectively, while the removal efficiencies of SWNTs and MWNTs were 72.9% and 51.9%, respectively. Isotherm and kinetic studies were undertaken to evaluate the characteristics of the Cr(VI) adsorption process. A well-fitted Langmuir isotherm model suggested that monolayer adsorption was the main process operating with an adsorption capacity ($q_m$) of 46.9, 35.6, 20.3, and 2.48 mg/g for PAC, chitosan, SWNTs, and MWNTs, respectively. Pseudo second-order fitted models revealed the importance of kinetic parameters (apart from adsorption capacity) in understanding the transport of Cr(VI) in the solution, while an intra-particle diffusion model fitted well for µg/L levels of Cr(VI) adsorption. This indicated that both physisorption and chemisorption were dominant, particularly for SWNTs. Anions such as $Cl^-$ and $SO_4^{2-}$ in the solution competed with $HCrO_4^-$ and this phenomenon resulted in negative effects on Cr(VI) adsorption.

*Keywords:* Hexavalent chromium; powdered activated carbon; chitosan; single-walled carbon nanotubes; multi-walled carbon nanotubes

## 4.1. Introduction

The release of chromium compounds having a large variety of valence states (range: –IV to +VI) to water systems may deleteriously affect aquatic life (Fukai 1967). To comply with the legal limits of 50 µg/L of total chromium concentration for drinking water (Khezami and Capart 2005) and 100 µg/L for discharges to surface water (US Environmental Protection Agency standards) (EPA 1990), chromium must be removed or alternatively converted into a less toxic soluble species (Pandey and Mishra 2011). However, industrial wastewater typically contains high concentrations of chromium,

26

ranging from 500 to 270,000 μg/L (Patterson 1985), and levels can reach 50–700 μg/L in groundwater (Oze, Bird, and Fendorf 2007). Detoxification of chromium is achieved by either conventional or biological treatment processes (Agrawal 2006). A range of approaches is taken in conventional and advanced chromium removal from water including the addition of alkaline solutions (e.g., increasing pH) and subsequent chemical precipitation, reduction of Cr(VI) to Cr(III) prior to precipitation using reducing agents, adsorption on synthetic or natural adsorbents, chelating, ion exchange, filtration (Basu 1989), solvent extraction (Beneitez and Ayllon 1987), membrane separation (Fraser, Pritzker, and Legge 1994), evaporation (Morisset et al. 1955), and electrolysis (Jacukowicz-Sobala 2009). In general, these processes require high levels of expertise and often generate toxic by-products, or combine low removal efficiencies with high operation and maintenance costs (Vaiopoulou and Gikas 2012).

Adsorption is widely used to remove heavy metals from industrial wastewaters. Detailed heavy metal adsorption studies involving equilibrium and kinetic data as well as the effects of pH, temperature, surface area, and other relevant conditions over the adsorption process have been undertaken (Aydin and Aksoy 2009). When compared to conventional methods, adsorption offers significant economic and environmental advantages such as low cost, availability, profitability, ease of operation, and high removal efficiency (Mittal, Krishnan, and Gupta 2005).

Various synthetic and natural materials have been used as Cr(VI) sorbents including activated carbon (AC), carbon nanotubes (CNTs), biological materials, zeolites, chitosan, and industrial wastes (Chen et al. 2012; Lv et al. 2011; Chen and Gu 2005; Leyva-Ramos et al. 2008; Sarin and Pant 2006). In particular, AC has been widely used as

27

an adsorbent for the removal of heavy metal contaminants because the large volume of micropores and mesopores provide a high surface area and they also have high chemical and thermal stability. AC has been modified (Dobrowolski and Otto 2010) or supplemented with surfactants (Chen, Zhou, and Zhu 2008) or tannic acid (Chen et al. 2012) to increase the Cr(VI) adsorption capacity. An effective strategy for improving the adsorption capacity of AC involves preparation of materials with a higher surface area by reducing the original particle size. These powdered activated carbons (PACs) are manufactured in the form of crushed or ground fine carbon particles, thereby having large surface to volume ratios and allowing an enhancement of the adsorption capacity per unit volume.

Chitosan is commercially produced by the deacetylation of chitin, the main structural component of the exoskeleton of crustaceans (e.g., crabs, shrimp) and the cell walls of fungi. Since chitosan contains amino groups (p$K$a ~6.5), it is protonated in acidic to neutral solutions generating a charge density that is pH-dependent (Ko et al. 2002). Chitosan has been widely used as a cationic coagulant supplier for water treatment (Huang, Chen, and Ruhsing Pan 2000). By taking advantage of this characteristic of chitosan, bound fine flocs can be subsequently removed during sand filtration. This process also allows the removal of phosphorus, heavy minerals, and oils from the water. Chitosan is inexpensive, abundant, and is a good adsorbent for heavy metals including chromium. Because of the free amino groups exposed during deacetylation, chitosan presents a high metal-chelating ability (more than five times greater than chitin (Yang and Zall 1984)). In addition, the high hydrophilicity of chitosan makes this material suitable for heavy metal adsorption (Owlad et al. 2009).

28

CNTs are a relatively new form of carbon materials discovered by Iijima (Iijima 1991). Owing to their outstanding properties, CNTs have been widely applied in various fields such as the fabrication of superconductors, optical devices, sensors, energy storage devices, fuel cells, and catalysts (Balasubramanian and Burghard 2005). With regard to water treatment applications, CNTs have also been used as carbonaceous adsorbents for the removal of heavy metals (Dennington et al. 2003), natural organic matter (NOM) (Hyung and Kim 2008), pharmaceuticals and personal care products (Ji, Liu, et al. 2010), and endocrine disrupting chemicals (Joseph et al. 2011; Kiran Kumar and Venkata Mohan 2012). CNTs can be manufactured in the form of single-walled carbon nanotubes (SWNTs) or multi-walled carbon nanotubes (MWNTs), distinguished by their number of graphite layers. The nano size of CNTs provides a high surface area, thereby leading to higher adsorption capacities and unique electrical properties. These characteristics have allowed CNTs to become attractive as adsorbents (Dennington et al. 2003).

Although each adsorbent has specific characteristics and different degrees of interaction with chromium, some studies have compared the abilities of carbonaceous adsorbents and biosorbents for Cr(VI) removal. However, only a few studies have focused on the removal of trace-level concentrations (µg/L) of Cr(VI) removal by adsorption, even though most potable waters contain Cr(VI) at these levels. Unlike previous studies focusing on Cr(VI) removal at high concentrations, this study considers trace level Cr(VI) adsorption onto four different types of adsorbent (i.e., PAC, chitosan, SWNTs, and MWNTs). The primary objective of the study was to compare the characteristics of these adsorbents and their removal mechanisms by means of Cr(VI) adsorption experiments.

The influence of various water chemistry conditions on the adsorption characteristics of each adsorbent was also studied by performing kinetic and isotherm experiments.

## 4.2. Materials and methods

### 4.2.1. Adsorbents and chemicals

The PAC (WPH) used in this study was supplied by Calgon Carbon Corp. (Pittsburgh, PA, USA) and had a mean diameter of 44 µm. The BET surface area and total pore volume (<400 Å) were determined to be 1027 $m^2$/g and 0.55 $cm^3$/g, respectively (Ludlow, Jain, and Adams 2007). High-molecular-weight chitosan flakes with a minimum deacetylation of 75% were obtained from Sigma-Aldrich (St. Louis, MO, USA). SWNTs (purity > 90%) and MWNTs (purity > 99%) were purchased from Cheap Tubes, Inc. (Brattleboro, VT, USA). As indicated by the manufacturer, SWNTs had a diameter of 1–2 nm and a length of 5–30 μm, with a specific surface area of 407 $m^2$/g. MWNTs had a diameter of 13–18 nm and a length of 1–12 μm, with a specific surface area of 233 $m^2$/g (CheapTubes 2012). All the adsorbents were used without further purification. All the chemicals used in this study were ACS certified grade or better and were supplied by Sigma-Aldrich. A 1000 mg/L stock Cr(VI) solution was prepared by dissolving $K_2Cr_2O_7$ in ultrapure water with subsequent mixing over a magnetic stirrer at 200 rpm. This stock solution was diluted to prepare a series of solutions of the required concentrations.

### 4.2.2. Characterization

The surface chemical characteristics of the adsorbents were determined by Fourier transform infrared (FTIR) spectroscopy (Model Spectrum 1000; Perkin Elmer, Waltham, MA, USA). The FTIR spectra were analyzed using the attenuated total reflectance technique. Each spectrum was a result of 32 scans with a resolution of 1.928 $cm^{-1}$. The pH

30

of the point of zero charge (pH$_{pzc}$: the pH above which the total surface of the adsorbent is negatively charged) was estimated for each adsorbent at a concentration of 100 mg/L by zeta potential measurements (Brookhaven ZetaPals, Holtsville, NY, USA). The pH of the testing solutions was adjusted from 3 to 10 by adding 1 M HCl or NaOH solutions. The calculation of the zeta potential was derived from the electrophoretic mobility ($\mu$) values by using the Smoluchowski Eq. (4.1):

$$\mu = \frac{\zeta \, \epsilon \, V}{4\pi\eta d} \cdot\cdot \,\cdots\cdots\cdots\cdots\cdots\cdots\cdots\cdots\cdots\cdots (4.1)$$

where $\zeta$ is the zeta potential, $\epsilon$ is the dielectric constant of the medium (water), $V$ is the applied voltage, $\eta$ is the viscosity of the suspension, and $d$ is the electrode separation (Saleh, Pfefferle, and Elimelech 2008).

### 4.2.3. Batch adsorption experiments

A stock suspension of 2000 mg/L of each adsorbent in ultrapure water was pre-equilibrated by mixing over a magnetic stirrer at pH 4. The effect of pH was investigated by varying this parameter from 4 to 9, while the dosages of adsorbent and initial Cr(VI) concentration were fixed at 100 mg/L and 500 μg/L, respectively. Adsorption kinetics and dose effect experiments were conducted simultaneously as follows: 1000 mL of a 500 μg/L Cr(VI) solution was placed in a beaker along with varying amounts (10–200 mg/L) of each adsorbent at pH 4. Fixed contact times (e.g., 0, 5, 15, 30, 45, 60, 90, 120, 180, and 240 min) were used for dose effect studies, while additional contact times were employed for kinetic measurements. Adsorption isotherm experiments were undertaken using the batch technique with 11 different initial concentrations (range: 250–50000 mg/L) of Cr(VI) with 100 mg/L of adsorbent. The samples were stirred at pH 4 for a time

31

sufficient to achieve pseudo-equilibrium (e.g., 12 h). The influence of competing anions (chloride and sulfate) on the adsorption process was studied by bringing 500 µg/L of Cr(VI) and either 0.1 M of NaCl or 0.1 M of $Na_2SO_4$ solutions into contact with 100 mg/L of each adsorbent at pH 4. To study the effect of mono- and divalent anions separately on the adsorption of hydrogen chromate ions, single- and multi-competition studies were conducted under the same conditions. As in the previous experiments, all the samples were agitated at 200 rpm for 12 h, for a total volume of solution of 500 mL. Aliquots were collected from the solutions and through a 0.45-µm Durapore membrane filter (Millipore, Ireland) before determining the total chromium (inductively coupled plasma mass spectrometry, ICP-MS) and hexavalent chromium (UV-visible spectroscopy at 540 nm; model 8453; Agilent, Santa Clara, CA, USA) concentrations with the 1,5-diphenylcarbazide method (Oleszczuk, Pan, and Xing 2009).

### 4.3. Results and discussion

### 4.3.1. FTIR

FTIR analyses of raw adsorbents (PAC, chitosan, SWNTs, and MWNTs) were performed to determine the surface functional groups (Figure 4.1). The overlapping bands resulting from two symmetrical peaks in the range of 3300–3500 $cm^{-1}$ were attributable to –OH and –NH stretching vibrations (Gupta, Agarwal, and Saleh 2011; Zhu and Pignatello 2005). The absorbance of this band followed the trend PAC > chitosan > SWNTs > MWNTs, which matched the Cr(VI) removal efficiency of these materials. Therefore, the amount of –OH and –NH surface groups seems to be an important factor controlling Cr(VI) adsorption on these materials. In addition, the presence of bands attributed to the –CH stretching vibration in –CH and $–CH_2$, the –NH bending vibration in $–NH_2$, and the –CO

32

stretching vibration in COH at 2924, 1635, and 1065 cm$^{-1}$, respectively, have previously been reported to significantly favor Cr(VI) adsorption (Pramod Kumar Heged 2010; Gurgel et al. 2009; Aydin and Aksoy 2009). Furthermore, the presence of carbonyl groups on the surface of the adsorbents, denoted by the band at 1740–1720 cm$^{-1}$, has been reported to favor the adsorption of Cr(VI) via the formation of –COOH by bonding with neighboring –OH groups (Mao et al. 1999). The background FTIR spectra indicated the presence of ambient water (3600 cm$^{-1}$) and carbon dioxide (1600, 2360, and 667 cm$^{-1}$), which have been shown to have a negligible influence on Cr(VI) adsorption (Fernandes, Hechenleitner, and Pineda 2006).
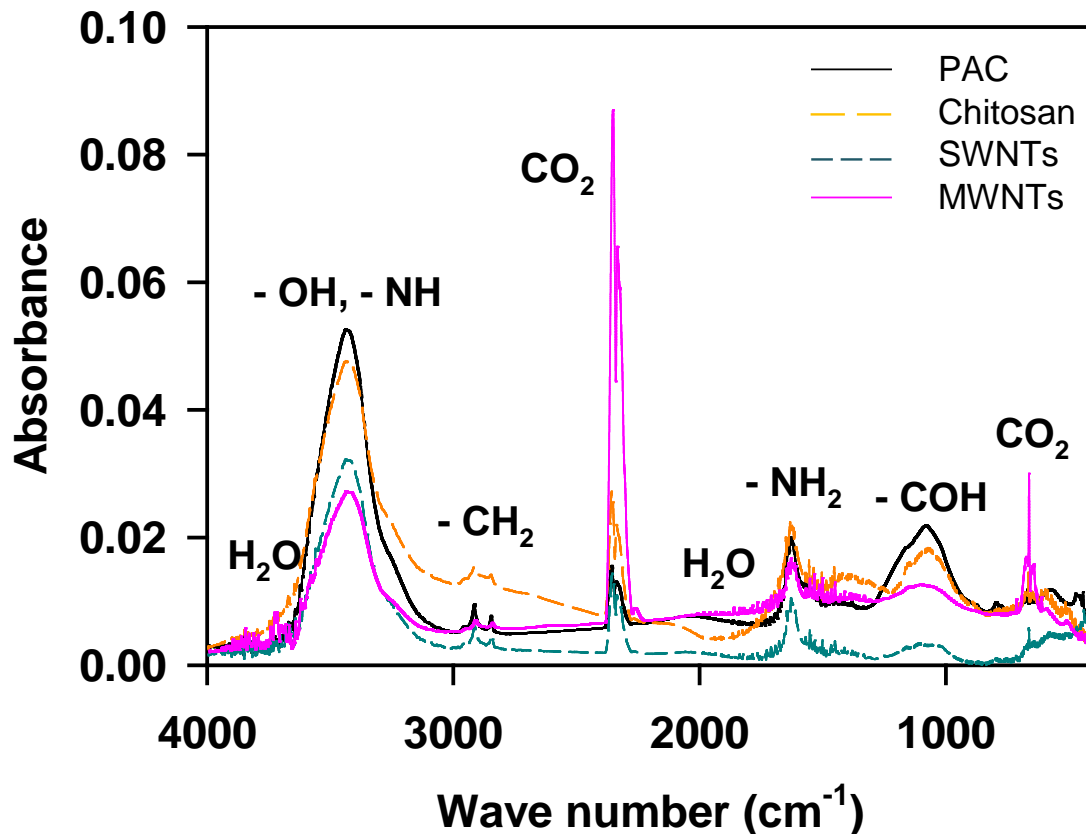


**Figure 4.1** FTIR spectrum adsorbents (PAC, chitosan, SWNTs, and MWNTs).

## 4.3.2. pH$_{pzc}$ and pH effect

pH$_{pzc}$ (i.e., the pH at which the electrical charge density on the surface of an adsorbent is zero) is a significant parameter for explaining the efficiency of the adsorption process in terms of ion attractions from oppositely charged surfaces. At pH < pH$_{pzc}$, the adsorbent surface is positively charged, thereby attracting anions and repelling cations or other positively charged adsorbent particles. For Cr(VI), hydrogen chromate (HCrO$_4^-$) and dichromate (Cr$_2$O$_7^{2-}$) are the predominant ions under acidic solutions, depending on the Cr(VI) concentration, whereas chromate (CrO$_4^{2-}$) prevails under alkaline conditions, depending on the oxidation states and concentrations with respect to different pH (Stumm and Morgan 1970). Therefore, pH determines the capability of a material to adsorb Cr(VI) at low concentrations of Cr(VI). As shown in Figure 4.2(a), pH$_{pzc}$ was 8.9, 9.4, 5.3, and 4.9 for PAC, chitosan, SWNTs, and MWNTs, respectively. The positively charged adsorbents at low pH adsorbed HCrO$_4^-$ and their adsorption capacities were related to the degree of charge. Because –OH, –NH, and –COOH are protonated at pH 4, a high concentration of these functional groups leads to a positively charged surface (Figure 4.3). Therefore, the higher pH$_{pzc}$ of chitosan, PAC, and SWNTs indicates that these materials are more efficient adsorbents for Cr(VI) compared to MWNTs.
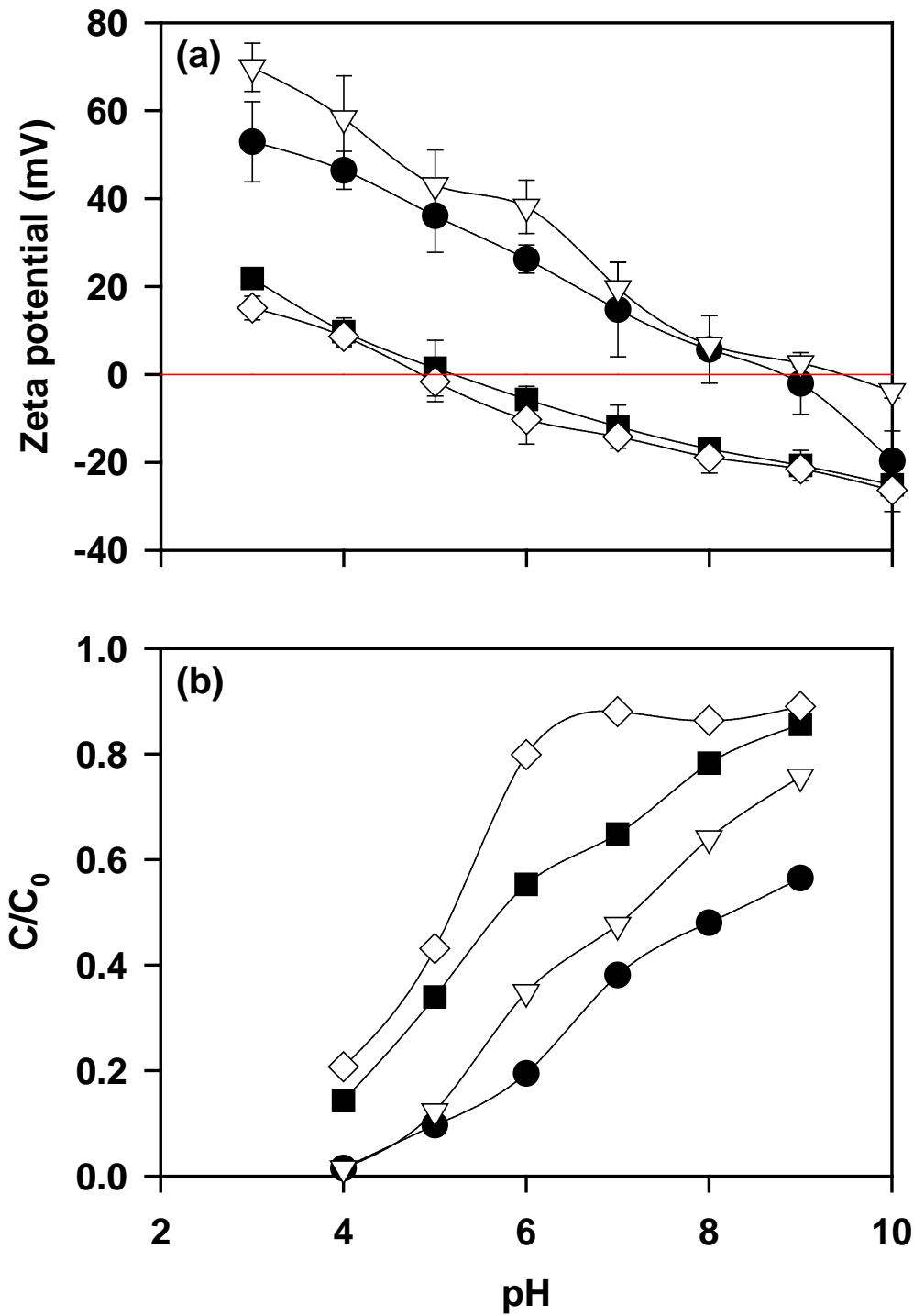
**Figure 4.2** Zeta potential curves (a) as a function of pH and (b) pH effect on removal ($C_0$ = 500 µg/L) for each type of adsorbent (dose of adsorbent = 100 mg/L; contact time = 12 h). Legend: PAC (●); chitosan (▽); SWNT (■); MWNT (◇).
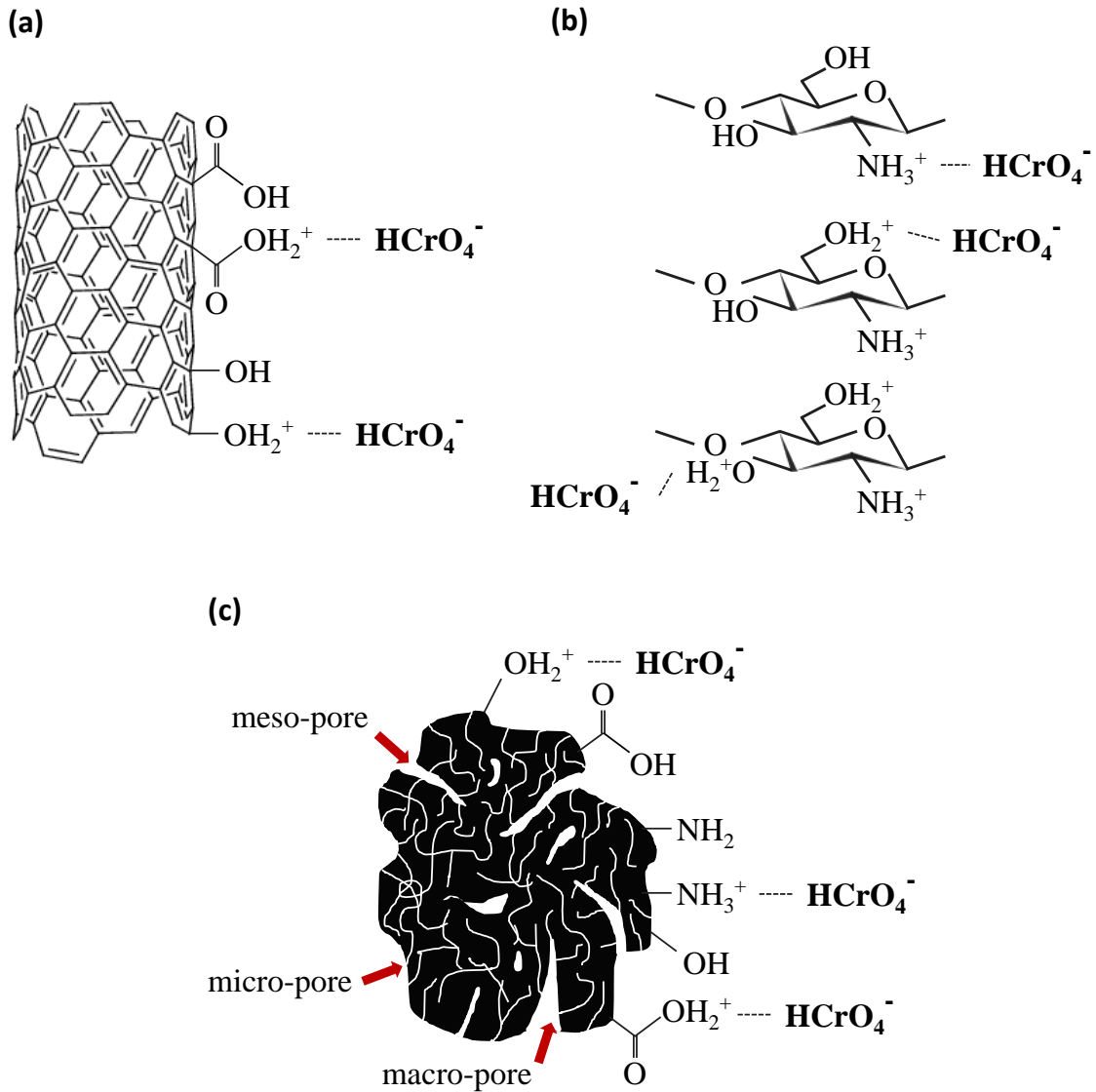
**Figure 4.3** Schematic diagram of Cr(VI) adsorption onto (a) CNTs, (b) chitosan, and (c) PAC.

Thermodynamically, pH determines the stability of Cr(VI) in solution (Cimino, Passerini, and Toscano 2000) and is a prominent parameter affecting the adsorption process. Because the stability and formation of different Cr(VI) species are important, the effect of pH (4–9, practical range in water) on the adsorption of Cr(VI) onto each adsorbent was considered in this study. Figure 4.2(b) shows that Cr(VI) adsorption was more

effective at lower pH values. PAC and chitosan were the most efficient adsorbents under these conditions, whereas SWNTs and MWNTs were not able to effectively remove Cr(VI) from solution. Remarkably, an increase in pH led to less Cr(VI) adsorption in all cases. Although $HCrO_4^-$ is the predominant species under conditions of low pH and trace concentrations of Cr(VI), we considered that both $HCrO_4^-$ and $CrO_4^{2-}$ were the primary species when evaluating the effect of pH at equilibrium for 500 μg/L of Cr(VI) (W. Stumm 1982) to cover the main reactions at all pH ranges. These two species and the protonated functional groups on the surface of the adsorbents electrostatically attract each other at pH 4 on all adsorbents, and this specific pH was therefore adopted for use in further studies. At higher pH values, Cr(VI) adsorption is negatively influenced by both the shift from $HCrO_4^-$ to $CrO_4^{2-}$ and the deprotonation of the adsorbent surface, resulting in the adsorption of $CrO_4^{2-}$ being limited by the presence of competing $OH^-$ ions and by a less-positive surface. This is in agreement with previous studies on the adsorption of other heavy metal anions (Aydin and Aksoy 2009; Kyzas, Kostoglou, and Lazaridis 2009). Adsorption on the MWNTs was relatively less sensitive to an increase in pH at values higher than 6. This indicates that the lower number of deprotonated functional groups on the MWNTs reduced the positive surface charge earlier than the other adsorbents, and that Cr(VI) adsorption slowed down at a lower $pH_{pzc}$. In contrast, the other three adsorbents displayed similar adsorption behaviors with pH changes because of their higher $pH_{pzc}$.

### 4.3.3. Contact time and initial concentration effects

To design efficient and economical water treatment technologies, it is important to determine the time required to reach equilibrium during Cr(VI) adsorption. The influence of contact time on the adsorption capacity of PAC, chitosan, SWNTs, and MWNTs (dose

of 100 mg/L at pH 4) at an initial Cr(VI) concentration of 500 μg/L and room temperature $(20 \pm 1^{o}C)$ was determined. The removal of Cr(VI) increased with contact time, while the rate of adsorption was found to decrease with this parameter to a varying extent, depending on the properties of each adsorbent (Figure 4.4a). Of the adsorbents tested, PAC had the highest Cr(VI) removal efficiency at the various contact times used; the trend continued as chitosan > SWNTs > MWNTs. These results differ from previous studies indicating that AC is a poor adsorbent for the removal of certain contaminants compared to MWNTs. AC is reported to be a poor adsorber of hydrophilic substances. However, the PAC used in this study had a higher affinity for Cr(VI) species compared to the MWNTs (Gupta, Agarwal, and Saleh 2011; Pillay, Cukrowska, and Coville 2009; Kandah and Meunier 2007), which led to better adsorption capacities. This can be explained by the presence of additional adsorbing sites (e.g., functional groups) on the surface of the PAC material and a higher surface area than the other adsorbents used in this study. The adsorption of Cr(VI) on different adsorbents as a function of Cr(VI) initial concentration (dose of 100 mg/L at pH 4) was investigated for different initial concentrations. As shown in Figure 4.4b, the adsorption capacity increased as the initial Cr(VI) concentration increased (250–5000 μg/L). An increase in initial Cr(VI) concentration boosted the uptake capacity proportionally, except for the SWNTs and MWNTs, which displayed a slight decrease in adsorption capacity when the Cr(VI) concentration was higher than 1000 μg/L. Normally, a higher initial concentration leads to a higher number of collisions between the Cr(VI) species and the adsorbent (especially for CNTs), generating a driving force that is able to overcome all mass transfer resistances between the aqueous and solid phases (Anupam et al. 2011). However, unlike unsaturated PAC and chitosan, Cr(VI) adsorption onto the
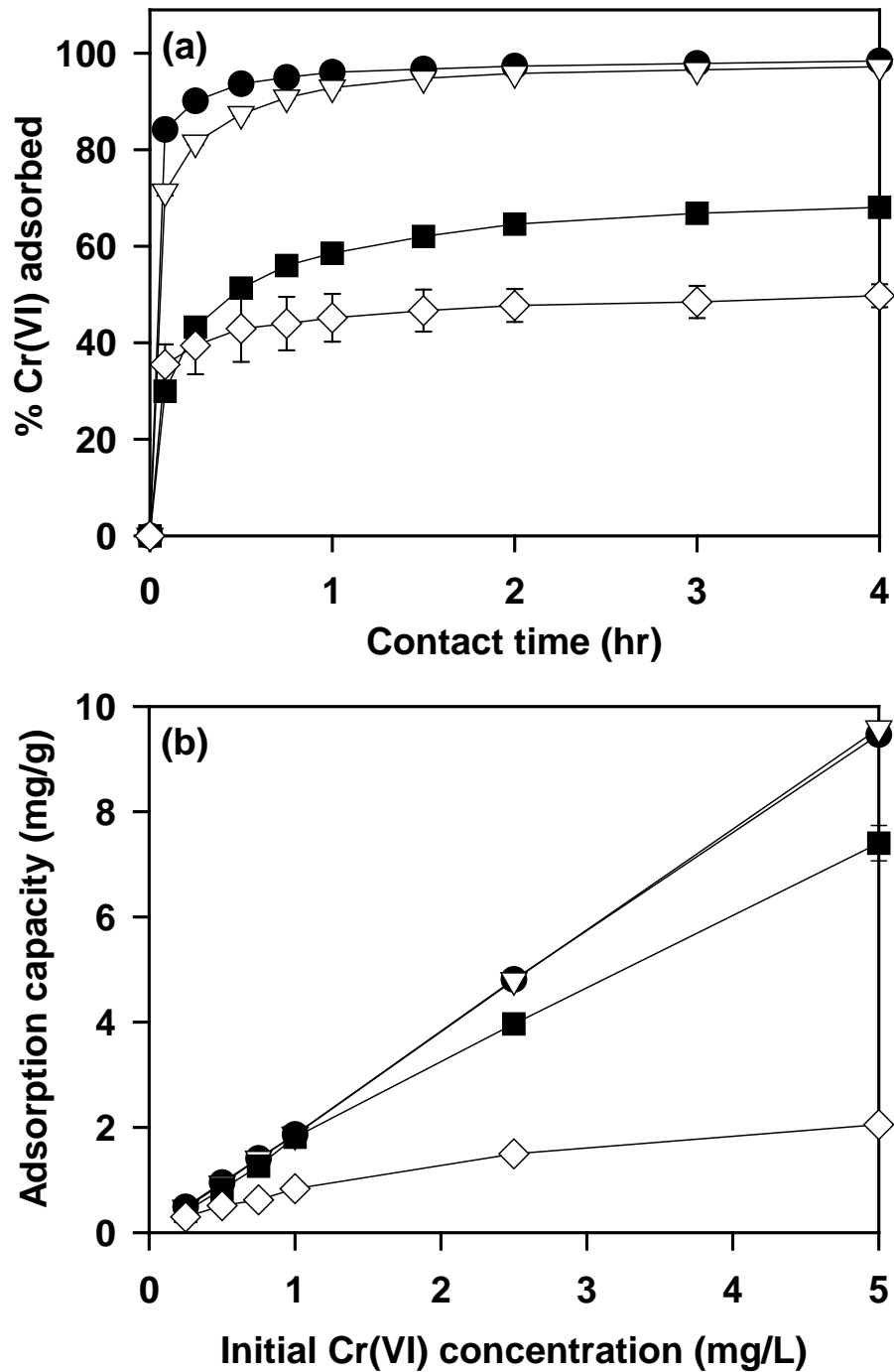
**Figure 4.4** Effect of contact time on (a) the amount of Cr(VI) ($C_0 = 500$ µg/L; dosage of adsorbent = 100 mg/L; pH = 4) and (b) initial Cr(VI) concentration on adsorption capacity on the adsorbents (dose of adsorbent = 100 µg/L; pH = 4). Legend: PAC (●);chitosan (▽); SWNT (■); MWNT (◇).

CNTs was restricted by saturation for concentrations of Cr(VI) over 1000 μg/L. Under these circumstances, adsorption sites are depleted by stagnation as concentration increases due to the presence of very small pores on the surface of the material (Figure 4.3) (Chun et al. 2004; Lee et al. 2005; Greenwood and Earnshaw 1998).

### 4.3.4. Dosage effect

The amount of adsorbent in solution is an important parameter as it determines the capacity of each adsorbent to remove a fixed initial concentration of Cr(VI). Varying amounts of adsorbent (range: 10–200 mg/L) were used for batch adsorption experiments with an agitation speed of 200 rpm and pH 4 for 4 h. As shown in Figure 4.5, the Cr(VI) adsorption capacity increased with increasing dosage (10–200 mg/L) to a different extent depending on the adsorbent (i.e., 65.7–99.6%, 70.0–96.4%, 11.1–88.8%, and 4.2–69.4% for PAC, chitosan, SWNTs, and MWNTs, respectively). This result indicates that the number of adsorption sites for Cr(VI) was proportional to the dose applied for each adsorbent. However, no further increase in adsorption capacity was found for PAC and chitosan at doses higher than 100 mg/L, which suggests that most molecules of Cr(VI) occupied surface sites (Muataz Ali Atieh 2010). Unlike PAC and chitosan, doses higher than 100 mg/L were required for SWNTs and MWNTs to achieve an adsorption capacity of 95%. This dose-dependent Cr(VI) adsorption behavior allowed the optimum and most economical dose for water treatment to be determined (e.g., 100 μg/L), and this value was subsequently used for the remainder of the study.
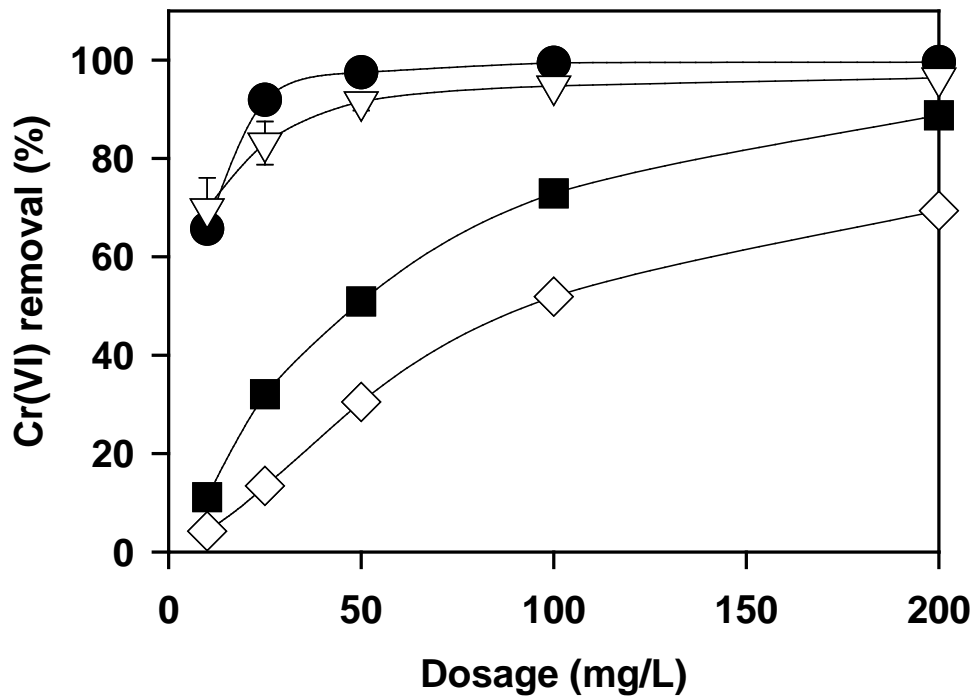
**Figure 4.5** Effect of dose on the amount of Cr(VI) adsorbed on each adsorbent ($C_0 = $ 500 µg/L; dose = 10–200 mg/L; pH = 4). Legend: PAC (●); chitosan (▽); SWNT (■); MWNT (◇).

### 4.3.5. Equilibrium isotherms

The relationship between adsorbed Cr(VI) and its concentration in solution under equilibrium conditions is described by the widely accepted Langmuir and Freundlich isotherm model. The Langmuir isotherm is valid for monolayer adsorption on an energetically homogeneous surface with a limited number of identical sites (Pandey and Mishra 2011). Both nonlinear and linear forms of the Langmuir isotherm can be expressed as Eqs. (4.2) and (4.3), respectively:

$$q_e = \frac{q_m b C_e}{1 + b C_e} \cdots\cdots\cdots\cdots\cdots\cdots\cdots\cdots\cdots\cdots\cdots\cdots (4.2)$$

41

$$\frac{1}{q_e} = \frac{1}{q_m} + \frac{1}{bq_mC_e} \dots\dots\dots\dots\dots\dots\dots\dots\dots\dots\dots\dots(4.3)$$

where $q_e$ is the equilibrium adsorption capacity (mg/g), $C_e$ is the equilibrium Cr(VI) concentration in solution (mg/L), and the Langmuir constants $q_m$ and $b$ represent the maximum adsorption capacity (mg/g) and the energy of adsorption (L/mg), respectively. The intercept and slope of the plot in Figure 4.6(a) provide reciprocal values of $q_m$ and $b$, respectively. A dimensionless separation factor ($R_L$) was evaluated for favorable adsorption conditions by Eq. (4.4):

$$R_L = \frac{1}{(1+bC_0)} \dots\dots\dots\dots\dots\dots\dots\dots\dots\dots\dots\dots(4.4)$$

where $b$ is the Langmuir constant (L/mg) and $C_0$ is the initial Cr(VI) concentration (mg/L). A separation factor $R_L > 1$ implies unfavorable adsorption, while values ranging from 0 to 1 are indicative of a favorable adsorption process (Aydin and Aksoy 2009; Rojas et al. 2005). In this study, all the $R_L$ values calculated for an initial concentration of 500 μg/L were within the range 0.599–0.8294 (Table 4.1), which indicates favorable Cr(VI) adsorption on all adsorbents tested.

Unlike Langmuir, the Freundlich isotherm describes multilayer adsorption well on an energetically heterogeneous surface. Both nonlinear and linear forms of the Freundlich isotherm can be expressed as Eqs. (4.5) and (4.6):

$$q_e = K_F C_e^{1/n} \dots\dots\dots\dots\dots\dots\dots\dots\dots\dots\dots\dots(4.5)$$

$$\ln q_e = \ln K_F + \frac{1}{n} \ln C_e \dots\dots\dots\dots\dots\dots\dots\dots\dots\dots(4.6)$$

42

where $K_F$ (mg/g) and $n$ provide an indication of the adsorption capacity and the intensity of the adsorbent, respectively. The intercept and slope of the plot in Figure 4.6(b) provided the reciprocal values of $n$ and $K_F$, respectively. In general, higher $K_F$ values are indicative of favorable adsorption processes, while the reciprocal of $n$ has a similar meaning to the $R_L$ value of the Langmuir isotherm parameter in terms of affinity to adsorption ($n > 1$) (Halling-Sørensen et al. 1998; Schoenborn 1969).

**Table 4.1** Isotherm constants for Cr(VI) adsorption on adsorbents.

| Initial Conc. (μg/L) | Adsorbent | *Langmuir* | | | | *Freundlich* | | |
|---|---|---|---|---|---|---|---|---|
| | | $q_m$ (mg/g) | $b$ (L/mg) | $R_L$ | $R^2$ | $K_F$ (mg/g)/ $(L/mg)^n$ | $n$ | $R_2$ |
| 250 to 50,000 | PAC | 46.9 | 1.022 | 0.662 | 0.998 | 13.3 | 1.583 | 0.971 |
| | Chitosan | 35.6 | 1.149 | 0.635 | 0.999 | 8.25 | 2.050 | 0.906 |
| | SWNTs | 20.3 | 1.831 | 0.522 | 0.997 | 5.90 | 1.285 | 0.999 |
| | MWNTs | 2.48 | 0.838 | 0.705 | 0.956 | 0.98 | 2.212 | 0.980 |
| 250 to 2500 | PAC | 55.6 | 1.212 | 0.623 | 0.997 | 55.4 | 0.946 | 0.986 |
| | Chitosan | 40.8 | 1.337 | 0.599 | 0.999 | 46.4 | 0.959 | 0.990 |
| | SWNTs | 9.18 | 0.798 | 0.715 | 0.998 | 6.74 | 1.198 | 0.996 |
| | MWNTs | 1.42 | 0.411 | 0.829 | 0.970 | 1.11 | 1.738 | 0.992 |
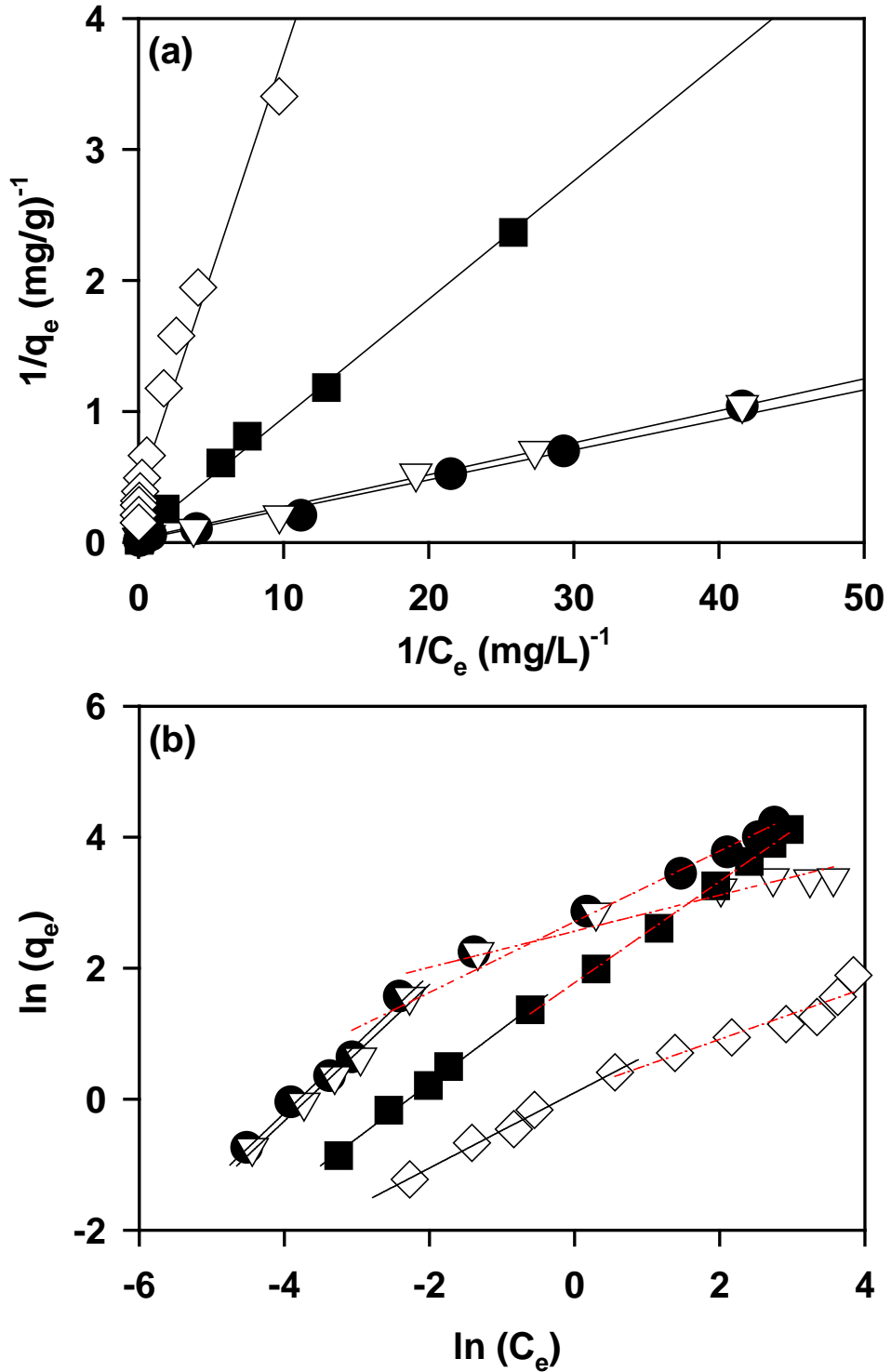
**Figure 4.6** (a) Langmuir and (b) Freundlich plot for adsorption of Cr(VI) on adsorbents
($C_0$ = 250–50,000 μg/L; dose = 100 mg/L; pH = 4). Legend: PAC (●); chitosan (▽);

SWNT (■); MWNT (◇).

The maximum adsorption capacities calculated by the Langmuir model ($q_m$) were 55.6, 40.8, 9.2, and 1.4 mg/g for PAC, chitosan, SWNTs, and MWNTs, respectively (Table 1). These values were similar to those of the $K_F$ calculated with the Freundlich model. However, the values of intensity of each adsorbent are higher than 1 excluding PAC and chitosan in the range of 250-2,500 μg/L, indicating that the non-linear Fruendlich model describes favorable adsorption condition in the order of MWNTs > SWNTs> chitosan > PAC. The energetic surface layer is not well determined with these data. However, the slopes in Figure 6b describe different values between low (250-2,500 μg/L) and high (5,000-50,000 μg/L) concentration ranges. The results suggest that it is difficult to determine the appropriation of Freundlich model in this study over the entire concentration ranges. In overall, the Langmuir model fitted better for initial Cr(VI) concentrations ranging from 250 to 25,000 μg/L, which indicates that monolayer adsorption occurs under these conditions. The equilibrium data for the initial Cr(VI) concentrations (250–50,000 μg/L) fitted well for both isotherms for SWNTs and MWNTs. However, the equilibrium data for PAC and chitosan showed variances, such as different slopes, and the Langmuir model fitted better (i.e., correlation above 0.99 $R^2$) than Freundlich for these materials. Therefore, from the isotherm study, the conclusion can be made that all adsorbents had higher adsorption capacities when the initial Cr(VI) concentrations were below 250 μg/L, and these data were able to describe the adsorption capacity of these adsorbents for μg/L levels of Cr(VI).

### 4.3.6. Kinetic analysis

Adsorption kinetic analysis is important for an understanding of the removal of contaminants as it reveals the transport mechanisms involved in the process. To determine

the kinetic behavior, experiments were conducted at an initial Cr(VI) concentration of 500 µg/L and at different time intervals (maximum 4 h) at a fixed dosage (100 mg/L) and pH 4. The Cr(VI) molecules were found to adsorb very rapidly during the early time intervals due to the presence of a large number of free adsorption sites. Equilibrium was reached within the first 2 h due to the increasing mass transfer driving force (Debnath and Ghosh 2008), as previously revealed by the contact time study (Figure 4.4(a)). To estimate the rate of adsorption and the adsorption capacity for Cr(VI) on adsorbents, various kinetic models were applied. Less applicable fits in the pseudo first-order kinetic model (Figure 4.7(a)) indicated that adsorption capacity alone was not the major factor controlling the adsorption mechanisms of all adsorbents (Álvarez-Ayuso, García-Sánchez, and Querol 2007) as expressed in Eq. (4.7),

$$\log(q_e - q_t) = \log q_e - \frac{k_1}{2.303} t \cdots\cdots\cdots\cdots\cdots\cdots\cdots(4.7)$$

where $q_e$ and $q_t$ represent the adsorption capacity (mg/g) at equilibrium and at time $t$, respectively, and $k_1$ is the adsorption rate constant.

The experimental data fitted well (see $R^2$ values in Table 4.2) with linearized forms of the pseudo second-order equation [Eq. (4.8)] for all the adsorbents (Figure 4.7(b)):

$$\frac{t}{q_t} = \frac{1}{k_2 q_e^2} + \frac{1}{q_e} t \cdots\cdots\cdots\cdots\cdots\cdots\cdots\cdots\cdots(4.8)$$

$$V_0 = k_2 q_e^2 \cdots\cdots\cdots\cdots\cdots\cdots\cdots\cdots\cdots (4.9)$$

where $V_0$ and $k_2$ refer to the initial adsorption rate (g/mg/h) and the pseudo second-order rate constant (g/mg/h), respectively (Hui Qiu 2009). $V_0$ was calculated by using Eq. (4.9) to be 187.2, 92.7, 20.2, and 27.4 g/mg/h for PAC, chitosan, SWNTs, and MWNTs,

46
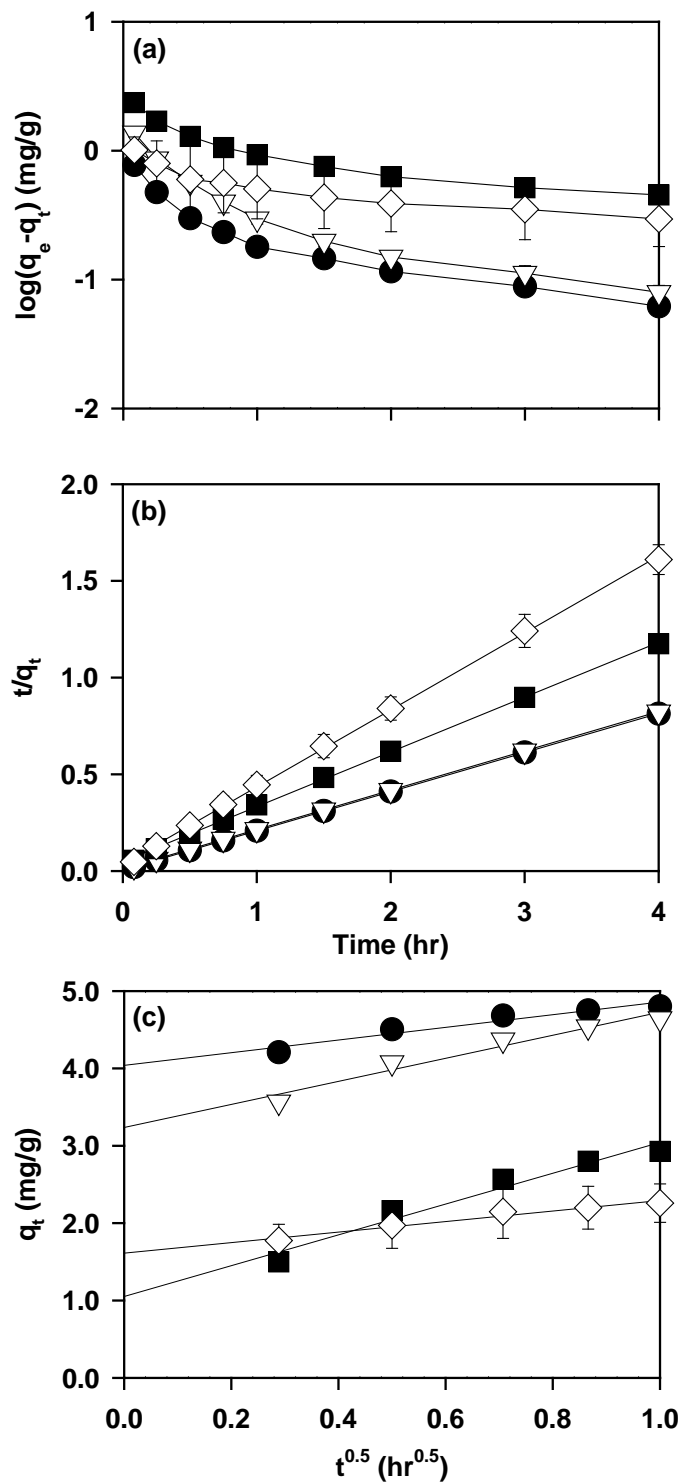
**Figure 4.7** Plot for (a) first-order kinetics, (b) second-order kinetics, and (c) the intra-particle diffusion model ($C_0 = 500$ µg/L; dose = 100 mg/L; time = 4 h; pH = 4).

Legend: PAC (●); chitosan (▽); SWNT (■); MWNT (◇).

respectively. This result indicates that PAC allows Cr(VI) to adsorb faster at equilibrium conditions, while adsorption on SWNTs (and not MWNTs) displayed the lowest rate. The good fit of this model indicates that the adsorption driving force, determined by ($q_e$ - $q_t$), was proportional to the number of free adsorption sites for Cr(VI) (Álvarez-Ayuso, García-Sánchez, and Querol 2007), while the adsorption kinetics were controlled by chemisorption (Pandey and Mishra 2011). Therefore, apart from the adsorption capacity, the kinetic rate is an important parameter determining the transport of Cr(VI) in the solution.

**Table 4.2** Kinetic parameters for Lagergren and intra-particle diffusion models.

| Adsorbent | Pseudo first-order | | | Pseudo second-order | | | Intra-particle diffusion | |
|---|---|---|---|---|---|---|---|---|
| | $k_1$ ($h^{-1}$) | $q_e$ (mg/g) | $R^2$ | $k_2$ (g/mg/h) | $q_e$ (mg/g) | $R^2$ | $K$ (mg/g/$h^{0.5}$) | $R^2$ |
| PAC | 0.560 | 0.442 | 0.848 | 7.661 | 4.943 | 1.000 | 0.819 | 0.935 |
| Chitosan | 0.677 | 0.802 | 0.869 | 3.834 | 4.917 | 0.999 | 1.490 | 0.957 |
| SWNTs | 0.380 | 1.630 | 0.846 | 1.618 | 3.531 | 0.999 | 1.992 | 0.959 |
| MWNTs | 0.271 | 0.757 | 0.832 | 4.348 | 2.512 | 0.999 | 0.681 | 0.963 |

The applicability of an intra-particle diffusion model, in which adsorption is proportional to $t^{1/2}$ rather than $t$ (Alkan, Demirbaş, and Doğan 2007), was investigated using Eq. (4.10) (Figure 4.7(c)):

$$q_t = Kt^{0.5} \cdots\cdots\cdots\cdots\cdots\cdots\cdots\cdots\cdots\cdots (4.10)$$

where $K$ is the intra-particle diffusion constant (mg/g/$h^{0.5}$). The probability of diffusion was calculated from the slope of the linear region for a contact time of 1 h, and values are summarized in Table 2. Unlike the driving force mechanism, the intra-particle diffusion

model did not explain the Cr(VI) adsorption mechanism, except for SWNTs. Unlike the other adsorbents, the adsorption of Cr(VI) onto SWNTs was attributed to intra-particle diffusion in the first hour (Figure 4.7(c)), followed by a gradual adsorption stage of Cr(VI) onto the SWNT material (Figure 4.4(a)). For the other adsorbents, it was difficult to observe not only the diffusion of Cr(VI) through the solution to the their surface, but also the boundary layer diffusion of Cr(VI) molecules. This difference suggests that the micropore-covered surface of SWNTs enabled the intra-diffusion of Cr(VI) molecules.

### 4.3.7. Anion effect

The Cr(VI) removal mechanism mainly involves ionic attraction between $HCrO_4^-$, $Cr_2O_7^{2-}$, or $CrO_4^{2-}$ species and positively charged adsorbents. Therefore, it is obvious that the coexistence of background anions in solution would inevitably compete with Cr(VI) anionic species at low pH values. To investigate the effect of competing anions, $Cl^-$ and $SO_4^{2-}$ ions were spiked in a 500 µg/L Cr(VI) solution (dose of 100 mg/L at pH 4). As with previous studies (Álvarez-Ayuso, García-Sánchez, and Querol 2007; Pillay, Cukrowska, and Coville 2009; Lv et al. 2011), 0.1 M of $Cl^-$ was found to interfere to a lesser extent on the adsorption process than 0.1 M of $SO_4^{2-}$ at similar concentrations (Figure 4.8). When compared to control experiments, $Cl^-$ and $SO_4^{2-}$ were found to reduce the Cr(VI) removal efficiency by more than 40% and 50%, respectively. When added simultaneously, these anions displayed very similar behavior regarding inhibition compared to their individual effects, indicating that $SO_4^{2-}$ preferentially occupies adsorption sites at the expense of Cr(VI) and $Cl^-$. In a similar study on competing anions, an ion-exchange mechanism was determined for metal adsorption on chitosan in the presence of oxyanions or anionic chloro complexes (Gupta, Agarwal, and Saleh 2011). This indicates that an interaction between

49

protonated functional groups in the adsorbents and Cr(VI) species occurs, and that this interaction is primarily based on electrostatic attraction. This electrostatic attraction, confirmed by infrared or ultraviolet spectral studies, allowed the identification of protonated carboxylic, alcohol, and hydroxyl groups as the main sorption sites in PAC, SWNTs, and MWNTs, while amine functional groups were prevalent in chitosan (Boddu et al. 2003; Dong, Ma, and Li 2011; Liu et al. 2011; Hu et al. 2009).
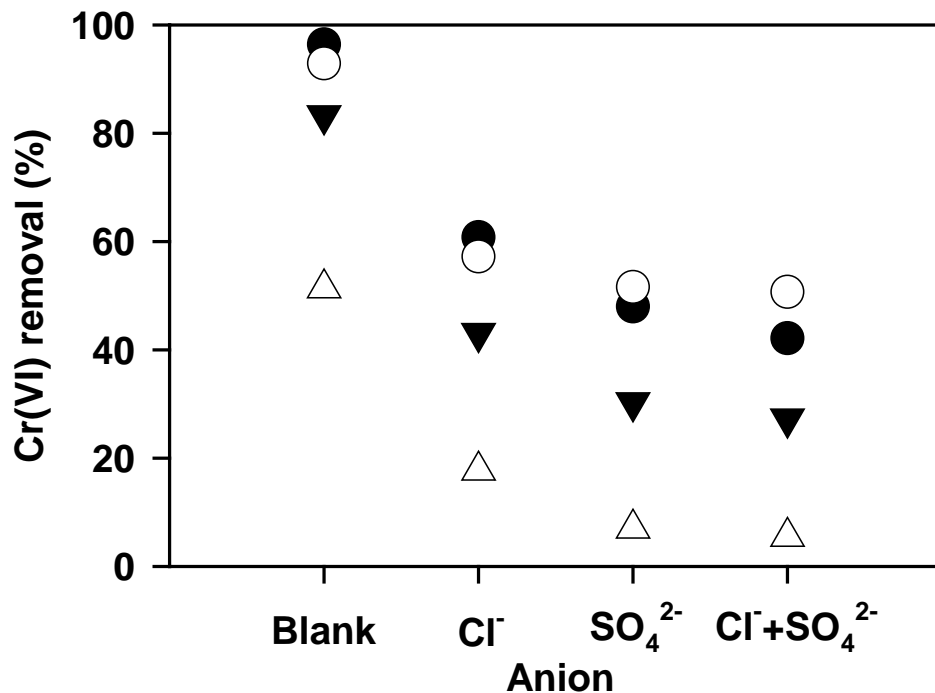


**Figure 4.8** Effect of anions on the adsorption of Cr(VI) on adsorbents ($C_0 = 500$ μg/L; dose = 100 mg/L; pH = 4; $Cl^- = 10$ mM, $SO_4^{2-} = 10$ mM). Legend: PAC (●); chitosan (○); SWNT (▼); MWNT (△).

**4.3.8. Adsorption mechanisms**

Most Cr(VI) was adsorbed by electrostatic attraction between $HCrO_4^-$ and positive charged adsorbents [Eqs. (4.11)–(4.13) and Figure 4.3]. Even though this is the main

mechanism considered in this study, additional Cr(VI) removal mechanisms were also determined.

$$Adsorbent - OH_2{}^+ + HCrO_4{}^- \leftrightarrow Adsorbent - OH_2CrO_4{}^- + H^+ \cdots\cdots\cdots (4.11)$$

$$Adsorbent - NH_2{}^+ + HCrO_4{}^- \leftrightarrow Adsorbent - NH_2CrO_4{}^- + H^+ \cdots\cdots\cdots (4.12)$$

$$Adsorbent - COOH_2{}^+ + HCrO_4{}^- \leftrightarrow Adsorbent - COOH_2CrO_4{}^- + H^+ \cdots\cdots (4.13)$$
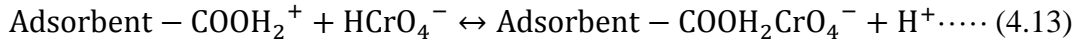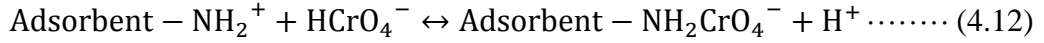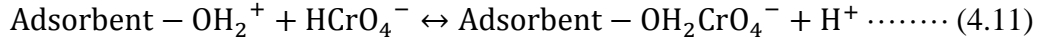
A physicochemical interaction occurred between Cr(VI) and adsorbents in acidic solution, and this contact was enabled by the strong oxidizing property and instability of Cr(VI) due to the presence of electron donors, such as the various carboxylic and hydroxyl functional groups in each adsorbent (determined by FTIR analysis). In acidic solution, the redox potential ($E^0$) of Cr(VI) is highly positive (range: 1.33–1.38 V) (Kotaś and Stasicka 2000) and the $HCrO_4{}^-$, which dominates under low concentrations of Cr(VI), was readily reduced to Cr(III) species in Eq. (4.14) (Durban and Brown 1939):

$$HCrO_4{}^- + 7H^+ + 3e^- \leftrightarrow Cr^{3+} + 4H_2O \qquad (E^0 = 1.20\,V)\cdots\cdots\cdots (4.14)$$
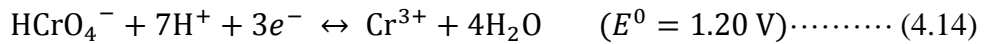
This reaction readily moves forward when enough protons and electrons are available due to high values of $E^0$ (log K = 62 at 20°C). At pH 4, with adsorbents containing acidic functional groups, this mechanism appeared to operate, but functional groups in the adsorbents did not perform well as electron donors for $HCrO_4{}^-$ reduction. This reaction was more applicable to CNTs than PAC and chitosan. Approximately 9–11% of the residual Cr was determined to be Cr(III), when residual Cr(VI) was subtracted from total Cr for SWNTs and MWNTs, while for PAC and chitosan, the values were only 1.5–4.0% and 2.1–2.8%, respectively. In addition, the final pH when CNTs were used was

51

slightly higher than for PAC and chitosan. These results indicate that functional groups in the CNTs provided more electrons, and a larger amount of protons ($H^+$), to reduce $HCrO_4^-$ to $Cr^{3+}$ than PAC and chitosan provided in acidic solution. This reaction was limited to the electron donor site on each adsorbent.

Cr(III) can form complexes such as $Cr(OH)^{2+}$ and $Cr(H_2O)_6^{3+}$ in acidic solution (Babel and Kurniawan 2004; Liu et al. 2011), although how much Cr(III) was oxidized remained unclear. Electrostatic attraction between these cations and acidic functional groups on the adsorbents was hypothesized, while competition for adsorption sites existed among cations, including $H^+$.

## 4.4. Conclusions

PAC, chitosan, SWNTs, and MWNTs were evaluated as adsorbents for Cr(VI) removal. A positively charged surface under acidic conditions (pH 4) attracted the predominant Cr(VI) species (i.e., $HCrO_4^-$). Isotherm data fitted well for both Langmuir and Freundlich models at the lower initial Cr(VI) concentrations (e.g., <2500 μg/L), although the Langmuir isotherm was determined to be the most suitable model over the entire range (250–50000 μg/L), indicating that a monolayer adsorption dominated for all adsorbents tested. Surface area, pore size, and surface functional groups had major roles in this reaction. Ion exchange and complexation were involved in the Cr(VI) adsorption process, although the most plausible Cr(VI) adsorption mechanism was electrostatic attraction. Protonated functional groups on the carbonaceous adsorbents and amine groups in chitosan were responsible for Cr(VI) electrostatic attraction. Owing to the large number of free adsorption sites (e.g., functional groups), PAC was the most efficient adsorbent followed by chitosan with a slightly lower capacity. Furthermore, the adsorption behavior of

52

chitosan for heavy metal removal is widely known to be attributable to its high hydrophilicity, with hydroxyl and primary amino groups allowing a high activity and a flexible structure of the polymer chains having suitable configurations for the adsorption of metal ions. Therefore, chitosan has the potential to be a prominent adsorbent for Cr(VI) removal. Also, chitosan has potential as a biosorbent, and therefore less post treatment is required compared to other adsorbents. SWNTs showed better adsorption capacities than MWNTs, but stagnation, derived from the small size of the pores and the lower number of functional groups per unit area and volume (compared to PAC and chitosan), made this material an inefficient adsorbent for Cr(VI) removal. A pseudo second-order kinetic model, determined by adsorption capacity and kinetic rate, fitted well for all the adsorbents, indicating that chemisorption dominated the adsorption process. An intra-particle diffusion model produced acceptable fittings at low concentrations ($<250$ μg/L), suggesting that diffusion also partially contributed to the rate of Cr(VI) adsorption, especially in the case of SWNTs. Based on this intensive study at μg/L levels for four different types of adsorbents, PAC may be considered to be an efficient material for Cr(VI) removal from ambient wastewater, although more specific comparison studies are required to definitively identify the best adsorbent for Cr(VI) removal.

**Acknowledgements**

# CHAPTER 5

## ADSORPTION OF SELECTED ENDOCRINE DISRUPTING COMPOUNDS AND PHARMACEUTICALS ON ACTIVATED BIOCHARS[2]

**Abstract**

Chemically activated biochar produced under oxygenated (O-biochar) and oxygen-free (N-biochar) conditions were characterized and the adsorption of endocrine disrupting compounds (EDCs); bisphenol A (BPA), atrazine (ATR), 17 α-ethinylestradiol (EE2), and pharmaceutical active compounds (PhACs); sulfamethoxazole (SMX), carbamazepine (CBM), diclofenac (DCF), ibuprofen (IBP) on both biochars and commercialized powdered activated carbon (PAC) were investigated. Characteristic analysis of adsorbents by solid-state nuclear magnetic resonance (NMR) was conducted to determine better understanding about the EDCs/PhACs adsorption. N-biochar consisted of higher polarity moieties with more alkyl (0-45 ppm), methoxyl (45-63 ppm), O-alkyl (63-108 ppm), and carboxyl carbon (165-187 ppm) content than other adsorbents, while aromaticity of O-biochar was higher than that of N-biochar. O-biochar was composed mostly of aromatic moieties, with low H/C and O/C ratios compared to the highly polarized

N-biochar that contained diverse polar functional groups. The higher surface area and pore volume of N-biochar resulted in higher adsorption capacity toward EDCs/PhACs along with atomic-level molecular structural property than O-biochar and PAC. N-biochar had a highest adsorption capacity of all chemicals, suggesting that N-biochar derived from loblolly pine chip is a promising sorbent for agricultural and environmental applications. The adsorption of pH-sensitive dissociable SMX, DCF, IBP, and BPA varied and the order of adsorption capacity was correlated with the hydrophobicity ($K_{ow}$) of adsorbates throughout the all adsorbents, whereas adsorption of non-ionizable CBM, ATR, and EE2 in varied pH allowed adsorbents to interact with hydrophobic property of adsorbates steadily throughout the study.

*Keywords*: Endocrine disrupting compounds; Pharmaceuticals; Biochar; Nuclear magnetic resonance; Adsorption mechanism

### 5.1. Introduction

Endocrine-disrupting compounds (EDCs) and pharmaceutically active compounds (PhACs) are trace-level organic contaminants that have been detected in aquatic environments such as surface waters, wastewater, runoff, and landfill leachates (Benotti et al. 2008a; Yoon et al. 2010; Kolpin et al. 2002). The widespread occurrence of these dissolved chemicals in water sources is of concern due to their adverse effects, such as mimicking or antagonizing natural hormones, hindering metabolic processes, occupying hormone receptors, and causing reproductive and development problems when consumed by humans and aquatic species (Rudder et al. 2004; Comerton, Andrews, and Bagley 2009).

55

A variety of EDCs exist, including pesticides, natural hormones, and industrial chemicals. Atrazine (ATR) is one of the most widely used herbicides and its continuous exposure into water causes its concentration to accumulate due to its poor degradability compared to other herbicides (Wackett et al. 2002). Recently, 17α-ethinylestradiol (EE2), an oral contraceptive, has been studied extensively due to its higher toxicity compared to other hormones such as estrone or 17β-estradiol (Segner et al. 2003). Similarly, bisphenol A (BPA), a main monomer in epoxy resin and polycarbonate plastic, has been studied due to the ubiquitous use of plastic in everyday living. In addition, because of the increasing demand for PhACs, the level of exposure has increased, paradoxically causing a threat to health. Certain pharmaceuticals have been studied widely, such as nonsteroidal anti-inflammatory drugs; diclofenac (DCF) and ibuprofen (IBP), as well as antibiotics (sulfamethoxazole; SMX) and antiseizure medicine (carbamazepine; CBM). EDCs/PhACs are metabolized and adsorbed by organisms at low levels, resulting in exposure to the residues of these compounds as their origin molecular forms or their transformed products when they enter the aquatic environment (Halling-Sørensen et al. 1998; Kolpin et al. 2002). Unfortunately, the treatment of EDCs/PhACs in wastewater and drinking water is inefficient (Xie et al. 2012; Ternes, Joss, and Siegrist 2004) and consequently more effective technologies are required to achieve their removal from drinking water.

Adsorption with a high-binding adsorbent has been used to eliminate various contaminants in the aqueous phase (Jung, Heo, et al. 2013). The well-established manufacturing process and relatively low cost of activated carbon has led to it becoming a common adsorbent for water treatment due to its strong interaction with hydrophobic organic contaminants. However, the physical properties of activated carbon, including the

56

irregular and closed pore structure with small micropore sizes (< 2 nm), precludes the adsorption of large molecules, leading to a size-exclusion effect (Kilduff et al. 1996). The improvement of this crucial role of pore size for the adsorption has been studied through physical and chemical activation of adsorbents (Ahmadpour and Do 1996; Ji, Shao, et al. 2010).

With an advance of biorefinery in the near future, it is expected to have biochar available for precursors for value-added products. Biochar is the byproduct of the pyrolytic processing of biomass to obtain biofuel such as controlled thermal process and gasification, and has a potential as a promising adsorbent for the elimination of micro-pollutants due to its superior properties including a highly condensed structure and surface density of functional groups, although its activated product provides a lower surface area and volume than commercialized activated carbon (Ji, Liu, et al. 2010; Chen, Zhou, and Zhu 2008). These properties are controlled by the pyrolysis conditions (residence time and temperature), activation, and type of feedstock; biochar pyrolyzed at a high temperature consists mainly of polyaromatic carbons and has a higher microporosity, which enhances the adsorption of organic compounds, while higher proportions of aliphatic carbons and functional groups are typical of biochars pyrolyzed at a low temperature (Chun et al. 2004; Chen, Zhou, and Zhu 2008). A separate study has shown that chemically activated biochar resulted in higher porous structure, surface area, and lower ash content than commercialized activated carbon (Azargohar and Dalai 2006). Since most of organic forms such as any kind of plants, domestic and industrial wastes, sewage sludge, and animal manures have used as a source in pyrolysis, their composition of elements and ratio of inorganic compounds in biomass varies the both product yield and quality of bio-oil and

57
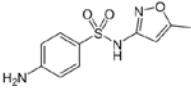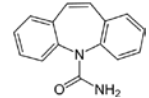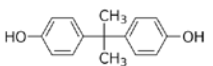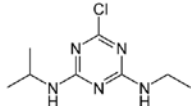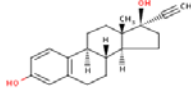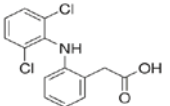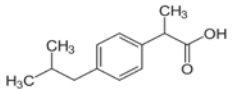
biochar (Laird et al. 2009). The overall objective of this study was to characterize activated biochars produced in a laboratory, where biochars were prepared at different gas environments using conventional analytical methods as well as advanced solid-state nuclear magnetic resonance (NMR) techniques and how these properties determine the competitive adsorption characteristics and mechanisms of EDCs/PhACs. Commercialized powdered activated carbon (PAC) was also examined as a comparison. Seven EDCs/PhACs commonly occurring in the aquatic environment were selected as adsorbates and the effects of their hydrophobicity and molecular size on adsorption capacity were also investigated. The competitive adsorption among EDCs/PhACs were investigated in terms of characteristic difference both adsorbents and adsorbates. Furthermore, adsorption inhibition by natural organic matters (NOMs), described by humic acid, in this study was determined for better understanding in real wastewater condition.

## 5.2. Materials and methods

### 5.2.1. Target adsorbates

Three EDCs (BPA, ATR, and EE2) and four PhACs (SMX, CBM, DCF, and IBP) were purchased from Sigma-Aldrich (St. Louis, MO, USA). Although the seven compounds have similar molecular weights (206–296 g/mol), their $pK_a$ values and octanol–water partition coefficients ($K_{ow}$) cover broad ranges. Detailed physicochemical properties are provided in Supporting Information (Table 5.1).

**Table 5.1** Physicochemical properties of the adsorbates used in this study.

| Compound (Formula) [ID] | Structure | MW (g/mol) | log $D_{ow}$[a] | | | Log $K_{ow}$ | $pK_a$[a] | Water Solubility[b] (g/L) | Mol. Dimens-ion (Å)[c] | Vol[a] (Å$^3$) | Mol. Polar-ity[a] | $\pi$ Energy[a] |
|---|---|---|---|---|---|---|---|---|---|---|---|---|
| | | | pH 3.5 | pH 7.0 | pH 10.5 | | | | | | | |
| Sulfamethoxazole ($C_{10}H_{11}N_3O_3S$) [SMX] | | 253.3 | 0.79 | 0.79 | 0.07 | 0.79 | 5.81 | 0.459 | L: 12.69 H: 3.45 W: 6.07 | 204.6 | 24.2 | 30.9 |
| Carbamazepine ($C_{15}H_{12}N_2O$) [CBM] | | 236.3 | 2.77 | 2.77 | 2.77 | 2.77 | 13.96 | 0.152 | L: 9.43 H: 5.92 W: 7.38 | 210.3 | 27.0 | 29.1 |
| Bisphenol A ($C_{15}H_{16}O_2$) [BPA] | | 228.3 | 3.64 | 3.64 | 2.87 | 3.64 | 9.78 -10.39 | 0.12-0.3[d] | L: 10.57 H: 4.33 W: 6.50 | 221.6 | 26.6 | 24.6 |
| Atrazine ($C_8H_{14}ClN_5$) [ATR] | | 215.7 | 2.08 | 2.20 | 2.20 | 2.20 | 14.48 | 0.030[e] | L: 10.22 H: 8.55 W: 6.27 | 190.9 | 21.2 | 19.2 |
| 17 α-ethinylestradiol ($C_{20}H_{24}O_2$) [EE2] | | 296.4 | 3.90 | 3.90 | 3.57 | 3.90 | 10.33 -10.47 | 0.011[f] | L: 12.28 H: 6.23 W: 3.77 | 291.7 | 33.9 | 18.5 |
| Diclofenac ($C_{14}H_{11}Cl_2NO_2$) [DCF] | | 296.2 | 4.26 | 1.55 | 1.08 | 4.26 | 4.15 | 0.004 | L: 10.14 H: 4.84 W: 7.19 | 236.8 | 29.0 | 33.2 |
| Ibuprofen ($C_{13}H_{18}O_2$) [IBP] | | 206.3 | 3.84 | 1.82 | 0.60 | 3.84 | 4.52 | 0.049 | L: 10.98 H: 4.33 W: 5.31 | 211.8 | 23.7 | 15.7 |

[a]chemicalize.org by ChemAxon (http://www.chemicalize.org); [b] drugbank.ca by DrugBank (http://www.drugbank.ca); [c] Molecular dimensions calculated using MacMolPlt v.7.4.2.; [d] ec.gc.ca by Environmental Canada (http://www.ec.gc.ca); [e] inchem.org by IPCS Inchem (http://www.inchem.org); [f] pharmacycode.com by Pharmacy Codes (http://pharmacycode.com).

## 5.2.2. Adsorbents

The N- and O-biochar samples were produced through the thermal treatment of torrefied loblolly pine chips (15 × 6 mm) containing bark at 300°C for 15 min in a laboratory-scale batch tube-furnace (OTF-1200X, MTI Corporation, Richmond, CA, USA), under pure nitrogen (N-biochar) and 7% oxygen + 93% nitrogen atmospheres (O-biochar). Due to the limitation of the loadable amount of samples in the tube furnace, N-/O-biochars were generated with several batches. After each batch, the weight loss from the thermal treatment was measured, and then the samples with a difference of ± 3% in weight loss were collected for further experiments. The yields for N-/O-biochar were 42.3% and 64.2%, respectively. 3 g of each pyrolyzed biochar was activated with 40 mL of 4 M NaOH for 2 hours and dried overnight at 105 °C. The NaOH-impregnated biochar samples were then heated at 800 °C for 2 hours under a nitrogen gas flow (2 L/min) and cooled down (10 °C/min) after being separated from the solution using a Buchner filter funnel. The dried samples were rinsed with 0.1 M HCl followed by deionized water until they reached neutral pH, dried at 105 °C, milled and passed through a 74-μm sieve. Coal-based virgin, high-performance PAC, Calgon WPH® (Pittsburgh, PA, USA) was used to compare its adsorption ability with that of the biochars manufactured in the lab.

## 5.2.3. Characterization of adsorbents

Elemental analysis was performed using a PerkinElmer 2400 Series II Elemental Analyzer (PerkinElmer, Waltham, MA, USA). Oxygen content was calculated by subtracting the ash and carbon, hydrogen, and nitrogen contents from the total mass of the samples. The BET surface area was measured with a Gemini VII 2390p surface area analyzer (Micromeritics, Norcross, GA, USA) and the total pore volume was calculated

from the adsorbed quantity of $N_2$ at $P/P_0 = 0.95$. Solid-state $^{13}C$ direct polarization/magic angle spinning (DP/MAS) NMR spectra were acquired with a 3.2 mm MAS probe, on a Varian Inova 500 spectrometer (Palo Alto, CA, USA). The $^{13}C$ NMR spectra combined with dipolar-recoupled NMR methods were used for quantitative structural analyses of the biochars and PAC. Detailed experimental conditions for the NMR experiments are described elsewhere (Boateng et al. 2013).

### 5.2.4. Adsorption experiments

Adsorption isotherms of the EDCs and PhACs on the adsorbents were undertaken through batch experiments as described in our previous study (Joseph et al. 2011) with a mixture of five different initial concentrations (10–50 $\mu$M). Each stock solution (10 mM), prepared in deionized water for DCF, and in acetonitrile for the others, was evaporated to minimize any cosolvent effect prior to addition to a 40-mL amber EPA vial equipped with a polytetrafluorethylene-lined screw cap. The pH and conductivity of aqueous background solution were adjusted using 1 N HCl or NaOH, and 0.1 M NaCl (to 150 $\mu$S/cm), respectively. A stock suspension of 2000 mg/L of each adsorbent (N/O-biochar and PAC) was prepared by adding 200 mg of each adsorbent to 100 mL of ultrapure deionized water (resistivity ~18 M$\Omega$/cm) and mixing over a magnetic stirrer at 500 rpm, and added to each vial at 50 mg/L. After capping (leaving minimal headspace), the vials were mixed under ambient conditions for 7 days and allowed to reach apparent equilibrium. The effect of natural organic matter (NOM) was determined by spiking 5.0 mg/L humic acid (Sigma-Aldrich) as dissolved organic carbon with 10 $\mu$M EDCs/PhACs mixed solution.

Single batch experiments were conducted to determine the adsorption kinetics for EDCs/PhACs on N-biochar, O-biochar, and PAC. Solutions of EDCs/PhACs (10 $\mu$M each

in 1000 mL) in beakers were transferred, and then the stock solution of each adsorbent was spiked to achieve 50 mg/L. The pH and conductivity were adjusted as described above. Under ambient conditions, the solutions were mixed over a magnetic stirrer at 150 rpm and sampled repeatedly at specific times. All adsorption experiments were conducted in duplicate.

After mixing, each aliquot was collected from the solution and filtered through a 0.22-μm Durapore® membrane filter (Millipore, Cork, Ireland), placed in a 2-mL amber vial, and analyzed using a high-performance liquid chromatograph equipped with a ultraviolet detector and a 4.6×150 mm LiChrosper RP-18 5$\mu$m column (Agilent, Santa Clara, CA, USA) at a constant flow rate of 0.75 mL/min for 23 min. The mobile phase was 5 mM phosphoric acid: acetonitrile (50:50 v/v). The detector wavelength was set at 210 nm for all EDCs and PhACs; SMX, CBM, BPA, ATR, EE2, DCF, and IBP eluted from the column at 3.8, 5.4, 7.1, 9.4, 10.6, 19.0, and 21.0 min, respectively.

### 5.2.5. Data analysis

The adsorption isotherms were analyzed with the Freundlich isotherm model (Eq. (5.1)).

$$q_e = K_F C_e^{1/n} \quad \text{……………………………………} (5.1)$$

where $q_e$ (mg/g) and $C_e$ (mg/L) are the concentration of adsorbate in adsorbent and solution at equilibrium condition, respectively. $K_F$ (mg/g) and $n$ provide a unit adsorption capacity parameter and dimensionless intensity of the adsorbent parameter, respectively. In general, high value of $K_F$ is indicative of favorable adsorption processes, while the reciprocal of $n$ has a meaning of the surface heterogeneity (homogeneous surface; $n = 1$).

Pseudo-second-order model was employed to analyze the kinetics of adsorption (Eq. (5.2)).

$$\frac{t}{q_t} = \frac{1}{k_2 q_e^2} + \frac{1}{q_e} \cdots\cdots\cdots\cdots\cdots\cdots\cdots\cdots\cdots\cdots\cdots(5.2)$$

where $q_t$ and $q_e$ are the amount of EDCs/PhACs adsorbed (mg/g) at time $t$ and equilibrium condition, respectively, while $k_2$ is the pseudo-second-order model rate constant (g/hr·mg) for the adsorption.

## 5.3. Results and discussion

### 5.3.1. Characterization of adsorbents

The activated biochars produced from two different precursor biochars were characterized by elemental analyses and solid-state NMR. The elemental composition and ^{13}C NMR spectra of N-/O-biochars and PAC were markedly different (Figure 5.1). The precursor biochar for the activated O-biochar was pyrolyzed in the presence of oxygen (3%), allowing the material to be partly combusted rather than fully charred (Chen, Zhou, and Zhu 2008). This nominal oxidation resulted in a significant difference in pyrolysis (Table 1). The oxygen content (13.0%) of the O-biochar was lower than the N-biochar (21.3%), resulting in carbon contents of 83.8% and 72.6%, respectively. The H/C ratio of 0.034 for O-biochar, and 0.127 for N-biochar indicated that O-biochar was slightly more carbonized than N-biochar.
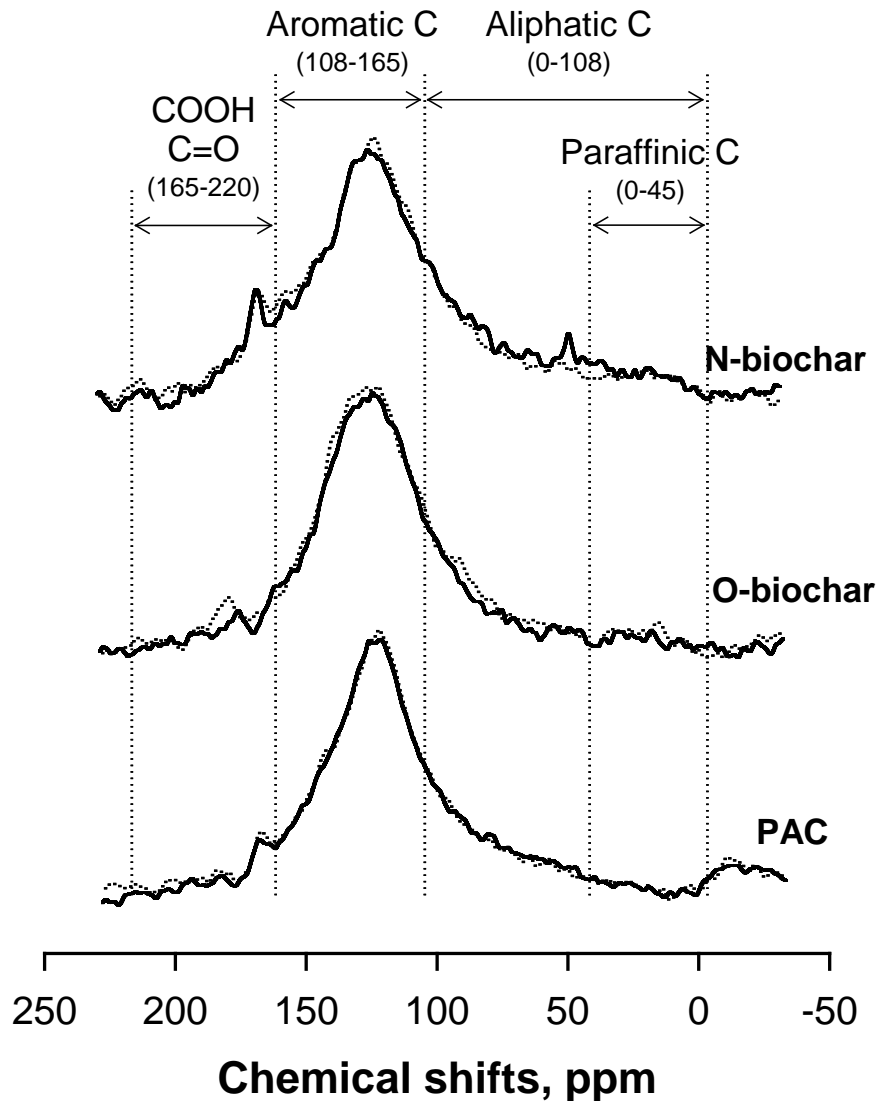
**Figure 5.1** Solid-state $^{13}C$ DP/MAS NMR spectra (solid line) with corresponding recoupled $^{1}H$-$^{13}C$ dipolar dephasing spectra (dotted line) for N-/O-biochars and PAC samples.

The elemental analyses are consistent with $^{13}C$ solid-state NMR results (Tables 5.2 and 5.3). The $^{13}C$ DP/MAS NMR spectra showed that O-biochar has more aromatic characters on the basis of a stronger peak at 108 – 148 ppm corresponding to aryl carbons than others. On the other hand, N-biochar has relatively higher aliphatic carbon fractions; paraffinic or alkyl (0-45 ppm), methoxyl (45-63 ppm), carbohydrate (63-108 ppm) and

carboxyl carbons (165-187 ppm). Quantitative analyses of the $^{13}C$ DP/MAS and dipolar dephasing experiments showed that O-biochar has a more condensed aromatic structure with higher aromaticity based on the larger non-protonated carbon fraction, which agrees well with its lower H/C and O/C ratios than those of N-biochar. These results indicate that O-biochar has a higher hydrophobicity than N-biochar.

Porous structures (BET surface area and pore volume) of the activated biochars and PAC were examined by $N_2$ adsorption experiments (Table 5.4). The chemically activated N-/O-biochars exhibit fairly large surface area (1360.3 and 1150.7 $m^2$/g) and pore volume (0.95 and 0.63 $cm^3$/g, respectively) that are comparable or better than those of commercial activated carbons (972.3 $m^2$/g and 0.53 $cm^3$/g). It is notable that N-biochar with relatively lower aromaticity has a higher surface area and pore volume, suggesting aromatic structures may not help develop porous structures of biochar. The high surface area and pore volume of the biochars render the activated carbons from the renewable biomass a promising sorbent that can potentially replace coal-based activated carbons such as PAC. In addition, the amount of ash in the activated biochar is far lower than the commercial PAC. The low ash content of both N-/O-biochar (4.2 and 2.7%, respectively) were derived from its property as a feedstock; following the order of soft wood < hard wood < corn or wheat stover < livestock manure (Laird et al. 2009). 20.1 % ash content of coal-based PAC hardly contributes to hydrophobic organic compounds, excepting for the interaction of ash-preferring species such as dyes and metal ions (Hameed, Ahmad, and Aziz 2007; Ahmaruzzaman 2009); therefore, not only the effective surface area and pore volume of adsorbent, but also absolute aromaticity may be diminished, resulting in losing its adsorption capacity.

**Table 5.2** Quantitative spectral analysis of solid-state $^{13}C$ DP/MAS NMR for biochars and PAC. The values were calculated based on 100% carbon in each biomass.

| Samples | Alkyls (%) | | | Aromatics (%) | | | Carbonyls (%) | | Aromaticity (%)[a] |
|---|---|---|---|---|---|---|---|---|---|
| | $CH_3$ (6-25 ppm) | $CH_{1.5}$ (25-50 ppm) | $HCO_{0.75}H_{0.5}$ (50-90 ppm) | Non-protonated (90-145 ppm) | Protonated (90-145 ppm) | O-Aryl $CO_{0.75}H_{0.5}$ (145-165 ppm) | COO- (165-183 ppm) | C=O (183-210 ppm) | |
| N-Biochar | 2.86 | 5.35 | 13.1 | 53.5 | 2.49 | 12.5 | 7.53 | 2.72 | 68.4 |
| O-Biochar | 1.13 | 2.22 | 8.31 | 66.5 | 0.65 | 13.2 | 4.44 | 3.49 | 80.4 |
| PAC | 0.58 | 2.69 | 12.5 | 61.1 | 2.31 | 12.5 | 4.88 | 3.42 | 75.9 |

[a] Aromaticiy (%) = [aromatic carbon fraction] / [total carbon fraction.]

**Table 5.3** Quantitative spectral analysis for solid-state $^{13}C$ DP/MAS NMR with corresponding recoupled $^{1}H$-$^{13}C$ dipolar dephasing spectra for biochars and PAC. The values were calculated based on 100% carbon in each biomass.

| Samples | Alkyl 0–45 ppm | Methoxyl 45–63 ppm | Carbohydrate 63–108 ppm | Aryl 108–148 ppm | O-Aryl 148–165 ppm | Carboxyl 165–187 ppm | Carbonyl 187–220 ppm | Aromaticity (%)[a] |
|---|---|---|---|---|---|---|---|---|
| N-Biochar | 7.14 | 4.81 | 21.5 | 45. 7 | 9.91 | 8.22 | 2.79 | 62.5 |
| O-Biochar | 2.80 | 2.42 | 18.5 | 57.8 | 10.1 | 5.07 | 3.32 | 74.1 |
| PAC | 2.78 | 3.70 | 21.4 | 53.5 | 9.67 | 5.55 | 3.43 | 69.4 |

[a] Aromaticiy = 100 × aromatic C (108–165 ppm) [aromatic C (108–165 ppm) + aliphatic C (0–108 ppm)].

**Table 5.4** Elemental composition, aromatic ratio, ash content, aromaticity, BET-$N_2$ surface area (SA-$N_2$), and cumulative pore volume of the adsorbents used in this study.

| Samples | C (%) | H (%) | N (%) | O (%) | H/C | Polarity index N/C | Polarity index O/C | Ash (%) | Aromaticity[a] | SA-$N_2$[b] ($m^2$/g) | Pore volume[c] ($cm^3$/g) micro-pore | Pore volume[c] ($cm^3$/g) macro-pore |
|---|---|---|---|---|---|---|---|---|---|---|---|---|
| N-Biochar | 72.6 | 0.77 | 0.65 | 21.3 | 0.127 | 0.001 | 0.221 | 4.7 | 62.5 | 1360.3 | 0.307 | 0.643 |
| O-Biochar | 83.8 | 0.24 | 0.30 | 13.0 | 0.034 | 0.003 | 0.116 | 2.7 | 74.1 | 1150.7 | 0.313 | 0.318 |
| PAC | 59.3 | 0.16 | 0.31 | 20.2 | 0.032 | 0.004 | 0.255 | 20.1 | 69.4 | 972.3 | 0.216 | 0.314 |

[a] Aromaticity = 100 × aromatic C (108–165 ppm)/[aromatic C (108–165 ppm) + aliphatic C (0–108 ppm)]. Data of aromatic C (108–165 ppm) and aliphatic C (0–108 ppm) are listed in Table 5.2.

[b] Calculated using the Brunauer–Emmett–Teller (BET) equation for data in the range less than 0.1 of relative pressure.

[c] Calculated from the adsorbed quantity of $N_2$ at $P/P_0 = 0.95$ with t-plot mod

## 5.3.2. Influence of physicochemical properties of the adsorbates on adsorption: Ionization and pK$_a$

The three EDCs and four PhACs are amphoteric species and consist of single or multiple charged groups, as well as polar groups (hydroxyl, carbonyl, carboxyl, amine, sulfonyl) with aromatic rings (benzene, isoxazole, 1,3,5-triazine, azepine). Under acidic conditions (pH 3.5), all of these EDCs/PhACs are predominantly neutral species. Increasing the pH varied the content of their ionic forms depending on each p$K_a$ value while basic compounds lose their proton, especially for SMX, DCF, and IBP whose p$K_a$ is relatively lower than those of other compounds. At pH values below their p$K_a$, the adsorption affinity toward adsorbents increased significantly with the pH, whereas the adsorption affinity dropped sharply at the pH above the p$K_a$ values (Hong et al. 2008). This difference occurs because the electronic coupling influences the adsorptive interaction with each adsorbent. The strong electron-withdrawing sulfonamide, carboxyl group, and hydroxyl groups on SMX, DCF/ IBP, and BPA, respectively, repulse π–electron–acceptor-rich aromatic ring(s) on adsorbents (Ji, Liu, et al. 2010), resulting in inhibition of π–π electron donor–acceptor (EDA) interaction, whereas less variation of adsorption affinity due to their higher p$K_a$ values (less variation in the ionic state from neutral to ionized form) allows CBM, ATR, and EE2 to show strong hydrophobic interactions throughout a wide range of pH values (Figure 5.2). Furthermore, CBM and EE2 were non–ionizable across the pH range from 3.5 to 10.5, and hence the influence of pH was negligible to the adsorption, while ATR was slightly protonated (28%) at pH 3.5, resulting in a reduction of the percent of non-ionized form (72%), (ChemAxon) and an increase in the π-H bond with adsorbent.
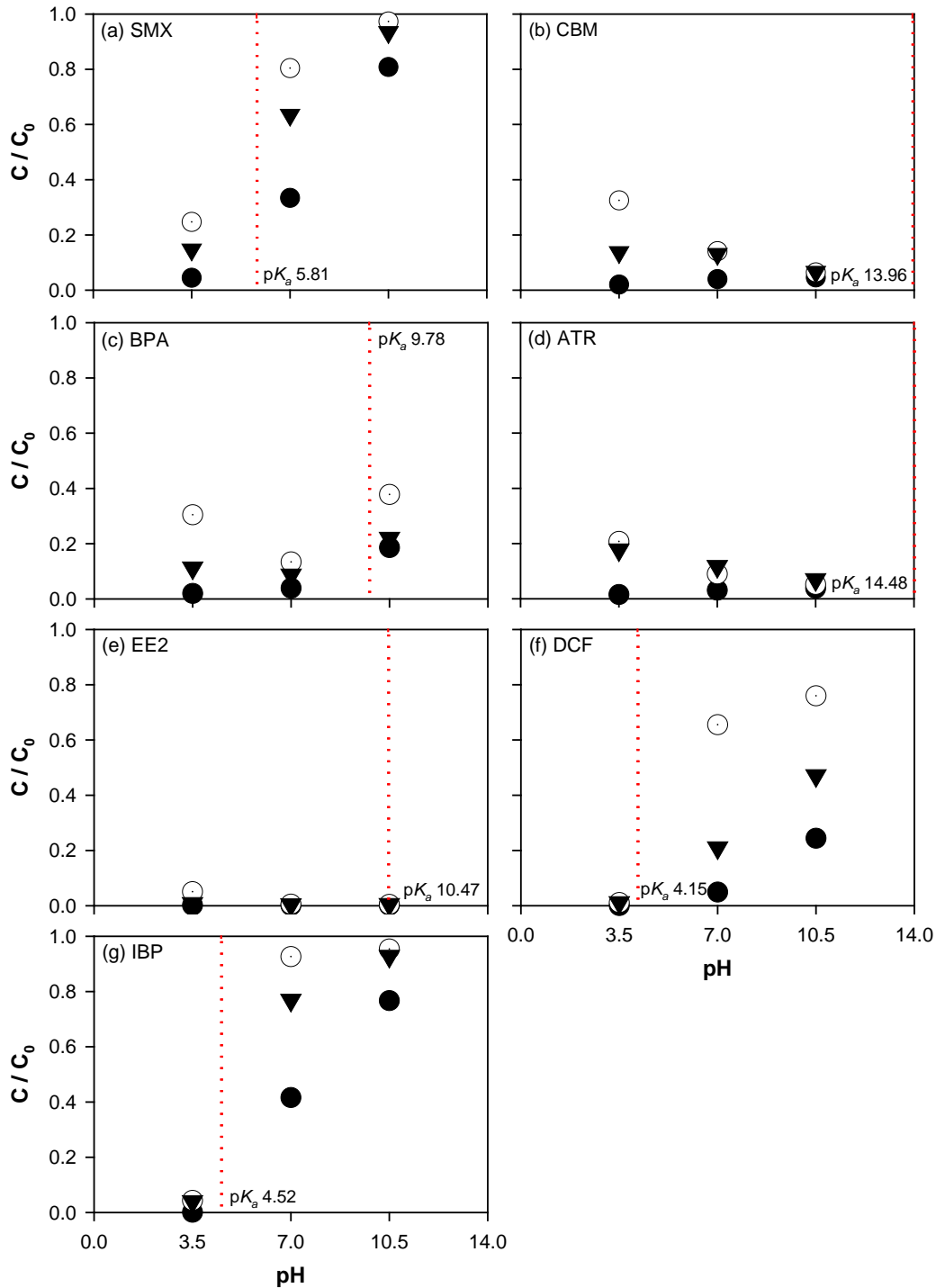
**Figure 5.2** Adsorption of EDCs/PhACs on each adsorbent as a function of pH, N-biochar (●); O-biochar (◌); PAC (▼). ($C_0$ = 10 µM, adsorbent dose = 50 mg/L. equilibrium contact time = 7 d at 20 °C). Vertical dashed lines represent $pK_a$ values of the respective adsorbates.

### 5.3.3. Distribution coefficient (D)

The octanol–water partition coefficient ($K_{ow}$) has been used to represent hydrophobicity. This is accurate if the compounds are non-ionizable, independent of pH. However, most EDCs and PhACs in solution coexist as ionized and neutral forms across the entire pH range. Therefore, for the seven adsorbates used in this study, the use of the distribution coefficient (*D*) is more reasonable and preferred because it prevents the overestimation of hydrophobicity (Kümmerer 2004). Each pH-dependent *D* value of EDCs/PhACs was calculated and reported in logarithmic scale at pH 3.5, 7.0, and 10.5 (Table 5.1). The adsorption affinity and correlation between p$K_a$ and hydrophobicity are depicted and ordered proportionally with the hydrophobicity of adsorbate (log *D*) in Figure 5.3. Under the condition of dominant hydrophobic interaction in the adsorption study of higher-aromatic-containing adsorbents, ionized molecules hardly attract to adsorbent through this mechanism. Therefore, a sharp drop in its hydrophobicity lowers the interaction with adsorbent when pH is greater than p$K_a$. The variable results of adsorption capacity were observed with DCF and IBP due to their lower p$K_a$ values (4.15 and 4.52, respectively). The higher ranked DCF and IBP in adsorption affinity at pH 3.5 dropped sharply, ranking fifth and sixth at pH 10.5, respectively, due to their declining values of log *D* (from 4.21 to 1.08 and 3.92 to 0.60, respectively). In contrast, the non-ionizable CBM and partially non-ionizable ATR and EE2 in basic conditions displayed less variable adsorption capacity for adsorbents, following the order of adsorption capacity, EE2 > CBM > ATR.

71
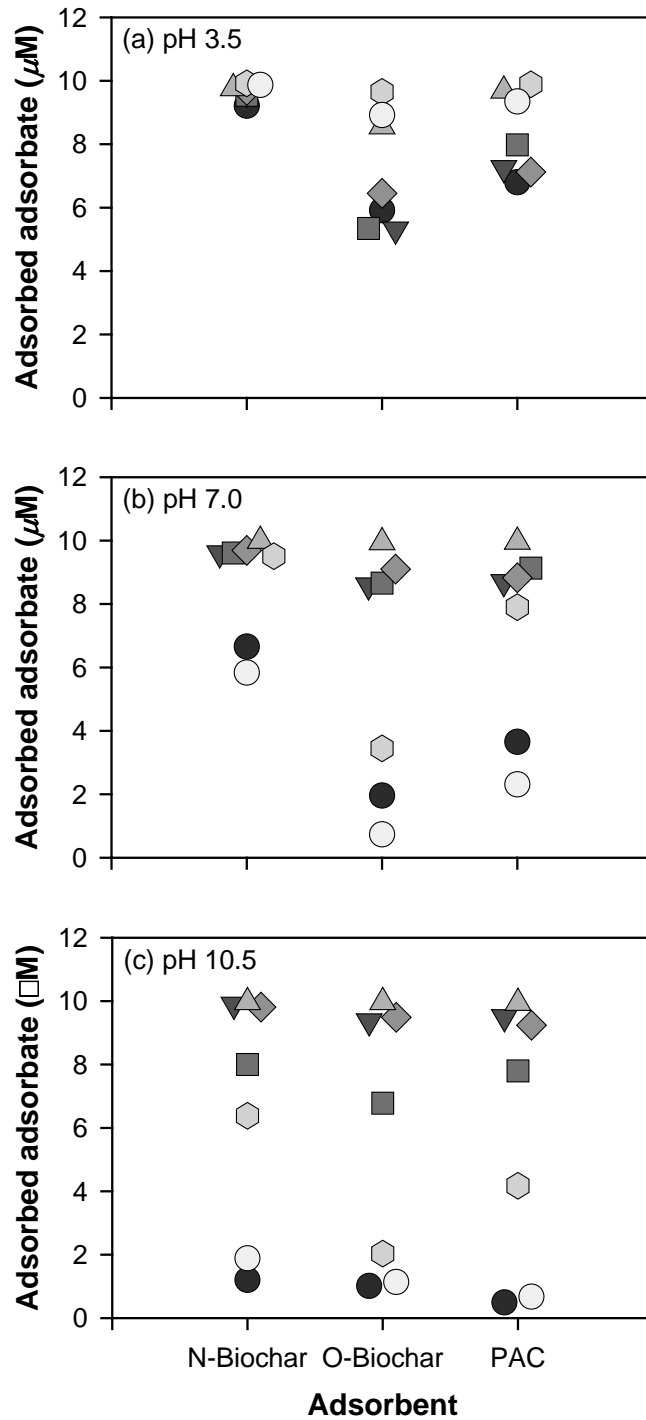
**Figure 5.3** Overall adsorbed EDCs and PhACs (SMX (●); CBM (▼); BPA (■); ATR (◆); EE2 (▲); DCF (⬡); IBP (○)) onto N-/O-biochars and PAC at various pH conditions; (a) pH 3.5; (b) pH 7.0; (c) pH 10.5 ($C_0 = 10$ μM, adsorbent dose = 50 mg/L, equilibrium contact time = 7 d at 20 °C).

### 5.3.4. Adsorption difference between N-biochar and O-biochar

Hydrophobic interactions were similarly emphasized in several adsorption studies of organic compounds in various solutions (Gotovac et al. 2007; Pyrzynska, Stafiej, and Biesaga 2007; Balavoine et al. 1999). However, the adsorption of organic chemicals cannot be interpreted by one or two mechanisms. The above results demonstrated that N-biochar allowed a higher adsorption for all seven EDCs/PhACs than O-biochar (Figure 5.4), although the aromaticity of N-biochar was lower than that of O-biochar (62.5% and 74.1%, respectively). The aromaticity determined by the sum of total aromatic carbon, the aryl (108-148 ppm) and O-aryl (148–165 ppm) groups, in the $^{13}$C NMR spectra increases hydrophobicity while aliphatic components cause lower aromaticity (Sun et al. 2011). Although high aromaticity contributes to the effective adsorption, the lower surface area and pore volume of O-biochar limited the adsorption capacity than that of N-biochar (Table 5.4).

Elemental composition, structural characteristics, and surficial properties of biochars affect their adsorption behavior. First, the higher polarity index (O/C+ N/C) and greater number of polar functional groups in the N-biochar (Table 5.4 and Figure 5.1) indicated that the polarity of N-biochar was higher than that of O-biochar. This higher polarity of N-biochar encouraged higher adsorption affinity toward polar compounds throughout this study due to delocalization of aromatic π-cloud. This role of polarizability may lead to induced electrostatic interaction (i.e. π-π interaction, π-stacking, and London dispersion forces (Martinez and Iverson 2012)) and the observed positive relationship between the polarities of adsorbates and the sorption coefficient, log $K_{oc}$ (Figure 5.4). The later may be interpreted by other intermolecular interactions such as dipolar and dispersion
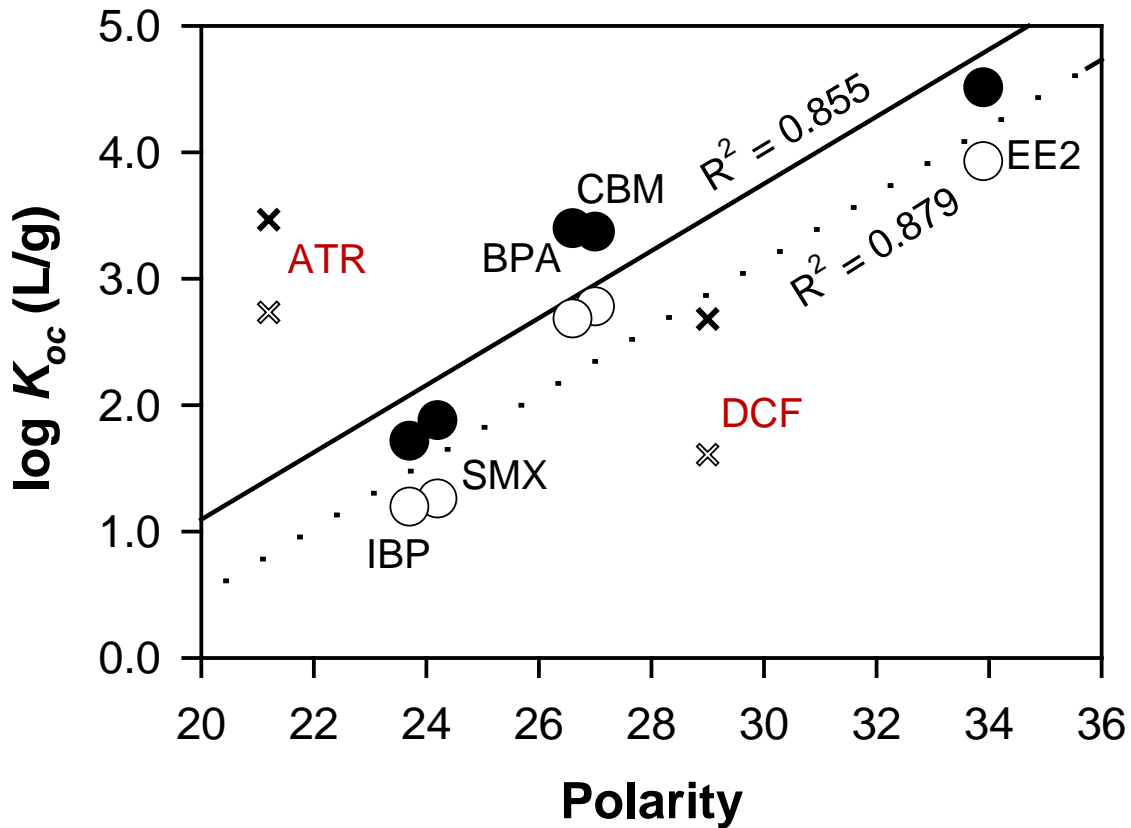
**Figure 5.4** Relationship between polarities of adsorbates (excluding ATR and DCF) and log $K_{oc}$ (calculated by dividing $q_e/C_e$ by the fraction of O/C in Table 1) at pH = 7; N-biochar (●) and O-biochar (○); ($C_0$ = 10 μM; adsorbent dose = 50 mg/L at 20°C).

forces, resulting in higher adsorption affinity (Pan and Xing 2008). In addition, the adsorption capacity was positively correlated with the O/C fraction of both biochars, implying that the polar functional groups of N-biochar have a significant role in the adsorption of EDCs/PhACs. Moreover, larger contributions of carbohydrate (63–108 ppm), carboxyl (165–187 ppm), and carbonyl carbons (187-220 ppm) revealed by $^{13}$C NMR spectra in N-biochar (Figure 5.1) are attributable to the polar functional groups, indicating that a polarity provider induces the higher adsorption capacity. These polar functional groups (O-containing groups) allow H-bonding interactions for adsorbents (H-bonding

donor) and chemicals (H-bonding acceptor) (Sun et al. 2010). The H-bonding donor groups of biochars and positively charged surface in the acidic condition (Figure 5.5) enable $\pi$–H-bonding interactions with the aromatic rings of EDCs/PhACs (Zhu et al. 2004). Due to the higher portion of such O-containing functional groups on N-biochar, the adsorption activity might be attributable to $\pi$–H-bonding interactions. Moreover, this allows adsorbents possessing hydrophilic and positively charged sites to interact with ionized molecules at pH ranges between above pH of lower $pK_a$ of adsorbates (SMX, DCF, and IBP) and each $pH_{zpc}$, although this mechanism was mostly suppressed by different values of $\pi$–electron-dependent polarizable interactions; EDA interaction, a specific noncovalent force existing between $\pi$-electron-rich moieties ($\pi$-electron donors) and $\pi$–electron-depleted moieties ($\pi$-electron acceptors) throughout the entire pH ranges (Hunter and Sanders 1990; Hunter et al. 2001). These resulted in both a strong interaction between EDCs/PhACs ($\pi$ acceptors) and the aromatic benzene-rings ($\pi$ donors) of adsorbents and hydrophobic interactions (Pan and Xing 2008).

Furthermore, previous studies have proposed micropore-filling and sieving effects to elucidate the adsorption of adsorbates (Ji, Liu, et al. 2010; Zhu and Pignatello 2005; Nguyen et al. 2007). Different from other single-solute and bi-solute adsorptions, less pore-filling and sieving effects occurred due to the larger micro- and macro-pore volumes of N-/O-biochar (0.31 and 0.64 $cm^3$/g, and 0.31 and 0.32 $cm^3$/g, respectively). The sieving effect of all EDCs/PhACs was elucidated by result of the positive correlation between the adsorption capacity and their molecular volume; a group of ionizable compounds followed the order of adsorption capacity as DCF > IBP > SMX (Figure 5.6), while that of

non-ionizable compounds was determined the similar trend of order as EE2 > BPA > CBM

> ATR (Figure 5.7).
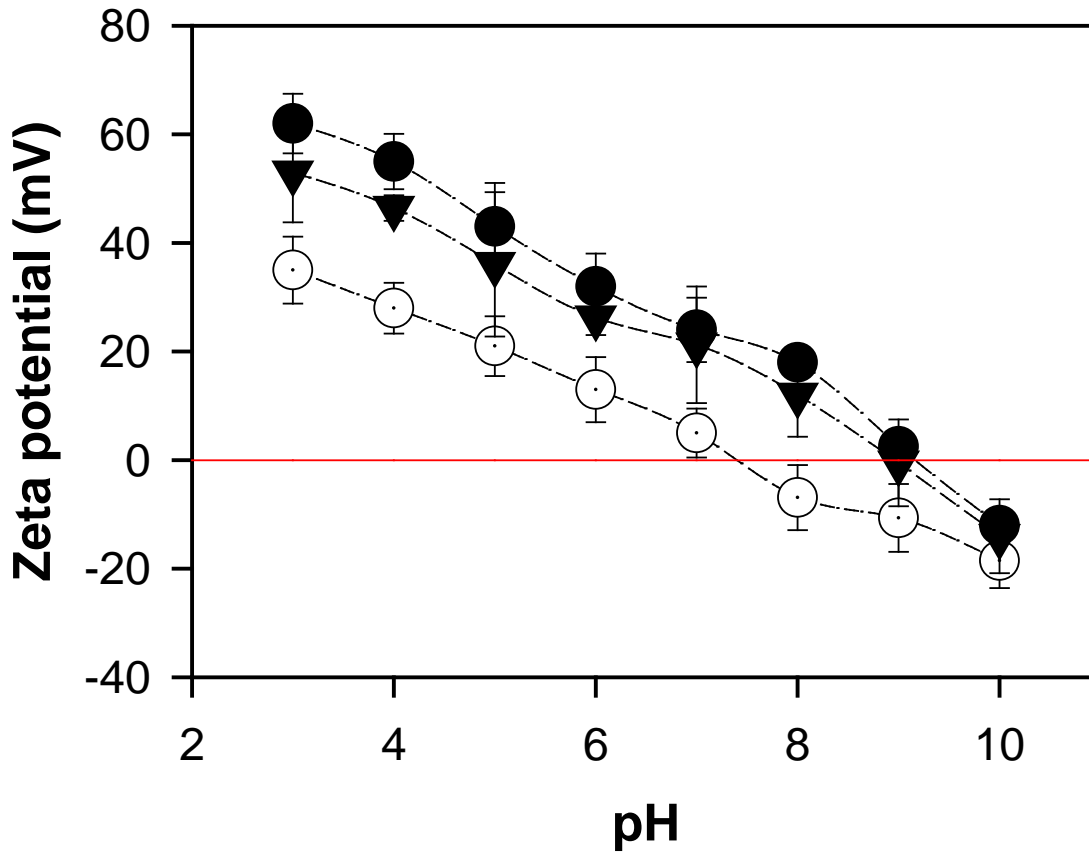


**Figure 5.5** Zeta potential curves as a function of pH for each type of adsorbent (dose of adsorbent = 50 mg/L). Adsorbent: N-biocahr (●); O-biocahr ( ⊙ ); PAC (▼).
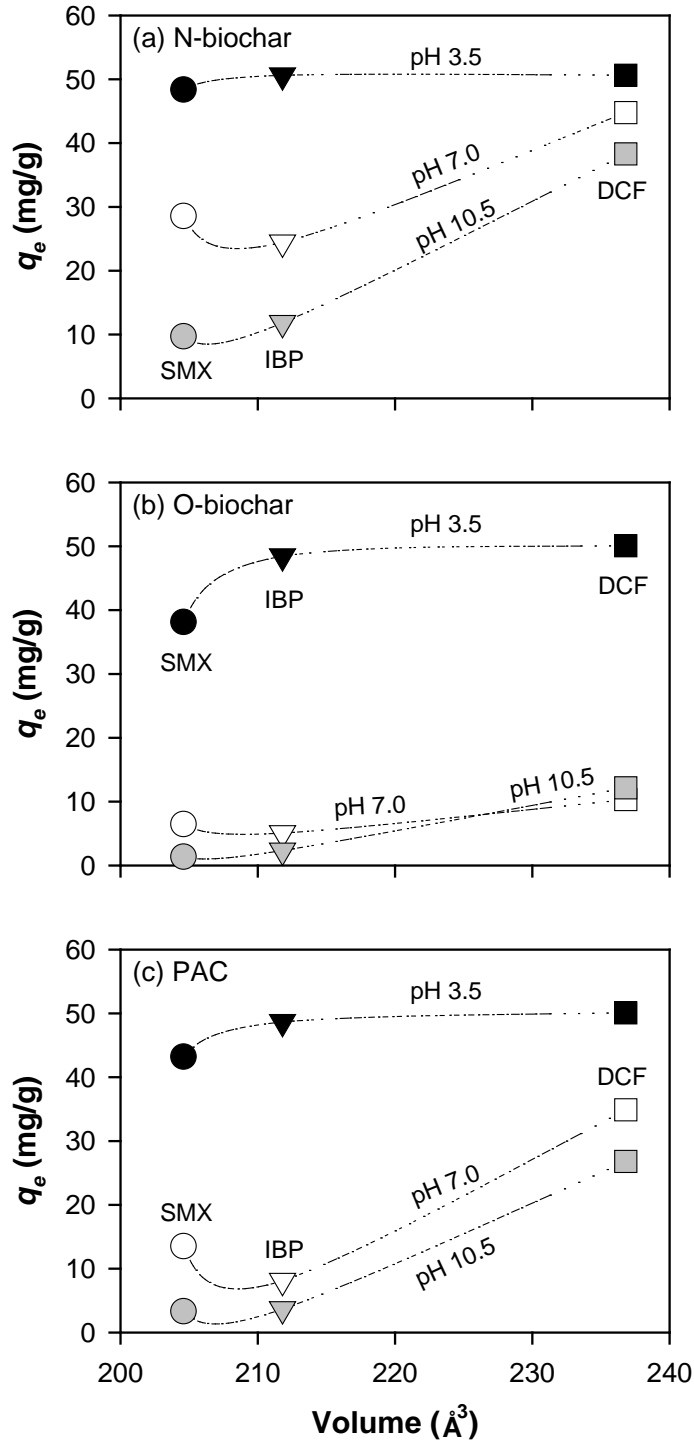
**Figure 5.6** Plot for relationship between volume and adsorption capacity of SMX (circle), IBP (triangle), and DCF (square) at various pH conditions ($C_0$ = 10 μM; adsorbent dose = 50 mg/L at 20 °C, $q_e$: amount of EDCs/PhACs adsorbed (mg/g) at equilibrium).
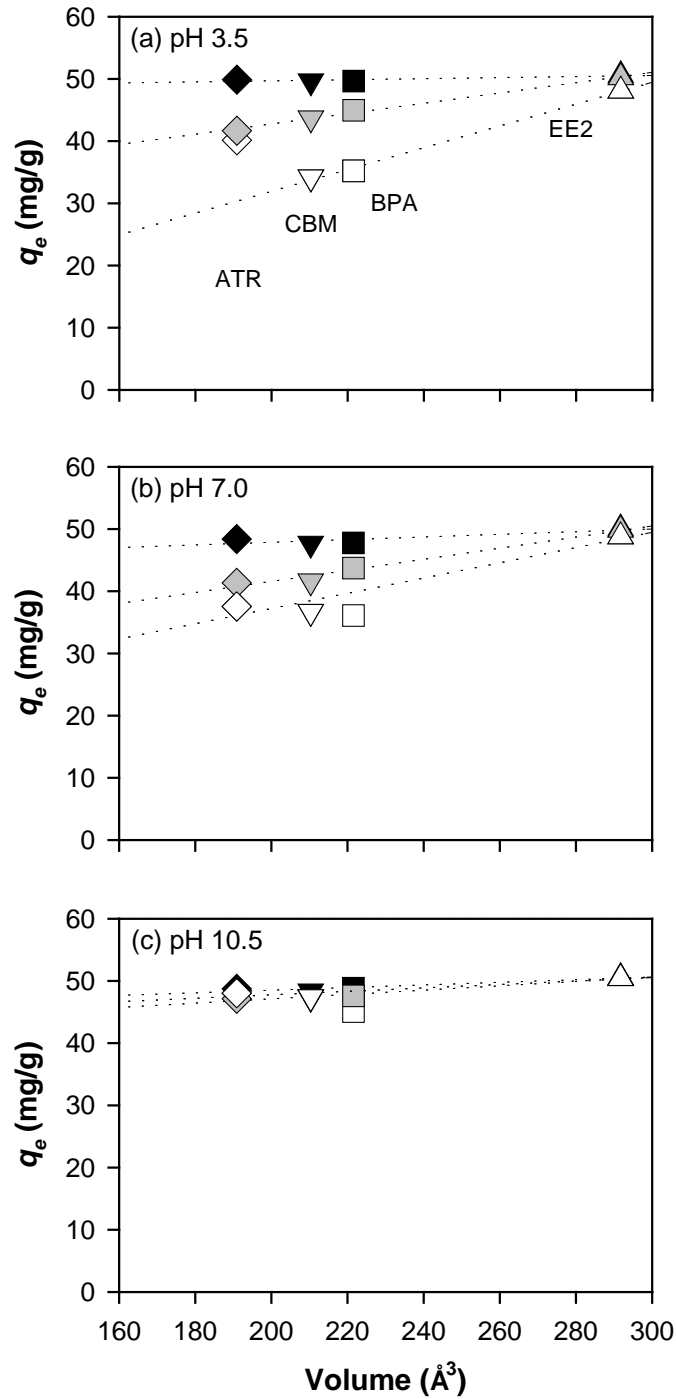
**Figure 5.7** Plot for relationship between volume and adsorption capacity of non-ionizable EDCs/PhACs (CBM, BPA, ATR, and EE2) at various pH conditions. Adsorbent type: N-biochar (black); O-biochar (white); PAC (gray), ($C_0$ = 10 μM; adsorbent dose 50 mg/L at 20 °C, $q_e$: amount of EDCs/PhACs adsorbed (mg/g) at equilibrium).

78

### 5.3.5. Competitive adsorption among EDCs and PhACs

The adsorption of EDCs/PhACs on biochars and PAC was regulated by the dissociable states of each adsorbate, displaying similar adsorption patterns in the order N-biochar > PAC > O-biochar. Unlike single-solute adsorption, multi-solute competitive adsorption was unable to describe the adsorption characteristics of each adsorbate through isotherm data; however, distinguishable adsorption layer type under competitive desorption was identified (Figure 5.8 and Table 5.5). The results of overall adsorption under a gradually increasing initial concentration (10 – 50 μM) of each adsorbate with limited adsorption sites were able to explain the competitive adsorption (Figure 5.9).

The desorption was clear for ionizable compounds. For instance, DCF mostly adsorbed proportionally with increasing initial concentration of adsorbent (N-biochar, 50 mg/L) predominately under acidic condition, while dissociated DCF lost its hydrophobicity and increased its solubility, resulting in poor adsorption under neutral and basic conditions. The adsorption site allowed DCF to interact via strong hydrophobicity, impeding the multi-layer adsorption of competitive adsorbates due to its poor polarity and high π energy (Liu et al. 2011; Ji, Shao, et al. 2010; Cho et al. 2008). Unlike dissociable DCF, relatively less dissocial EE2 predominated in both the aromatic and polar functionalized sites under neutral and basic conditions via its strong hydrophobicity and higher polarity and lower π-energy, respectively (Cho et al. 2008; Chen, Zhou, and Zhu 2008). The overall adsorbed EE2 under this condition was higher than that under acidic conditions and indicated that EE2 replaced and occupied the site at which DCF was adsorbed.
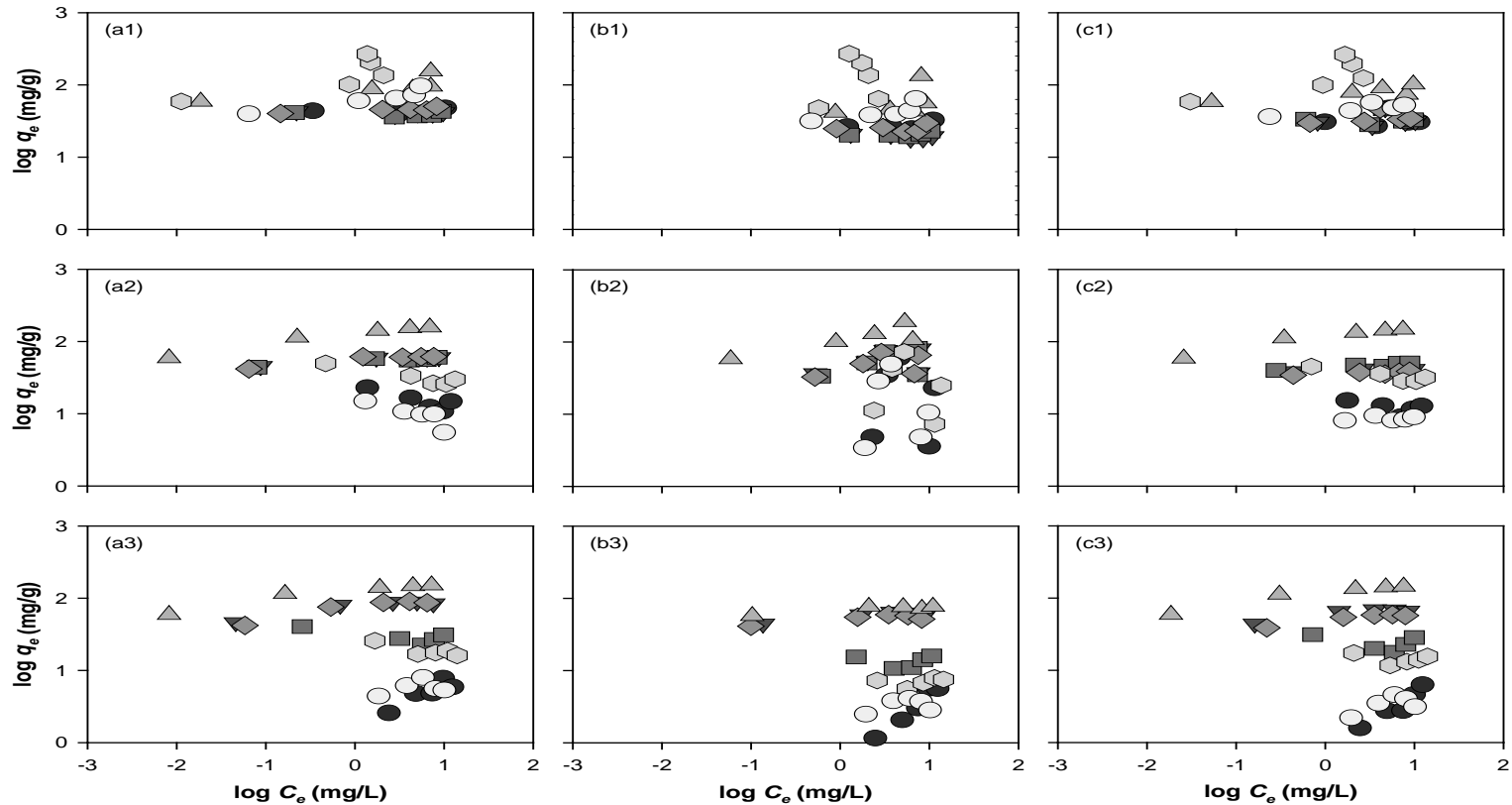
**Figure 5.8** Freundlich isotherm ($q_e = K_F \cdot C_e^n$) for EDCs and PhACs (SMX (●); CBM (▼); BPA (■); ATR (◆); EE2 (▲); DCF (⬡); IBP (◯)) adsorption onto N-biochar (a), O-biochar (b), and PAC (c) at various pH conditions (3.5 (a1, b1, c1); 7.0 (a2, b2, c2); 10.5 (a3, b3, c3)), ($C_0$ = 10-50 μM; adsorbent dose = 50 mg/L; equilibrium contact time = 7 d at 20 °C, $q_e$: amount of EDCs/PhACs adsorbed (mg/g) at equilibrium, $K_F$: Freundlich affinity coefficient, EDCs/PhACs aqueous phase concentrations($C_e$)).

**Table 5.5** Freundlich isotherm parameters for adsorption of EDCs and PhACs on various adsorbents.

| Adsorb-ent | pH | SMX | | | CBM | | | BPA | | | ATR | | | EE2 | | | DCF | | | IBP | | |
|---|---|---|---|---|---|---|---|---|---|---|---|---|---|---|---|---|---|---|---|---|---|---|
| | | $K_F$ | $1/n$ | $R^2$ | $K_F$ | $1/n$ | $R^2$ | $K_F$ | $1/n$ | $R^2$ | $K_F$ | $1/n$ | $R^2$ | $K_F$ | $1/n$ | $R^2$ | $K_F$ | $1/n$ | $R^2$ | $K_F$ | $1/n$ | $R^2$ |
| N-Biochar | | 42.6 | 0.00 | 0.002 | 41.1 | -0.01 | 0.234 | 39.5 | -0.01 | 0.040 | 43.7 | 0.04 | 0.772 | 88.8 | 0.11 | 0.648 | 155 | 0.22 | 0.639 | 61.1 | 0.17 | 0.875 |
| O-Biochar | 3.5 | 25.3 | 0.05 | 0.172 | 21.2 | -0.06 | 0.527 | 19.4 | 0.04 | 0.239 | 24.4 | 0.02 | 0.026 | 39.2 | 0.26 | 0.254 | 103 | 0.35 | 0.080 | 34.7 | 0.19 | 0.644 |
| PAC | | 31.8 | 0.02 | 0.008 | 31.6 | 0.03 | 0.014 | 33.8 | 0.01 | 0.001 | 31.8 | 0.07 | 0.161 | 74.5 | 0.08 | 0.696 | 140 | 0.25 | 0.621 | 43.1 | 0.11 | 0.727 |
| N-Biochar | | 24.5 | -0.29 | 0.732 | 53.8 | 0.06 | 0.896 | 52.3 | 0.06 | 0.864 | 54.6 | 0.08 | 0.874 | 127 | 0.15 | 0.968 | 42.7 | -0.02 | 0.886 | 19.0 | -0.39 | 0.752 |
| O-Biochar | 7.0 | 18.4 | -0.11 | 0.004 | 46.0 | 0.15 | 0.207 | 42.6 | 0.18 | 0.210 | 42.3 | 0.15 | 0.218 | 103 | 0.19 | 0.738 | 33.4 | -0.21 | 0.027 | 14.6 | -0.13 | 0.007 |
| PAC | | 15.8 | -0.14 | 0.332 | 39.9 | 0.03 | 0.345 | 43.7 | 0.07 | 0.882 | 35.4 | 0.03 | 0.639 | 114 | 0.16 | 0.943 | 42.6 | -0.15 | 0.837 | 8.3 | 0.03 | 0.086 |
| N-Biochar | | 1.7 | 0.57 | 0.818 | 73.7 | 0.13 | 0.862 | 33.3 | -0.11 | 0.582 | 72.5 | 0.16 | 0.886 | 124 | 0.14 | 0.929 | 26.7 | -0.19 | 0.733 | 4.7 | 0.13 | 0.160 |
| O-Biochar | 10.5 | 0.4 | 1.05 | 0.961 | 54.3 | 0.08 | 0.804 | 13.3 | -0.00 | 0.000 | 50.2 | 0.07 | 0.696 | 67.5 | 0.06 | 0.806 | 6.14 | 0.06 | 0.100 | 2.7 | 0.13 | 0.157 |
| PAC | | 0.7 | 0.79 | 0.909 | 57.2 | 0.11 | 0.838 | 27.0 | -0.10 | 0.185 | 48.1 | 0.12 | 0.902 | 115 | 0.15 | 0.936 | 16.1 | -0.06 | 0.100 | 2.1 | 0.28 | 0.426 |

Unit of $K_F$ : $(mg/g)/(mg/L)^{1/n}$
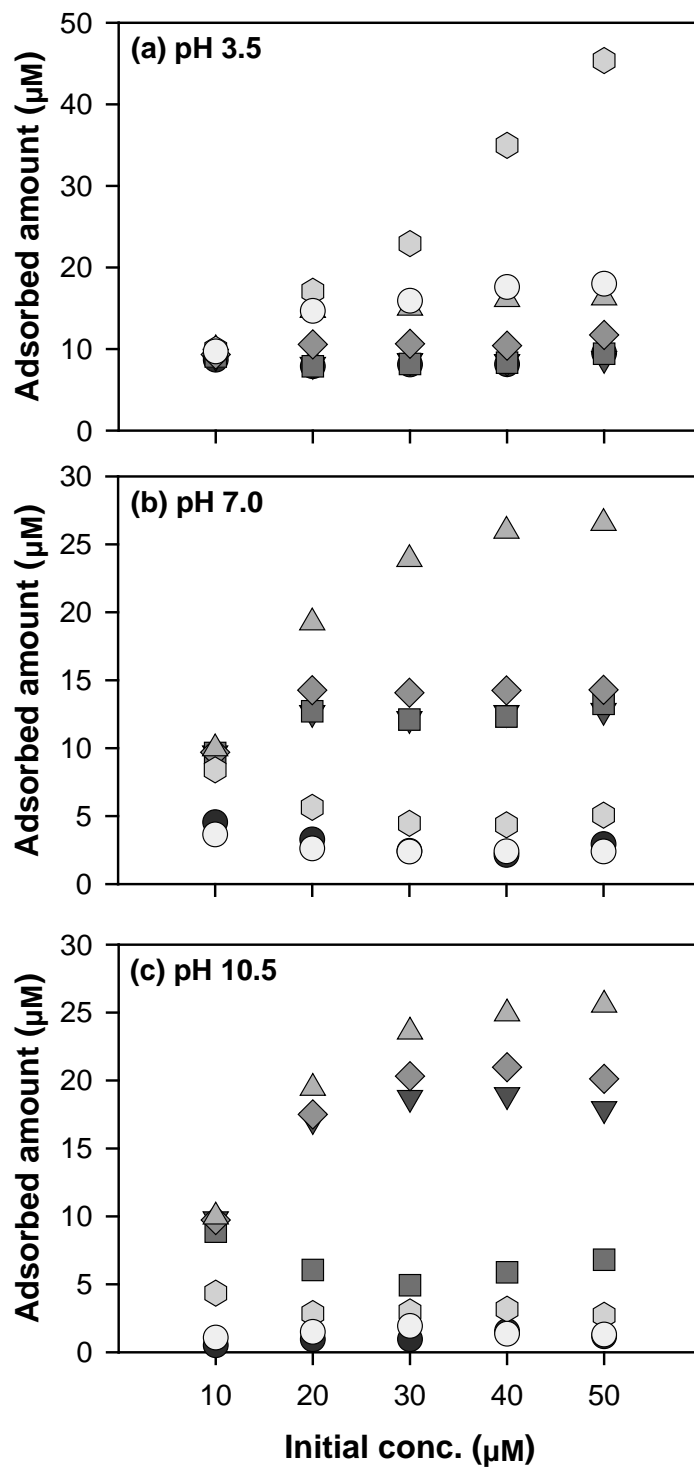
**Figure 5.9** Limited adsorbed adsorbates as a function of various initial concentrations (SMX (●); CBM (▼); BPA (■); ATR (◆); EE2 (△); DCF (⬡); IBP (○)) onto 50 mg/L of N-biochar; (a) pH 3.5; (b) pH 7.0; (c) pH 10.5 ($C_0$ = 10 – 50 μM, equilibrium contact time = 7 d at 20 °C).

82

The linear Fruendlich isotherm of EE2 in Figure 5.8 implies that EE2 allowed multi-layer adsorption to other competitors in terms of additional hydrogen bonding, which facilitated interactions among competitors. IBP performed similarly to the dissociable and hydrophobic pattern of DCF. Lower $\pi$-energy allowed stronger $\pi$-$\pi$ EDA interactions in conjunction with hydrophobic interactions under acidic conditions; however, the former was negligible when hydrophobicity decreased sharply. ATR displayed a stable adsorption capacity toward the adsorbent under neutral and basic conditions, while it was suppressed by more hydrophobic competitors, DCF, IBP and EE2, under acidic conditions. Although the hydrophobicity of ATR was intermediate among the competitors, its lower $\pi$-energy and smaller size encouraged $\pi$-acceptors to interact with $\pi$-donors on the adsorbent, which caused a $\pi$-$\pi$ EDA interaction and alleviated both the sieving effect and size-exclusion and allowed occupation of the adsorption site on the micropores (Dennington et al. 2003).

The hydrophobicity of CBM was steady over a wide range of pH values due to its high p$K_a$ 13.96, as was ATR (p$K_a$ 14.48). This property was scarcely exhibited under conditions of coexistence with higher hydrophobic adsorbates under acidic conditions, while the relatively higher hydrophobicity resulted in strong adsorption with constant removal efficiency. The adsorption of BPA was determined to have a similar pattern to that of CBM, which was correlated with hydrophobicity, while having a slightly higher hydrophobicity than ATR and CBM with a polarity derived from two hydroxyl functional groups occupying the adsorption sites at which ATR and CBM were located under lower initial concentrations (< 20 $\mu$M) (Figure 5.9(c)). SMX exhibited inferior adsorption by virtue of its low hydrophobicity and $\pi$-energy, while the amino functional group and

83

N-heteroaromatic rings of neutral SMX contributed to $\pi$-$\pi$ EDA interactions under acidic conditions (Sun et al. 2010).

Another competitive adsorption was conducted in the presence of NOM. NOM adsorption on the adsorbent was negligible in this study. Several explanations include competition against occupying active adsorption sites and hydrophobic interaction between EDCs/PhACs and NOM. A slightly diminished adsorption capacity of chemicals was observed in the presence of NOM (Figure 5.10). This explains how NOM failed not only to occupy the adsorption sites on the adsorbent, but also to interact with adsorbates in the solution, except for atrazine. NOM reduced atrazine adsorption to 34–35% under no-adsorbent conditions; this was derived from precipitation with a hydrophobic interaction between the heterocyclic aromatic ring (1,3,5-triazine) and NOM and direct site competition and pore blockage due to the small size of Atrazine (Dennington et al. 2003). Nonetheless, the predominant adsorption capacity of hydrophobic adsorbates on adsorbent was prevalent while NOM disperses not only particles (Aydin and Aksoy 2009), but also the molecules (Konradt Moraes et al. 2008) in the solution or instigates ionization through interactions with diverse functional groups on NOM.

### 5.3.6. Adsorption kinetics on adsorbents

Adsorption kinetics are often controlled simultaneously by film diffusion and intra-particle diffusion (Hui Qiu 2009). However, the adsorption kinetics in the current study were complex due to both the mixture conditions and desorption of compounds with weak adsorption bonding energy. Both diffusion theories barely applied to the kinetics in this study, except for the initial reaction. Thus, the tendencies of adsorption capacity and rates to reach the equilibrium concentration were investigated using the pseudo second

84
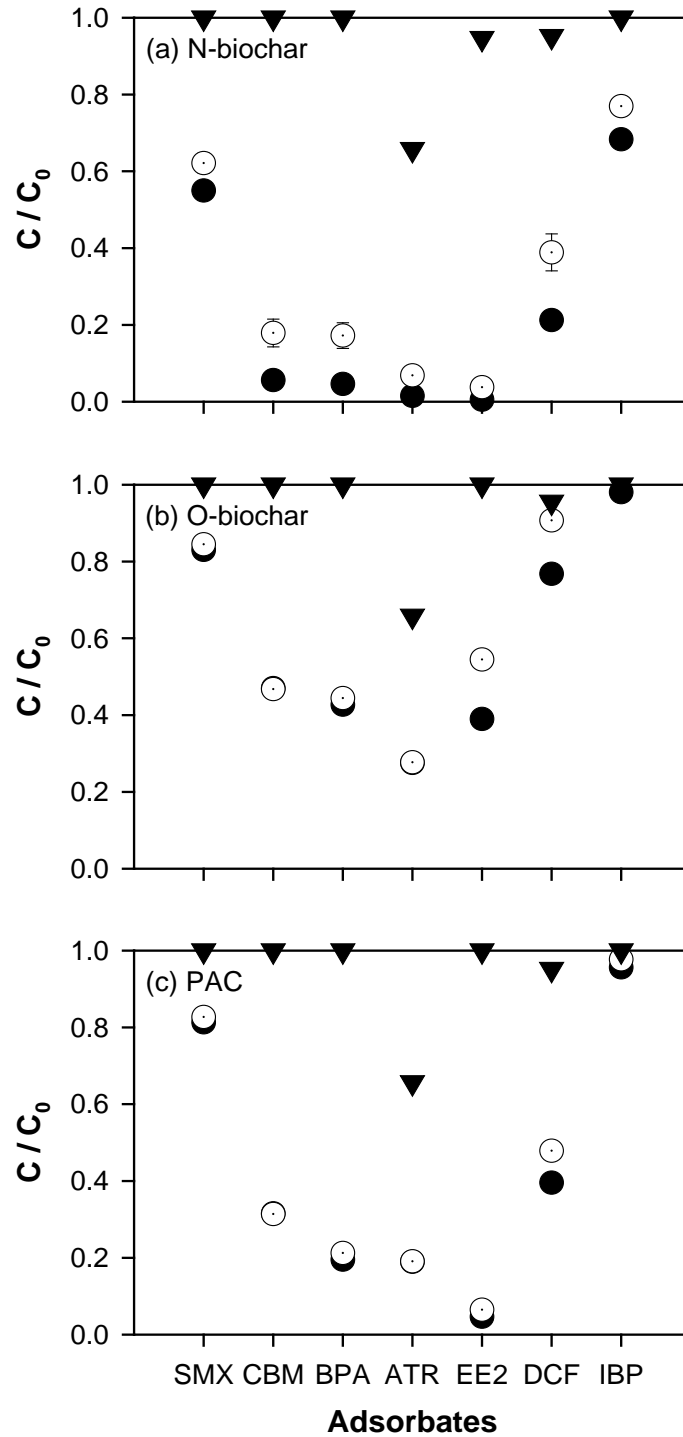
**Figure 5.10** Plot for NOM inhibition effect on EDCs/PhACs adsorption; in the presence (●) or absence ( ☐ ) of humic acid, and only interaction between adsorbates and humic acid without adsorbent (▼), ($C_0$ = 10 μM; humic acid = 5 mg/L; adsorbent dose = 50 mg/L; pH = 7.0 at 20 °C).

85

order model (Figures 5.11 and 5.12, and Table 5.6). This well-fit pseudo second-order model implies that the rate limiting step is chemical adsorption involving electronic forces through the sharing or exchange of electrons between the adsorbent and ionized species as a function of electron donor or acceptor, respectively, regardless of equilibrium concentrations (Hui Qiu 2009). Therefore, π–π bonding and hydro-bonding interactions should be considered to evaluate the competitive adsorption in the mixture. The aromatic rings in all seven EDCs/PhACs and adsorbents form a π-system and enable π–π interactions.

Due to the π-energy, calculated by the Huckel method (Table 5.1) (Cioslowski 1988), smaller π-energy is more reactive with higher π-energy at the atomic location (Shaik et al. 2001); the graphite form of carbonaceous adsorbents (biochars and PAC) in the order of π–π interactions was determined to be IBP > EE2 > ATR > BPA > CBM > SMX > DCF. This property correlates with adsorption capacity for hydrophobic compounds (EE2 > ATR > BPA > CBM), while that of dissociated compounds was negligible. Moreover, the steady and faster kinetic adsorption of predominantly hydrophobic compounds would occupy active pore sites so that fewer hydrophobic or ionized molecules would have the opportunity to occupy those sites.

## 5.4. Conclusions

Biochars used in this study were produced at 300 °C under controlled thermal process, which resulted in great physicochemical properties for adsorption to reduce the micro-pollutants. This controlled thermal process to produce biochar under oxygen-limited condition with simple activation allowed higher surface area and condensed aromatic carbon structure to contribute better adsorption performance. In addition, this controlled
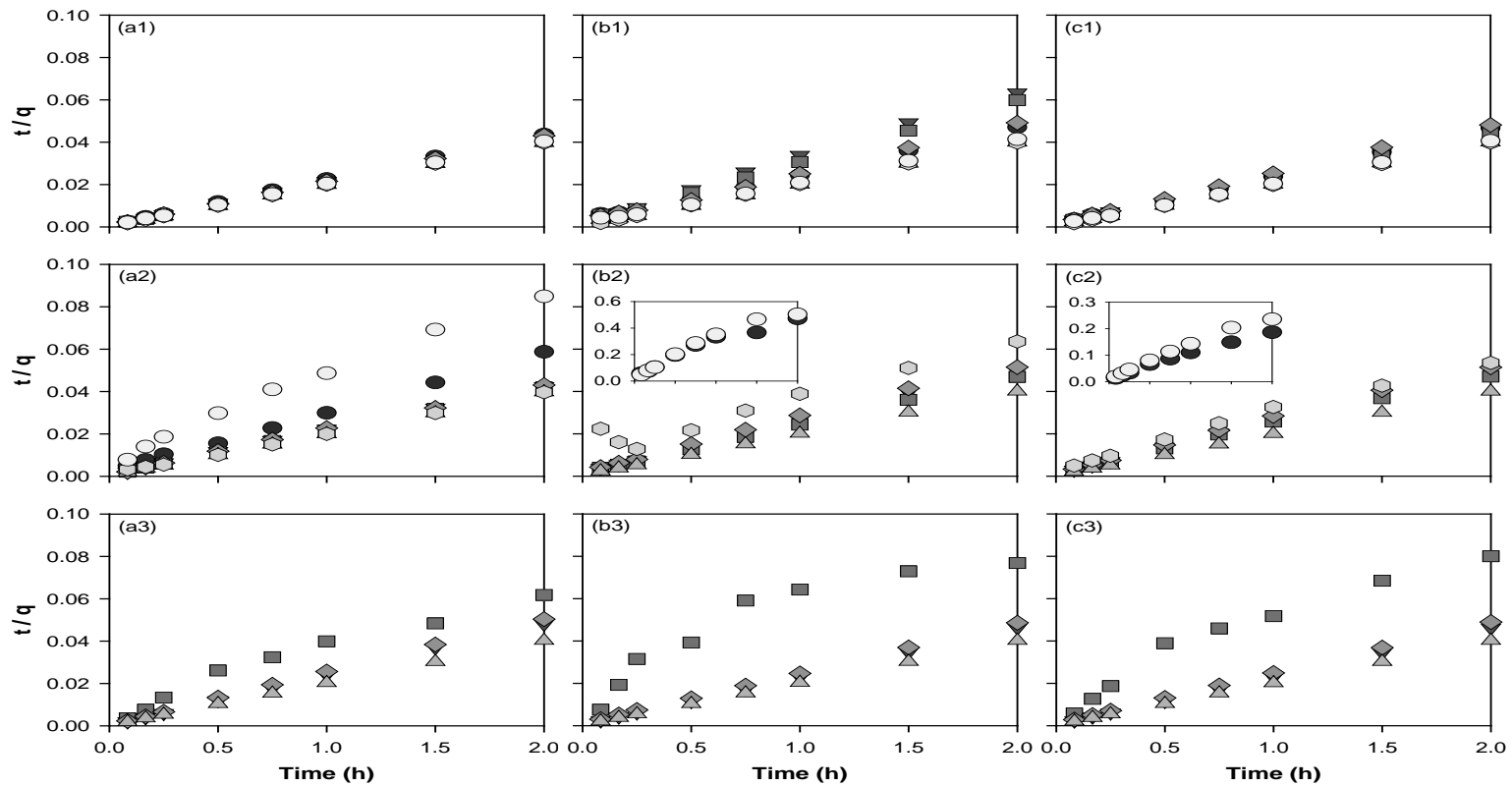
**Figure 5.11** Plots of pseudo second-order kinetic model ($\frac{t}{q_t} = \frac{1}{k_2 q_e^2} + \frac{1}{q_e}$) for EDCs and PhACs (SMX (●); CBM (▼); BPA (■); ATR (◆); EE2 (▲); DCF (◓); IBP (◯)) adsorption onto N-Biochar (a), O-Biochar (b), and PAC (c) at various pH conditions, (3.5 (a1, b1, c1); 7.0 (a2, b2, c2); 10.5 (a3, b3, c3)) ($C_0$ = 10 μM; adsorbent dose = 50 mg/L at 20 °C, $q_t$: amount of EDCs/PhACs adsorbed (mg/g) at time $t$, $k_2$: rate constant (g/hr·mg) of pseudo-second-order model, $q_e$: amount of EDCs/PhACs adsorbed (mg/g) at equilibrium).
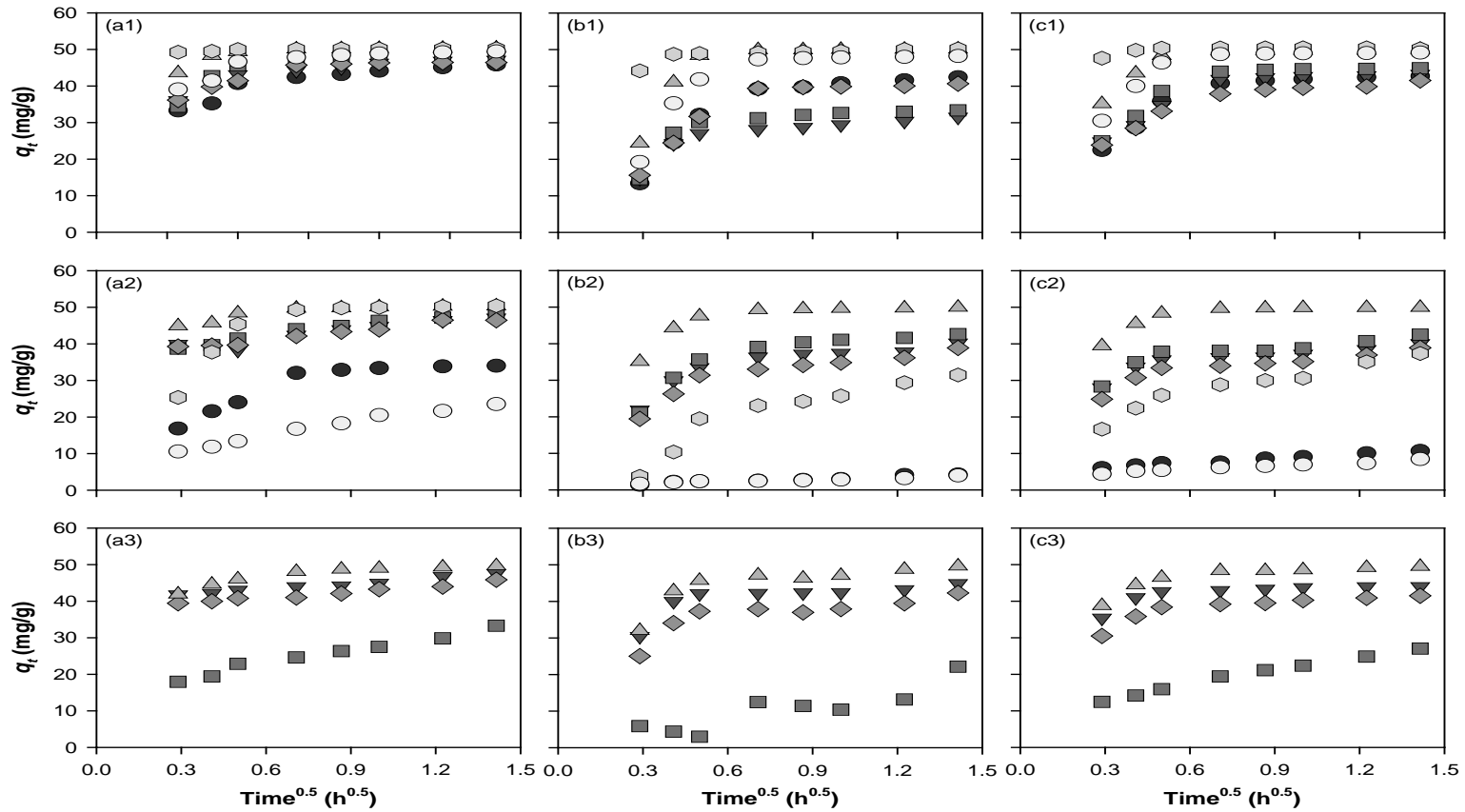
**Figure 5.12** Plots of intra-particle diffusion model ($q_t = k_p \cdot t^{0.5}$) for EDCs and PhACs (SMX (●); CBM (▼); BPA (■); ATR (◆); EE2 (▲); DCF (⬡); IBP (◯)) adsorption onto N-biochar (a), O-biochar (b), and PAC (c) at various pH conditions, (3.5 (a1, b1, c1); 7.0 (a2, b2, c2); 10.5 (a3, b3, c3)) ($C_0 = 10$ μM; adsorbent dose = 50 mg/L at 20 °C, $q_t$: amount of EDCs/PhACs adsorbed (mg/g) at time $t$, $k_p$: rate constant (mg/g h$^{0.5}$) for intra-particle diffusion).

**Table 5.6** Kinetic parameters for pseudo second-order and intra-particle diffusion models at various pH conditions.

**Pseudo second-order model**

Unit: $q_e$ (mg/g); $k_2$ (g/mg h)

| Adsorb-ent | pH | SMX | | | CBM | | | BPA | | | ATR | | | EE2 | | | DCF | | | IBP | | |
|---|---|---|---|---|---|---|---|---|---|---|---|---|---|---|---|---|---|---|---|---|---|---|
| | | $q_e$ | $k_2$ | $R^2$ | $q_e$ | $k_2$ | $R^2$ | $q_e$ | $k_2$ | $R^2$ | $q_e$ | $k_2$ | $R^2$ | $q_e$ | $k_2$ | $R^2$ | $q_e$ | $k_2$ | $R^2$ | $q_e$ | $k_2$ | $R^2$ |
| N-Biochar | | 46.7 | 0.455 | 1.000 | 47.8 | 0.636 | 1.000 | 18.6 | 0.917 | 1.000 | 47.2 | 0.848 | 1.000 | 50.6 | 2.539 | 1.000 | 50.3 | 10.85 | 1.000 | 50.1 | 0.801 | 1.000 |
| O-Biochar | 3.5 | 45.6 | 0.169 | 0.997 | 32.4 | 0.400 | 0.999 | 34.5 | 0.472 | 0.999 | 43.1 | 0.237 | 0.998 | 51.5 | 0.491 | 0.999 | 50.4 | 1.838 | 1.000 | 50.4 | 0.286 | 0.998 |
| PAC | | 44.4 | 0.336 | 0.999 | 44.9 | 0.352 | 0.999 | 46.4 | 0.406 | 0.999 | 42.6 | 0.322 | 0.999 | 50.6 | 0.950 | 1.000 | 50.4 | 33.75 | 1.000 | 50.2 | 0.643 | 1.000 |
| N-Biochar | | 35.9 | 0.302 | 0.999 | 47.9 | 0.414 | 0.999 | 48.4 | 0.510 | 1.000 | 47.3 | 0.470 | 0.999 | 50.7 | 1.574 | 1.000 | 52.0 | 0.373 | 0.999 | 25.2 | 0.192 | 0.993 |
| O-Biochar | 7.0 | 4.6 | 0.699 | 0.950 | 40.8 | 0.357 | 0.998 | 44.0 | 0.315 | 1.000 | 39.6 | 0.262 | 0.997 | 50.6 | 0.908 | 1.000 | 39.3 | 0.053 | 0.950 | 4.0 | 1.050 | 0.955 |
| PAC | | 11.1 | 0.591 | 0.990 | 40.3 | 0.498 | 0.999 | 42.8 | 0.413 | 0.998 | 39.2 | 0.383 | 0.998 | 50.4 | 1.416 | 1.000 | 38.9 | 0.162 | 0.992 | 8.6 | 0.753 | 0.986 |
| N-Biochar | | - | - | - | 41.2 | 2.216 | 1.000 | 34.1 | 0.138 | 0.961 | 39.8 | 1.424 | 1.000 | 50.0 | 1.289 | 1.000 | - | - | - | - | - | - |
| O-Biochar | 10.5 | - | - | - | 43.6 | 1.542 | 1.000 | 28.9 | 0.062 | 0.847 | 42.2 | 0.458 | 1.000 | 50.3 | 0.847 | 1.000 | - | - | - | - | - | - |
| PAC | | - | - | - | 43.8 | 1.614 | 1.000 | 26.4 | 0.133 | 0.945 | 41.8 | 0.552 | 1.000 | 50.3 | 0.919 | 1.000 | - | - | - | - | - | - |

**Intra-particle diffusion model**

Unit: $k_i$ (mg/g h$^{0.5}$)

| Adsorb-ent | pH | SMX | | CBM | | BPA | | ATR | | EE2 | | DCF | | IBP | |
|---|---|---|---|---|---|---|---|---|---|---|---|---|---|---|---|
| | | $k_i$ | $R^2$ | $k_i$ | $R^2$ | $k_i$ | $R^2$ | $k_i$ | $R^2$ | $k_i$ | $R^2$ | $k_i$ | $R^2$ | $k_i$ | $R^2$ |
| N-Biochar | | 23.0 | 0.871 | 19.0 | 0.836 | 28.3 | 0.769 | 22.3 | 0.989 | 14.1 | 0.723 | 2.1 | 0.850 | 21.9 | 0.856 |
| O-Biochar | 3.5 | 60.6 | 0.935 | 29.3 | 0.725 | 35.9 | 0.683 | 56.4 | 0.963 | 57.1 | 0.745 | 10.1 | 0.566 | 63.5 | 0.849 |
| PAC | | 44.0 | 0.938 | 41.5 | 0.989 | 45.6 | 0.944 | 33.6 | 0.971 | 32.9 | 0.790 | 6.1 | 0.659 | 42.2 | 0.834 |
| N-Biochar | | 35.9 | 0.997 | 6.8 | 0.391 | 13.2 | 0.984 | 7.0 | 0.855 | 12.2 | 0.910 | 55.2 | 0.858 | 15.0 | 0.992 |
| O-Biochar | 7.0 | 2.5 | 0.745 | 33.0 | 0.861 | 41.34 | 0.865 | 31.7 | 0.837 | 31.5 | 0.778 | 47.0 | 0.895 | 1.8 | 0.824 |
| PAC | | 3.6 | 0.832 | 18.2 | 0.734 | 21.8 | 0.712 | 20.5 | 0.751 | 23.1 | 0.806 | 28.2 | 0.907 | 4.1 | 0.961 |
| N-Biochar | | - | - | 5.6 | 0.971 | 16.6 | 0.919 | 3.8 | 0.853 | 14.3 | 0.954 | - | - | - | - |
| O-Biochar | 10.5 | - | - | 25.1 | 0.631 | 16.5 | 0.487 | 28.3 | 0.712 | 33.0 | 0.726 | - | - | - | - |
| PAC | | - | - | 16.4 | 0.686 | 16.8 | 0.998 | 19.6 | 0.781 | 21.4 | 0.838 | - | - | - | - |

thermal process also provides efficient adsorbent, less product waste, and energy source simultaneously under tangible economical beneficial in terms of biofuel by-product use. In real aquatic environments, exposure to EDCs/PhACs occurs in either a neutral or dissociated form, resulting in specific competitive adsorption characteristics. Determination of physicochemical properties of these organic compounds; hydrophobicity, polarity, $\pi$-energy, and molecular size, and that of adsorbent; aromaticity, polarity, ash content, surface area, and the pore volume, provided better understanding of reduction of adsorbates in the aquatic system through adsorption process. Characterization of adsorbents via NMR analysis improved the interpretation of the structure and properties and allowed objective comparisons among adsorbents. Through this study, the importance of analysis both adsorbate and adsorbent is described under various attraction mechanisms and probabilities. This fundamental fate of selected micro-pollutants and an understanding of the adsorption system in biochar contribute to not only improving the removal efficiency of adsorbents, but also preventing exposure to harmful chemicals under more complex environmental conditions.

# CHAPTER 6

## COMPETITIVE ADSORPTION OF SELECTED NON-STEROIDAL ANTI-INFLAMMATORY DRUGS ON ACTIVATED BIOCHAR: EXPERIMENTAL AND MOLECULAR MODELING STUDY[3]

**Abstract**

The adsorption of targeted non-steroidal anti-inflammatory drugs: diclofenac (DCF), naproxen (NPX), and ibuprofen (IBP)) by two types of activated biochar (N-/O-biochar) produced in the lab was studied in single- and multi-solute adsorption experiments in conjunction with molecular modeling. The carbonaceous structure of the biochars was elucidated via nuclear magnetic resonance and the intensity of the interactions between the solute and adsorbent was also determined. Using fractions of the carbonaceous functional group on the adsorbent for the single-solute adsorption, the overall binding energies were determined to be in the order of DCF > NPX > IBP (-21.8 > -17.5 > -14.1 kcal/mol for N-biochar and -21.2 > -17.3 > -14.2 kcal/mol for O-biochar). A strong interaction between the DCF and the adsorbent resulted in the occupation of effective adsorption sites as compared to other solutes, while blocking the pores in which smaller sized NPX and IBP that may have been adsorbed.

---

[3] Jung *et al.*, Submitted to Chemical Engineering Journal (in review).

## 6.1. Introduction

Environmental biochar is a byproduct from the pyrolytic processing of biomass. Its presence significantly improves not only mechanical features of industrial materials, but also chemical properties of soil. It is also plays a critical role in environmental remediation of soil and water by acting as an adsorbent for natural organic matters and trace organic compounds (Ni, Pignatello, and Xing 2011). These potentialities are controlled by feedstock source and pyrolytic profiles (time, temperature, and gasfication). The carbon and ash content are governed by the feedstock (livestock manure > plant > wood ) (Novak et al. 2009) and the condensed aromatic carbon (400 to 700 °C) as well as the fraction of functional groups (250 to 400 °C) are governed by the pyrolysis temperature (Chen, Zhou, and Zhu 2008).

Non-steroidal anti-inflammatory drugs (NSAIDs) are often prescribed for the treatment of headaches, arthritis, ankylosing, spondylitis, sports injuries, and menstrual cramps. In fact, they are one of the most prescribed pharmaceuticals. Unfortunately, NSAIDs often pass through the patients' digestive system and eventually made their way to water systems via incomplete treatment of human waste. NSAIDs have been detected in trace to considerable levels in the environment (Benotti et al. 2008b), and they are known to cause significant renal, degenerative, and necrotic changes on vertebrates (Treadgold et al. 2012). Therefore it is critical to study and understand their fates in order to develop effective treatment and mitigation strategies (Packer et al. 2003).

Adsorption has been considered as an efficient treatment strategy for organic contaminants in aqueous environment. The use of carbon nanotubes and activated carbons in this strategy has garnered significant attention due to their high-binding energy and inducement of hydrophobic interaction (Salloum and Schlenoff 2004). However, these approaches are insufficient to reveal the adsorption mechanism due to their diversity and intricateness. Therefore, it is required to investigate the additional adsorption mechanisms toward chemicophysical properties of both adsorbent and adsorbate. Consideration of the accessibility of the adsorptive sites and pore size of adsorbent in order to minimize the size-exclusion effect and desorption is able to ensure the adsorption mechanism influenced and crucial role in competitive adsorption by characteristics of adsorbent (Yang et al. 2006).

It is hypothesized that the adsorption of NSAIDs onto activated biochar is related to the binding of NSAIDs onto the surface of the adsorbent at the molecular level. Therefore molecular level simulation of the adsorption process can potentially provide valuable mechanistic insight into the adsorption strength differences between different NSAIDs and various char surface functional groups. Various computational techniques have been employed to study the physisorption of different chemicals onto graphene (Cortés-Arriagada, Sanhueza, and Santander-Nelli 2013), single-walled carbon nanotubes, and multi-walled carbon nanotubes (Boateng et al. 2013). However, molecular level studies involving adsorption of chemicals onto biochar has not been explored. This is probably due to the difficulty in generating the exact molecular structure of the char. Previous work by our research group reported the interaction energy associated with the

adsorption of atrazine onto hydrochar (Flora et al. 2013). In that study, it was found that atrazine was more strongly adsorbed to surfaces without weakly associated alkyl groups.

In this study, the adsorption of three NSAIDs; diclofenac (DCF), naproxen (NPX), and ibuprofen (IBP), onto representative biochar structures was investigated. More specifically we used dispersion-corrected density functional theory in single or competitive adsorptive conditions under consideration of conformation and chemical properties of both solute and adsorbent. Interaction energies between the NSAIDs and the biochar were also calculated to characterize the strength of adsorption and the effect of the various surface functional groups on the adsorption capacity of the char.

## 6.2. Materials and methods

### 6.2.1. Materials

Biochars produced by pyrolyzing torrefied loblolly pine chip ($15 \times 6$ mm) at 300 °C for 15 min were classified as either N-biochar or O-biochar in terms of pyrolysis with pure nitrogen or 7% oxygen with 93% nitrogen gas, respectively. Both biochars were activated by NaOH to increase the surface area and pore volume of the biochars. Here are detailed pyrolysis and activation procedures, described in the previous work (Jung, Heo, et al. 2013).

### 6.2.1.1. Biochar pyrolysis condition

3 grams of biomass were loaded in a porcelain boat and put into tube furnace. Tube furnace was preheated to target temperature (300 °C), and the sample-containing porcelain boat in loaded in the tube, but outside of the heating element to prevent the exposure to the heat. Sealed tube was purged with 1 L/min nitrogen to ensure the non-oxidative gas environment inside the furnace for N-biochar, while nitrogen with additional 7% oxygen (1

L/min) was purged in the furnace for O-biochar. The porcelain boat was loaded inside the preheated area, and held for 15 min. The boat was retracted outside the heating element, then cooled down to ambient temperature (samples were under continuous 1 L/min nitrogen flow inside the sealed tube during the pyrolysis). Samples were stored in a desiccator for further analysis.

### 6.2.1.2. Biochar activation

3 grams of sample (N-biochar and O-biochar) were soaked with 40 mL of 4 M NaOH solution, and incubated with shaking (15-min interval) for 2 hours at room temperature. NaOH-impregnated samples were filtered (Buchner filter funnel) to remove excess NaOH solution, and dried overnight at 105 °C oven. Dried samples were loaded in a porcelain boat and put into tube furnace. With continuous nitrogen flow (2 L/min), temperature was elevated with 3°C/min heating rate, and held for 2 hours at 800°C. The samples were cooled down to reach the ambient temperature with about 10 °C/min cooling rate. Activated samples were washed with 2 L of deionized water, followed by 100 mL of 0.1 M HCl solution, and then washed again with deionized water. Washed samples were dried overnight at 105 °C oven, and stored in a desiccator for further analysis.

Biochars were milled and passed through a 200-mesh (74-µm) sieve, and then stored with ultrapure water (2000 mg/L) for 24 h as a stock solution to hydrate before use. Three NSAIDs (DCF, NPX, and IBP) and acetonitrile were purchased from Sigma-Aldrich (St. Louis, MO, USA). Their detailed physicochemical properties are provided in the Supporting Information (Table 6.1). A 10 mM stock solution for each NSAID was prepared with acetonitrile solution (anhydrous, 99.8%). The solution was diluted to a target NSAID concentration with ultrapure water after pre-evaporating a known amount of

NSAID to minimize any cosolvent effect. Ultrapure water produced by a Milli-Q water filtration system (Millipore, Billeriac, MA, USA) was used for the preparation of all solutions.
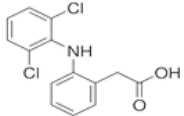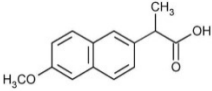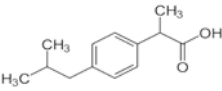
### 6.2.2. Adsorption Experiments.

A 20 µM of each pharmaceutical solution was added to 40-mL glass vials equipped with a polytetrafluoroethylene-lined screw cap, and then six known volumes (0.1 to 0.8 mL) of biochar stock solution were spiked for the production of a single-solute adsorption isotherm. The pH of the aqueous phase was adjusted to 7 with 1.0 M HCl and NaOH prior to the addition of the adsorbent. Following solute and adsorbent addition, the vials were shaken for 7 d under ambient conditions to achieve equilibrium. After equilibrium, each sample was filtered (0.22 µm) and concentrations of NSAIDS were analyzed using an Agilent 1100 series high-performance liquid chromatograph (Agilent technologies, Santa Clara, CA, USA). To produce competitive isotherms, bi- and tri-solute adsorption experiments were also performed, and the adsorption method was identical to that used to produce the single-solute isotherm, except for the addition of two or three solutes in the vials. All adsorption experiments were conducted in duplicate or triplicate.

### 6.2.3. Characterization of Adsorbents.

Elemental analysis of the adsorbent was performed on a PerkinElmer 2400 Series II CHNS/O Elemental analyzer (PerkinElmer, Waltham, MA, USA). The ash content was determined by heating the biochars to 750 °C and the oxygen content was calculated by subtracting the ash, and carbon, hydrogen and nitrogen contents from the total mass of the samples. Surface and pore characteristics were examined by gas adsorption using a Gemini VII 2390p surface area analyzer (Micromeritics, Norcross, GA, USA).

**Table 6.1** Physicochemical properties of the solutes used in this study.

| Compound (Formula) [ID] | Structure | MW (g/mol) | Log $K_{ow}$ | log $D_{ow}$[a] pH 7.0 | $pK_a$[a] | Water solubility[b] (mg/L) | Mol. polariz-ability[a] | $\pi$ energy[a] | Mol. dimen-sion (Å)[a] | Volume[a] (Å$^3$) |
|---|---|---|---|---|---|---|---|---|---|---|
| Diclofenac ($C_{14}H_{11}Cl_2NO_2$) [DCF] | | 296.2 | 4.26 | 1.55 | 4.15 | 2.37 [b] | 29.0 | 33.2 | L: 10.1 H: 4.8 W: 7.2 | 236.8 |
| Naproxen ($C_{14}H_{14}O_3$) [NPX] | | 230.3 | 2.99 | 0.32 | 4.19 | 15.9 [c] | 26.4 | 25.7 | L: 11.7 H: 5.6 W: 5.3 | 213.1 |
| Ibuprofen ($C_{13}H_{18}O_2$) [IBP] | | 206.3 | 3.84 | 1.82 | 4.52 | 21.0 [c] | 23.7 | 15.7 | L: 11.0 H: 4.3 W: 5.3 | 211.8 |

[a] Chemicalize.org by ChemAxon (http://www.chemicalize.org); [b] Fini. A. et al. (1986); [c] Yalkowsky. S. and Dannenfelser. R. (1992);

L, H, and W stand for the minimum value of a length, height, and width of molecule.

The total pore volume was calculated from the adsorbed quantity of $N_2$ at $P/P_0 =$ 0.95, and the surface area was determined by the Brunaer-Emmett-Teller (BET) equation with multipoint adsorption isotherms of $N_2$ at 77 K. Solid-state $^{13}C$ DP/MAS (direct polarization/magic angle spinning) nuclear magnetic resonance (NMR) spectra were acquired using a 3.2-mm MAS probe on a Varian Inova 500 spectrometer (Palo Alto, CA, USA). The $^{13}C$ NMR spectra combined with dipolar-recoupled NMR methods were used for quantitative structural analyses of the biochars. The detailed experimental conditions used for the NMR experiments are described elsewhere (Park et al. 2013).

### 6.2.4. Molecular Modeling for Solutes and Adsorbents.

The initial structures for seven representative biochar configurations were generated in Gaussview based on NMR surface functional group measurements and char structures proposed in the literature (Cao et al. 2011). The geometries of the biochar structures and NSAIDs were optimized using dispersion-corrected density functional theory (Grimme, Ehrlich, and Goerigk 2011) with the BLYP functional, and the 6-31++G(d,p) basis set in TeraChem (Kastner et al. 2009). The initial configurations for the biochar-NSAID complexes (BIO-DCF, BIO-NPX and BIO-IBP) were obtained by optimizing fragments of the biochar-NSAID complexes by following the geometry optimization procedures described in a previous study (Zaib et al. 2012). Competitive adsorption of the different NSAIDs onto the biochar surfaces was simulated by randomly locating the center of a competing NSAID molecule between 1.5 to 5 Å from the center of a fixed BIO-NSAID complex. A total of 10,000 optimized configurations were collected and the lowest-energy configurations that were representative of competitive adsorption were selected for further geometry optimization at the DFT-D/BLYP/6-31++G(d,p) level.

Aqueous phase adsorption energies were calculated using the SMD continuum solvation model implemented in GAMESS. Final solvated energy calculations for the complexes were performed at the DFT-D/BLYP/6-31++G(d,p) level, and the binding energies ($\Delta E$) between the biochar and the NSAIDs were calculated as:

$$\Delta E \ = \ E \ (BIO + NSAID) - E(BIO) - \ E(NSAID)$$

In the case of competitive adsorption, the binding energies between the biochar and the competing NSAIDs were calculated as:

$$\Delta E_C \ = \ E(BIO + NSAID^1 + \ NSAID^2) - E(BIO + NSAID^1) - \ E(NSAID^2)$$

where $\Delta E_C$ is the binding energy (kcal/mol) between the biochar and the $NSAID^2$ in the presence of a competitor $NSAID^1$. Binding energies between the NSAIDs and N-biochar and O-biochar were approximated based on the NMR surface functional group measurements.

## 6.3. Results and Discussion

### 6.3.1. Characterization of Biochars.

The ^{13}C NMR spectra and elemental composition of two different precursor biochars were markedly different. A quantitative spectral analysis for ^{13}C DP/MAS NMR revealed that both aromatic and aryl carbon (108-148 ppm) were dominant in N-biochar and O-biochar, while N-biochar was composed of higher aliphatic carbon; alkyl (0-45 ppm), methoxyl (45-63 ppm), carbohydrate (63-108 ppm), and carboxyl carbons (165-187 ppm). This indicated that N-biochar had a higher surface polarity than O-biochar, whereas

99

O-biochar contained more aromatic carbon than N-biochar, with higher peak values (Figure 6.1 and Table 6.2). More condensed aromatic carbon, as indicated by the higher fraction of non-protonated carbon in O-biochar than in N-biochar, was analyzed by the $^{13}$C DP/MAS and dipolar dephasing experiments (Table 6.3). The increased aromaticity of O-biochar resulted from the supplemental combustion between alkyl carbons and oxygen, which produced additional heat in the pyrolysis process (Drnevich et al. 2006). A higher pyrolysis temperature produced a higher carbon content, an aromatic carbon fraction with a more condensed cluster, and a higher surface area, while it produced a lower biochar yield, and low oxygen and ash contents (Chen, Zhou, and Zhu 2008). This additional heat resulted in not only an increased aromaticity but also lower ash content in O-biochar (Table 6.2).
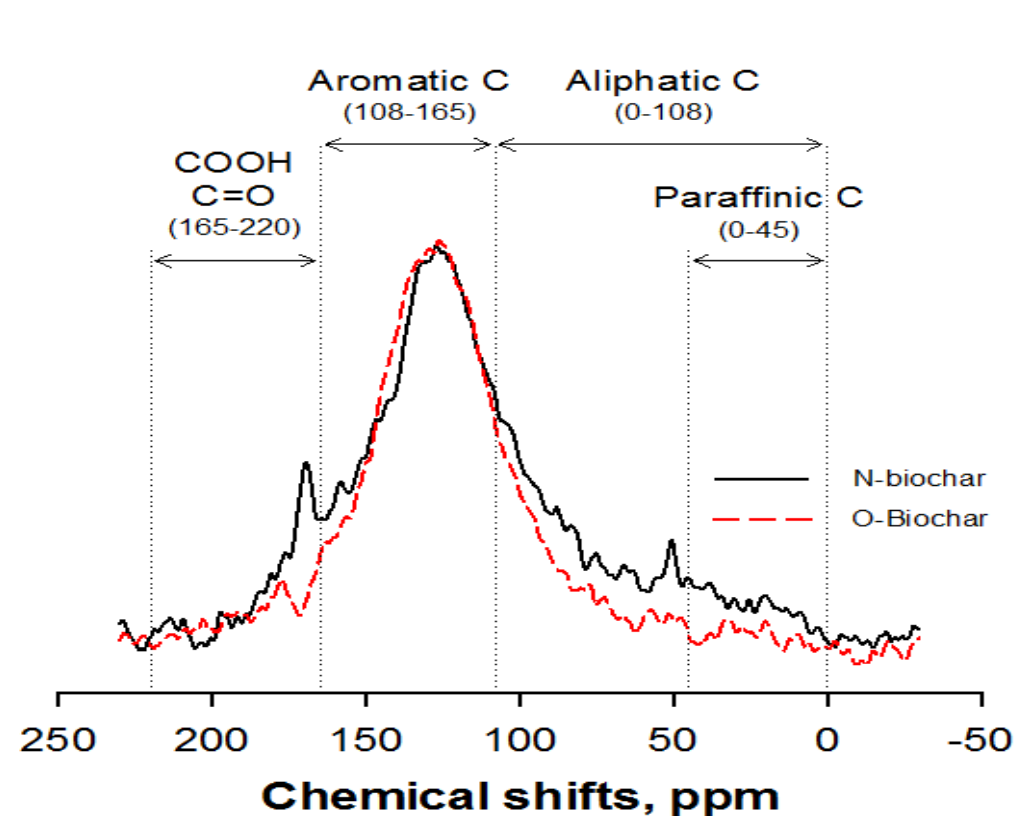


**Figure 6.1** Solid-state $^{13}$C DP/MAS NMR spectra (solid line) for N-/O-biochars.

100

**Table 6.2** Properties of activated biochars.

Elemental composition, aromatic ratio, ash content, BET-N$_2$ surface area (SA-N$_2$), and cumulative pore volume of biochars

| Samples | C (%) | H (%) | N (%) | O (%) | H/C | Polarity index | | Ash (%) | SA-N$_2$ (m$^2$/g) | Pore volume (cm$^3$/g) | |
|---|---|---|---|---|---|---|---|---|---|---|---|
| | | | | | | N/C | O/C | | | micro-pore | macro-pore |
| N-biochar | 72.6 | 0.77 | 0.65 | 21.3 | 0.127 | 0.001 | 0.221 | 4.7 | 1360 | 0.307 | 0.643 |
| O-biochar | 83.8 | 0.24 | 0.30 | 13.0 | 0.034 | 0.003 | 0.116 | 2.7 | 1151 | 0.313 | 0.318 |

Quantitative spectral analysis for solid-state $^{13}$C DP/MAS NMR for biochars (calculated based on 100% carbon in each biomass)

| Samples | Aliphatic C (%) | | | Aromatic C (%) | | Carbonyls (%) | | Aliphatic C (%) | Aromatic C (%) | Aromati-city (%)[a] | Polar C (%)[b] |
|---|---|---|---|---|---|---|---|---|---|---|---|
| | Alkyl 0–45 ppm | Methoxyl 45–63 ppm | Carbo-hydrate 63–108 ppm | Aryl 108–148 ppm | O-aryl 148–165 ppm | Carboxyl 165–187 ppm | Carbonyl 187–220 ppm | | | | |
| N-biochar | 7.14 | 4.81 | 21.5 | 45. 7 | 9.91 | 8.22 | 2.79 | 33.5 | 55.6 | 62.5 | 47.2 |
| O-biochar | 2.80 | 2.42 | 18.5 | 57.8 | 10.1 | 5.07 | 3.32 | 23.7 | 67.9 | 74.1 | 39.4 |

[a] Aromaticity = aromatic C (108–165 ppm) / [ aliphatic C (0–108 ppm) + aromatic C (108–165 ppm)];

[b] Total polar carbon = (45-108 ppm) + (148-220 ppm)

**Table 6.3** Quantitative spectral analysis of solid-state $^{13}C$ DP/MAS NMR for biochars. The values were calculated based on 100% carbon in each biomass.

| Samples | Alkyls (%) | | | Aromatics (%) | | | Carbonyls (%) | | |
|---|---|---|---|---|---|---|---|---|---|
| | $CH_3$ 6-25 ppm | $CH_{1.5}$ 25-50 ppm | $HCO_{0.75}H_{0.5}$ 50-90 ppm | Non-protonated 90-145 ppm | Protonated 90-145 ppm | O-aryl $CO_{0.75}H_{0.5}$ 145-165 ppm | COO- 165-183 ppm | C=O 183-210 ppm | Aromati-city (%)[a] |
| N-biochar | 2.86 | 5.35 | 13.1 | 53.5 | 2.49 | 12.5 | 7.53 | 2.72 | 68.4 |
| O-biochar | 1.13 | 2.22 | 8.31 | 66.5 | 0.65 | 13.2 | 4.44 | 3.49 | 80.4 |

[a] Aromaticiy (%) = [aromatic carbon fraction] / [total carbon fraction.]

The 7% oxygen content available for pyrolysis in O-biochar resulted in partial combustion (Chen, Zhou, and Zhu 2008), which produced lower oxidation levels during chemical activation. In contrast, fully charred N-biochar allowed an enhancement of oxygen during activation, with a higher polarity on the surface of the material itself due to the accessible activated layers (Vinke et al. 1994). The examination of the pore structure of the biochars identified a reasonably large surface area and pore volume. More disordered structures provide more open and closed sectors on the biochar (Gustafsson et al. 2001; Braida et al. 2003). An adsorption facilitative open sector allows interaction with molecules in solution (Yang et al. 2006), and it was assumed that N-biochar, with twice as much marco-pore volume compared to O-biochar, would achieve a higher level of adsorption in this study. The more condensed aromatic carbon cluster in O-biochar mitigated the effect of chemical activation, resulting in less effective porous structural properties.

### 6.3.2. Interaction Energy.

The interactions between activated biochar and NSAIDs were mainly due to hydrophobic interactions and π–π electron donor–acceptor (EDA) interactions. Figure 6.2 and 6.3 show the optimized configurations of the biochar-NSAID complexes. DCF interacted more favorably than NPX and IBP with the biochar structures as a result of its larger molecular butterfly structure, which maximizes π-π interactions between the surface of the biochar and the solute. In its lowest energy configuration, DCF interacted with the biochar structures at a minimum distance of 3.5 Å, with one aromatic ring oriented parallel to the surface of the biochar and the other perpendicular to the adsorbent surface. The

103

simulation results were consistent with the experimental observations, where a higher fraction of DCF was adsorbed onto the biochar.

Interactions between biochar and NPX were more favorable than for IBP with one methyl group directed toward the surface of the adsorbents, although the carbohydrate functional group on the biochar was an exception with the carboxyl group of NPX oriented away from the biochar surface with a minimum intermolecular distance of 3.5 Å (Figure 6.2). The smaller molecular structure of IBP resulted in reduced π-π interactions and dispersion forces between the solute and adsorbent due to less surface area exposure to the biochar surface, which resulted in an overall reduction in the binding energies. Single-solute adsorption experiments however indicated preferential adsorption of IBP onto biochar, compared to DCF and NPX. This could be attributed to the higher dependence of IBP adsorption on a hydrophobicity effect, which was not fully captured in the simulations. The gas phase and implicit SMD simulations estimated binding energies on the basis of available molecular surface area and did not fully account for the hydrophobicity effect on the adsorption process.

The interaction energies associated with the binding of the NSAIDs onto N-biochar and O-biochar were estimated based on the percentage of carbon in each functional group. The results together with the energy contribution from the individual functional groups are presented in Figure 6.4 and Tables 6.4 and 6.5. Overall, the NSAIDs interacted more favorably with N-biochar than O-biochar despite the high aromaticity value of O-biochar. The high interaction strength of the NSAIDs with N-biochar can be attributed to its high BET-$N_2$ surface area, which has an overall greater impact on the adsorption capacity than the aromatic carbon fraction in the functional groups. A significant energy contribution
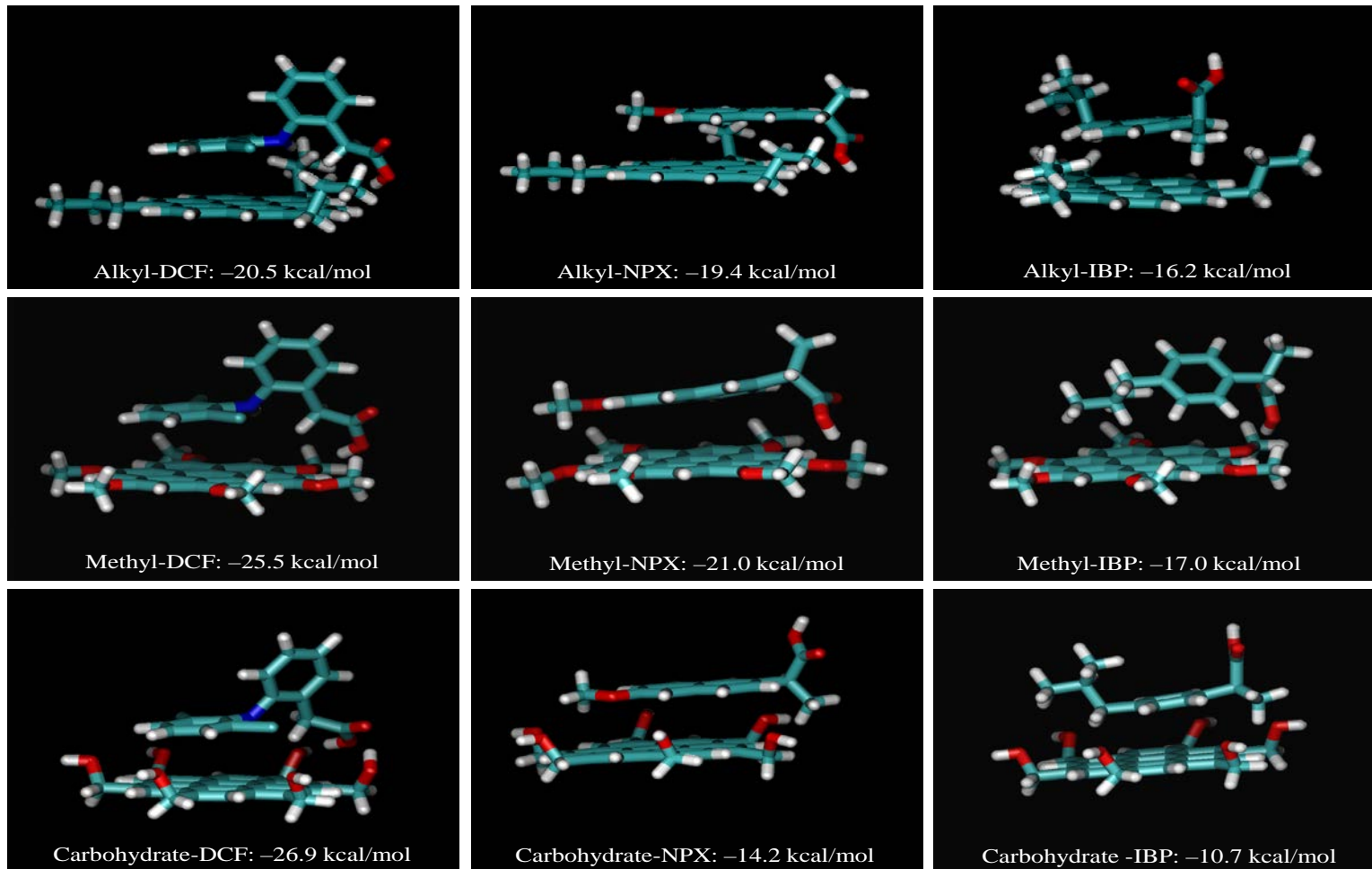
104

**Figure 6.2** BLYP-D3/6-31++G(d,p) optimized geometries of the biochar and BIO-NSAID complexes in single solute system.

**Figure 6.2** BLYP-D3/6-31++G(d,p) optimized geometries of the biochar and BIO-NSAID complexes in single solute system (continued).

Carboxyl-DCF: –22.8 kcal/mol     Carboxyl-NPX: –20.7 kcal/mol     Carboxyl -IBP: –14.6 kcal/mol

**Figure 6.2** BLYP-D3/6-31++G(d,p) optimized geometries of the biochar and BIO-NSAID complexes in single solute system (continued).

Carbohydrate-DCF-NPX: –22.2 kcal/mol

Carbohydrate-NPX-IBP: –10.3 kcal/mol

Aryl-IBP-NPX: –14.5 kcal/mol

Carbohydrate-NPX-DCF: –16.7 kcal/mol

Carbohydrate-IBP-NPX: –20.1 kcal/mol

Aryl -NPX-IBP: –15.3 kcal/mol
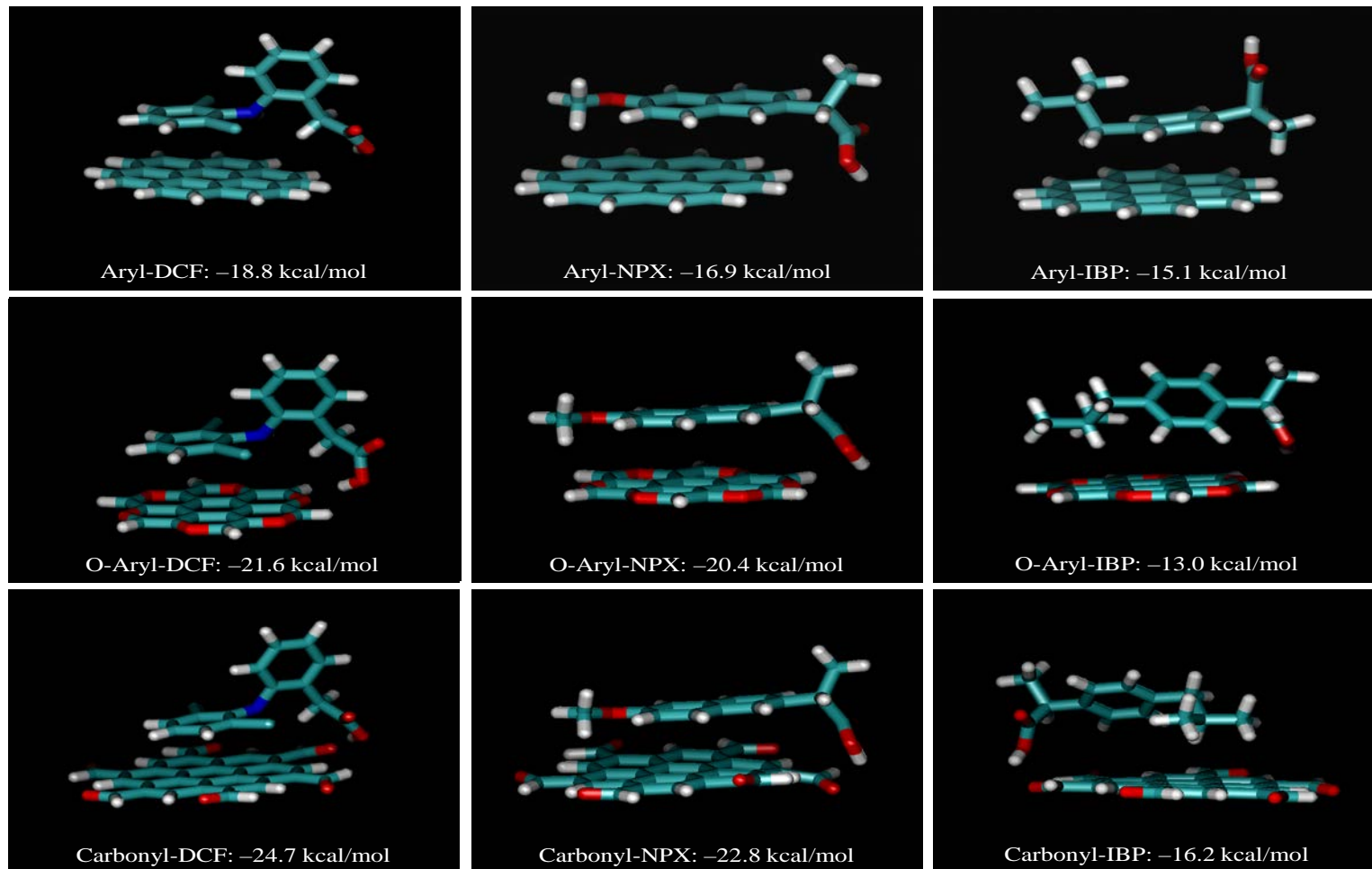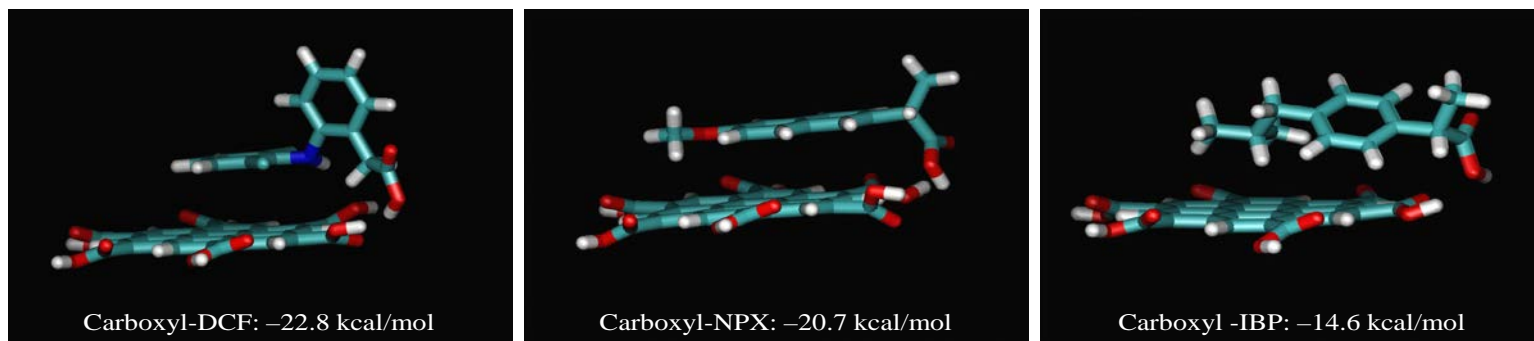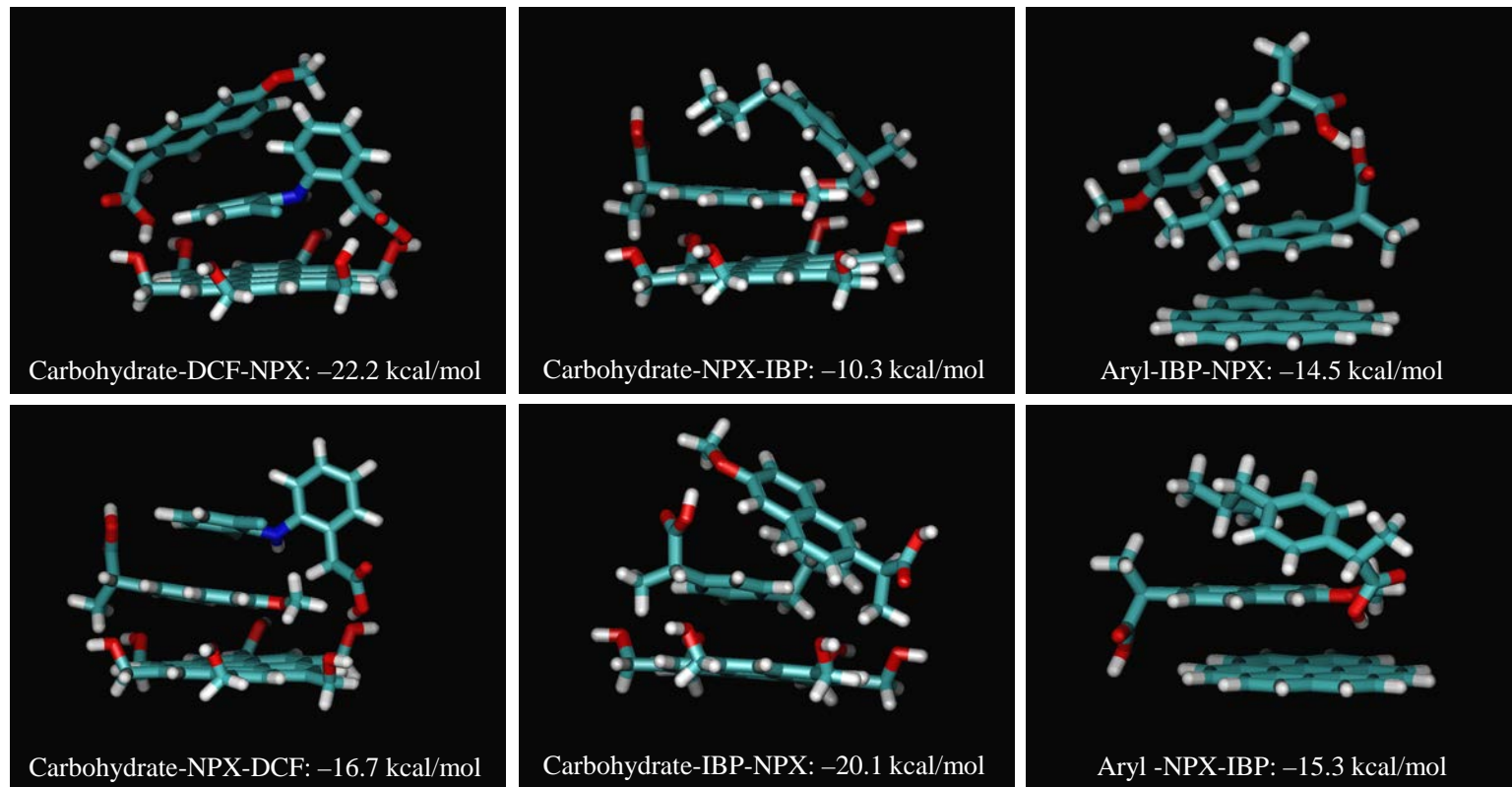
**Figure 6.3** BLYP-D3/6-31++G(d,p) optimized geometries of the biochar and BIO-NSAID complexes in bi-solute system.
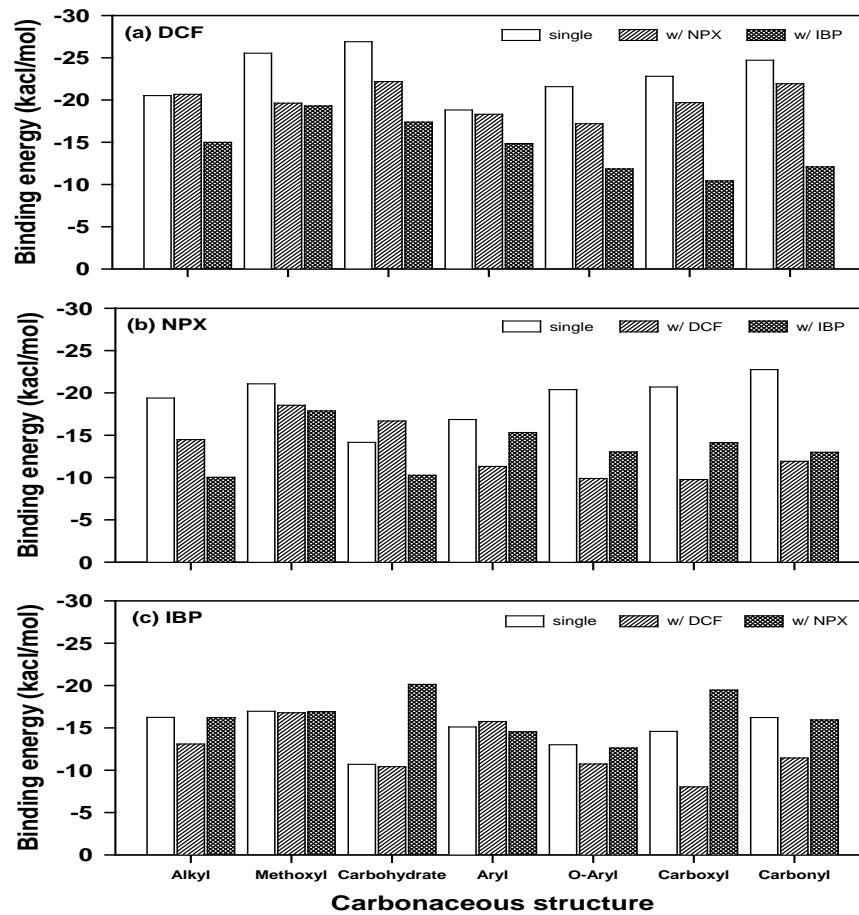
| (a.1) DCF overall binding energy (kcal/mol) | | |
|---|---|---|
| Competitor | N-biocahr | O-biochar |
| None | -21.8 | -21.2 |
| NPX | -19.5 | -19.2 |
| IBP | -14.9 | -14.8 |

| (b.1) NPX overall binding energy (kcal/mol) | | |
|---|---|---|
| Competitor | N-biocahr | O-biochar |
| None | -17.5 | -17.3 |
| DCF | -12.8 | -12.4 |
| IBP | -13.6 | -13.9 |

| (c.1) IBP overall binding energy (kcal/mol) | | |
|---|---|---|
| Competitor | N-biocahr | O-biochar |
| None | -14.1 | -14.2 |
| DCF | -13.2 | -13.7 |
| NPX | -16.2 | -15.8 |

**Figure 6.4** Binding energy distribution of (a) DCF, (b) NPX, and (c) IBP with respective to carbonaceous structure base analyzed by NMR and overall binding energies (a.1, b.1, and c.1) in the condition of non-competitive and competitive adsorption.

**Table 6.4** Binding energies for non-competitive and competitive adsorption of NSAIDs onto each carbon based functional groups of biochar (kcal/mol).

| Binding energy between solutes and each carbon based functional group | | | | | | | | | |
|---|---|---|---|---|---|---|---|---|---|
| Main NSAID | | DCF | | | NPX | | | IBP | |
| Competitor | None | NPX | IBP | None | DCF | IBP | None | DCF | NPX |
| Alkyl | -17.7 | -20.7 | -15.0 | -13.3 | -14.5 | -10.0 | -19.6 | -13.1 | -16.2 |
| Methoxyl | -18.7 | -19.6 | -19.3 | -16.8 | -18.5 | -17.9 | -9.26 | -16.8 | -16.9 |
| Carbohydrate | -21.8 | -22.2 | -17.4 | -22.2 | -16.7 | -10.3 | -15.3 | -10.4 | -20.1 |
| Aryl | -16.8 | -18.3 | -14.8 | -17.1 | -11.3 | -15.3 | -17.5 | -15.8 | -14.5 |
| O-Aryl | -12.7 | -17.2 | -11.8 | -16.8 | -9.89 | -13.0 | -8.44 | -10.7 | -12.6 |
| Carboxyl | -15.4 | -19.7 | -10.4 | -20.9 | -9.76 | -14.1 | -8.23 | -8.04 | -19.5 |
| Carbonyl | -11.4 | -21.9 | -12.1 | -16.9 | -11.9 | -13.0 | -7.67 | -11.4 | -15.9 |

**Table 6.5** Energy contribution from biochar functional groups for single NSAIDs interacting with N-biochar and O-biochar (kcal/mol).

| Functional group | N-biochar | | | O-biochar | | |
|---|---|---|---|---|---|---|
| | DCF | NPX | IBP | DCF | NPX | IBP |
| Alkyl | 0.07 | 0.08 | 0.08 | 0.03 | 0.03 | 0.03 |
| Methoxyl | 0.06 | 0.06 | 0.06 | 0.03 | 0.03 | 0.03 |
| **Carbohydrate** | **0.27** | 0.17 | 0.16 | **0.23** | 0.15 | 0.14 |
| **Aryl** | **0.39** | **0.44** | **0.49** | **0.51** | **0.56** | **0.62** |
| O-Aryl | 0.10 | 0.12 | 0.09 | 0.10 | 0.12 | 0.09 |
| Carboxyl | 0.09 | 0.10 | 0.08 | 0.05 | 0.06 | 0.05 |
| Carbonyl | 0.03 | 0.04 | 0.03 | 0.04 | 0.04 | 0.04 |

111

from the aryl and carbohydrate functional groups was observed in both N-biochar and O-biochar. This was apparently due to the high percentages of the functional groups in both types of biochar, which affected the overall binding energies between solute and adsorbent.

The interaction strength of DCF and NPX decreased during competitive adsorption in the presence of other NSAIDs. For a given adsorption site, the presence of a competing solute may lead to a reduction in the available adsorption sites that are accessible to the main NSAIDs. In the simulations, this translated to a reduction in the accessible adsorbent surface area, which resulted in an overall reduction in the interaction strength between the main NSAIDs and the adsorbent. The interaction strength of DCF with N-biochar decreased by 6.9 and 2.3 kcal/mol in the presence of IBP and NPX competitors, respectively. For O-biochar, reductions of 6.4 and 2.0 kcal/mol were observed. Similarly, the interactions of NPX with the adsorbents were mitigated by reduction of binding energy of 3.9 and 4.7 kcal/mol for N-biochar and 3.4 and 4.9 kcal/mol for O-biochar in the presence of IBP and DCF as a competitor, respectively. However, the interaction of IBP with N-biochar and O-biochar increased by 2.1 and 1.6 kcal/mol, respectively, in the presence of NPX as a competitor; while the presence of DCF reduced the overall binding energy between biochars and IBP.

### 6.3.3. Single-solute Adsorption.

The Langmuir adsorption model was applied to adsorption data in this work, due mainly to the comparison between experimental results and monolayer adsorption-based molecular modeling. The model has the following linear form:

$$\frac{C_e}{q} = \frac{C_e}{q_{max}} + \frac{1}{K_L q_{max}} \quad \cdots\cdots\cdots\cdots\cdots\cdots\cdots\cdots\cdots\cdots\cdots\cdots\cdots\cdots (6.1)$$

where $C_e$ is the solute equilibrium concentration (mg/L) in the aqueous phase; $q$ is the mass

of adsorbed solute on a unit mass of adsorbent (mg/g); $q_{max}$ is the maximum mass adsorbed at the saturated adsorption capacity of adsorbent (mg/g); and $K_L$ is the empirical constant (L/mg).

Adsorption isotherms on N- and O-biochars are displayed for NSAIDs in Figure 6.5. Although the adsorption affinity of NSAIDs onto the biochar determined by molecular modeling followed the order of DCF > NPX > IBP, the experimental adsorption results differed slightly from those of molecular modeling due to limited consideration of open sectors on the biochar and the physicochemical properties of both the solute and adsorbent (Table 6.6).

### 6.3.3.1. Diclofenac Adsorption.

DCF adsorption behavior differed between N- and O-biochars, with a maximum adsorption capacity of 372 and 214 mg/g, respectively. A strong interaction between aromatic carbon on the biochar and DCF was dominant due to the π-π EDA interaction between polar aromatic DCF (electron acceptors) and the polarizable biochars (electron donors) (Chen, Duan, and Zhu 2007). Relatively large size of DCF molecules appeared to be an important factor for DCF adsorption. For the micro-sized pores in the open sector it was assumed that a sieving effect occurred in DCF adsorption. The greater number of large sized pores on N-biochar allowed better contact with DCF, resulting in considerable adsorption differences to smaller pore-sized other carbonaceous adsorbents (Jung, Park, et al. 2013). This sieving effect was identified by surface area normalized isotherms (Figure 6.5 and Table 6.7). The area normalized maximum adsorption capacity values for DCF indicated that N-biochar was a superior adsorbent with respect to DCF adsorption than O-biochar. Despite the higher aromaticity and binding energy with DCF of the O-biochar,

113
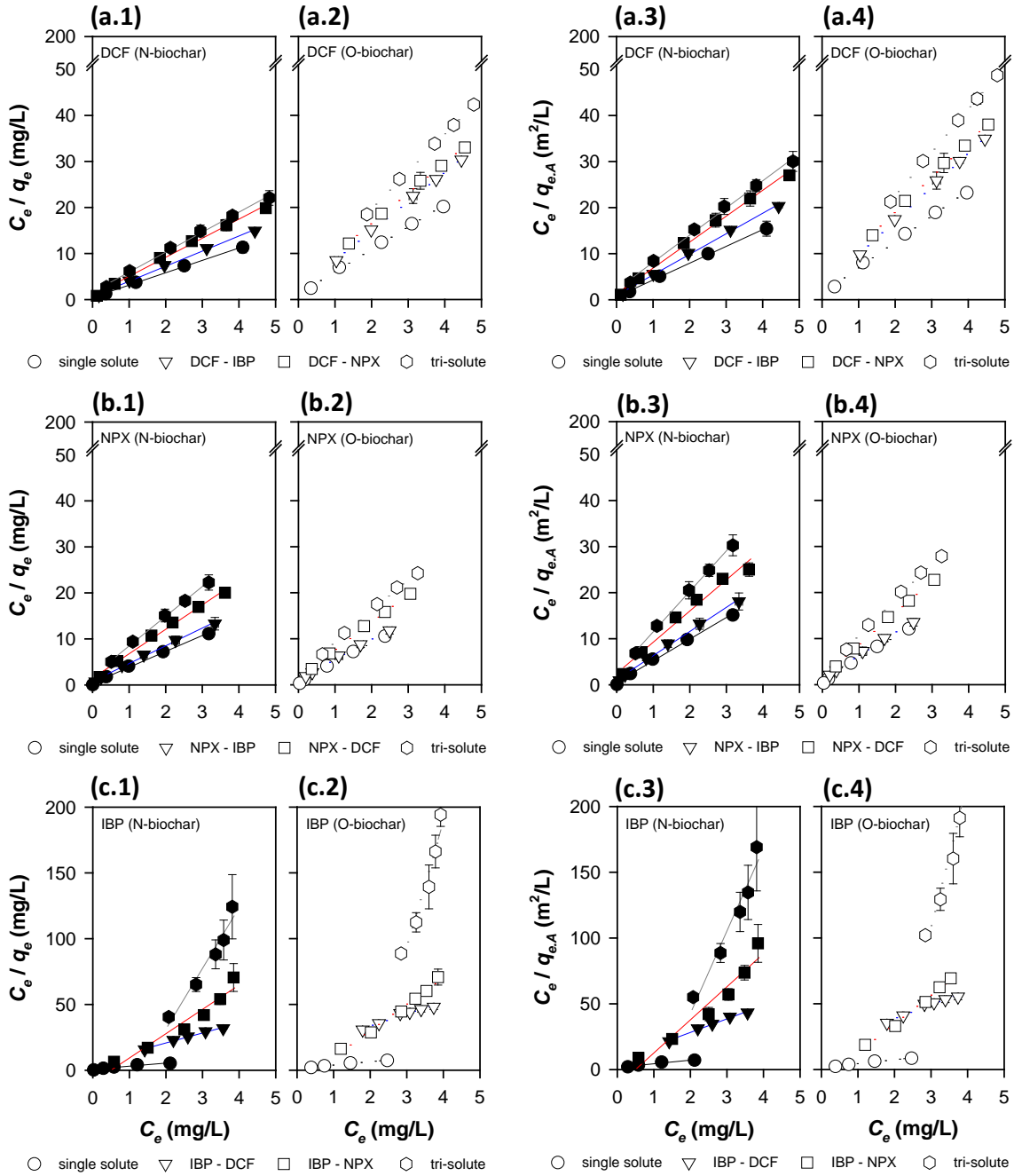
**Figure 6.5** Langmuir model data fitting for NSAIDs by N-biochar (black) and O-biochar (white) in the condition of single-solute (circle), bi-solute (triangle and square), and tri-solute system (hexagon) ($C_0 = 20$ μM).

**Table 6.6** Langmuir isotherm parameters for adsorption of NSAIDs on biochars (mass).

| | DCF | | | | NPX | | | | IBP | | | |
|---|---|---|---|---|---|---|---|---|---|---|---|---|
| | Single | Double | | Triple | Single | Double | | Triple | Single | Double | | Triple |
| Competitor | - | IBP | NPX | All | - | IBP | DCF | All | - | DCF | NPX | All |
| N-biochar | | | | | | | | | | | | |
| $q_{max}$ | 372 | 305 | 242 | 231 | 290 | 243 | 178 | 155 | 311 | 132 | 62.6 | 25.3 |
| $K_L$ | 5.89 | 4.80 | 4.59 | 2.67 | 8.90 | 6.59 | 4.85 | 3.20 | 8.02 | 1.35 | -3.02 | -0.903 |
| $R^2$ | 0.990 | 0.996 | 0.993 | 0.990 | 0.994 | 0.992 | 0.994 | 0.990 | 0.983 | 0.986 | 0.965 | 0.929 |
| O-biochar | | | | | | | | | | | | |
| $q_{max}$ | 214 | 161 | 155 | 124 | 228 | 213 | 166 | 147 | 286 | 109 | 52.6 | 14.6 |
| $K_L$ | 3.19 | 2.46 | 1.73 | 2.25 | 10.9 | 5.07 | 3.95 | 2.70 | 6.81 | 0.601 | -2.40 | -0.635 |
| $R^2$ | 0.994 | 0.997 | 0.995 | 0.998 | 0.997 | 0.995 | 0.998 | 0.996 | 0.991 | 0.940 | 0.986 | 0.910 |

Unit of $q_{max}$ : (mg/g); $K_L$ : (L/mg)

**Table 6.7** Comparison maximum sorption capacity of both N-biochar and O-biochar in single- and multi-sorption system under mass/surface area base.

| Competitor | DCF Single - | DCF Double IBP | DCF Double NPX | DCF Triple All | NPX Single - | NPX Double IBP | NPX Double DCF | NPX Triple All | IBP Single - | IBP Double DCF | IBP Double NPX | IBP Triple All |
|---|---|---|---|---|---|---|---|---|---|---|---|---|
| **Mass** | | | | | | | | | | | | |
| $q_{max}^N$ | 372 | 305 | 242 | 231 | 290 | 243 | 178 | 155 | 311 | 132 | 62.6 | 25.3 |
| $q_{max}^O$ | 214 | 161 | 155 | 124 | 228 | 213 | 166 | 147 | 286 | 109 | 52.6 | 14.6 |
| $q_m^O : q_m^N$ | **0.57** | **0.53** | **0.64** | **0.54** | **0.79** | **0.88** | **0.93** | **0.95** | **0.92** | **0.83** | **0.84** | **0.58** |
| **Surface area** | | | | | | | | | | | | |
| $q_{max.A}^N$ | 274 | 224 | 178 | 170 | 213 | 179 | 131 | 114 | 229 | 97.0 | 46.1 | 18.6 |
| $q_{max.A}^O$ | 186 | 140 | 135 | 108 | 198 | 185 | 144 | 128 | 248 | 94.7 | 45.7 | 12.7 |
| $q_{m.A}^O : q_{m.A}^N$ | **0.68** | **0.62** | **0.76** | **0.63** | **0.93** | **1.03** | **1.10** | **1.12** | **1.09** | **0.98** | **0.99** | **0.68** |
| $q_m^{multi} : q_m^{single}$ | | | | | | | | | | | | |
| N-biocahr | | 0.18 | 0.35 | 0.38 | | 0.16 | 0.38 | 0.46 | | 0.58 | 0.80 | 0.92 |
| O-biochar | | 0.25 | 0.27 | 0.42 | | 0.07 | 0.27 | 0.35 | | 0.62 | 0.82 | 0.95 |

Unit of $q_{max}$ (mg/g) for mass base and $q_{max.A}$ (mg/m$^2$) for surface area base.

the contribution of the polarity of N-biochar increased the adsorption affinity of DCF (Küsgens et al. 2009) due to the relatively high molecular polarizability and $\pi$-energy values of DCF compared to NPX and IBP. Regardless of the elemental composition and the ratio of carbonaceous structure, the binding energy between each structure and DCF was estimated to be above -20 kcal/mol, except for that between aryl carbon and DCF (-18.8 kcal/mol). Although non-aromatic carbon, aliphatic carbon, and carbonyls had higher binding energies with DCF, the small fraction of non-aromatic carbon did not play a critical role in DCF adsorption, while aromatic carbon did encourage the hydrophobic interaction due to the component ratio.

### 6.3.3.2. Naproxen Adsorption.

NPX adsorption behavior on N- and O-biochars displayed a similar tendency to DCF adsorption, with maximum adsorption capacities of 290 and 228 mg/g, respectively. The maximum adsorption capacity ratio of O-biochar to N-biochar was 0.79, and this value was higher than the ratio for DCF (0.57) (Table 6.7). This distinctive NPX adsorption capacity of each biochar was dissipated with surface area normalization, with only 7% difference, due to the smaller size of the NPX molecule, less influenced sieving effect, compared to DCF. NPX was able to occupy both open and closed sectors with no hindrances. The lower adsorption capacity of NPX than DCF was due to the lower hydrophobicity. Due to the relatively low $K_{ow}$ and p$K_a$ values of NPX, the hydrophobicity expressed was lower than 1 in log $D$, resulting in a lesser overall binding energy compared to DCF. However, naphthalene-based aromatic structures of NPX employed not only strong $\pi$-$\pi$ EDA interaction but also high Van der Waals force with the biochars, and improved the adsorption behaviors such as an adsorption strength and capacity (Table 6.6)

117

(Chakarova-Käck et al. 2006).-based aromatic structures and the biochars improved the adsorption behavior.

### 6.3.3.3. Ibuprofen Adsorption.

IBP was estimated from the molecular modeling to be the least favorable solute for adsorption onto biochars. The adsorption experiments, however, indicated preferential adsorption of IBP onto the biochars compared to DCF and NPX. This discrepancy could be attributed to the higher dependence of IBP adsorption on not only the hydrophobicity effect, which was not fully captured in the simulations, but also its smaller molecular structure, which enabled it to occupy more small sites on the exposed surface area of the biochar (Xu et al. 2009). The relatively higher hydrophobicity (log $D_{ow}$ = 1.82 at pH = 7) led to the binding energy deficiency derived from the single benzene ring structure to be overcome, and the small molecular dimensions were considered to be sufficient for adsorption onto the small sized pores in the open sector of the biochars. This strong hydrophobic interaction was explained by surface area nominalization at the maximum adsorption capacity. Macro-sized pores in N-biochar were regarded as a closed sector for IBP, and mitigated the sieving effect due to the small size of IBP, resulting in a ratio of the surface area normalized maximum adsorption capacity of O-biochar to that of N-biochar of 1.09 (Table 6.7). This excess led to magnification of the hydrophobic interactions in IBP adsorption.

Another factor affecting the evaluation of IBP adsorption is partitioning. A partitioning coefficient is usually calculated by means of dual-mode sorption in a single-solute system (Graber et al. 2007), and its effect is correlated with the conformation and polarity of an adsorbent for the removal of organic pollutants (naphthalene,

118

nitrobenzene, and m-dinitrobenzene) that is dominated by a monolayer surface cover (Chen, Zhou, and Zhu 2008; Chen et al. 2012). However, the conformation of both biochars was only marginally correlated to the partition of NSAIDs (Figure 6.6 and Table 6.8). The partitioning of NSAIDs was inversely proportional to molecular polarity for O-biochar due to its lower polarity and higher aromatic carbon content (Sawhney and Brown 1989). These hydrophobic interaction favored properties may interrupt the partitioning, which was evident in the inverse relation between the adsorptive role of hydrophobic interaction and the partitioning. The lower polarity of IBP promoted partitioning along with total adsorption, and this adsorption mechanism was attributed to the partition between trichloroethene and other low polarity compounds, and soil organic matter (Xing, Pignatello, and Gigliotti 1996). Therefore, this weak binding between the low-polarity IBP and the polar section of the biochars could describe partitioning and total sorption, while the lower polarity was negligible in terms of controlling the adsorption behavior.

### 6.3.4. Bi-solute Adsorption.

To compare competitive effect of individual cosolutes with the adsorption of each NSAID onto the biochars, the competitive adsorption between DCF vs. NPX, NPX vs. IBP, and IBP vs. DCF is plotted in Figure 6.5. The maximum adsorption capacity was compared to that in the single adsorption system and is listed in Table 6.6 and 6.7.

Competition of cosolutes with DCF on both biochars followed the order at the same thermodynamic state: NPX > IBP. The DCF maximum adsorption capacities on N- and O-biochars were 18% and 25%, respectively, in the presence of IBP, and 35% and 27%, respectively, in the presence of NPX compared to the value of its single adsorption

119
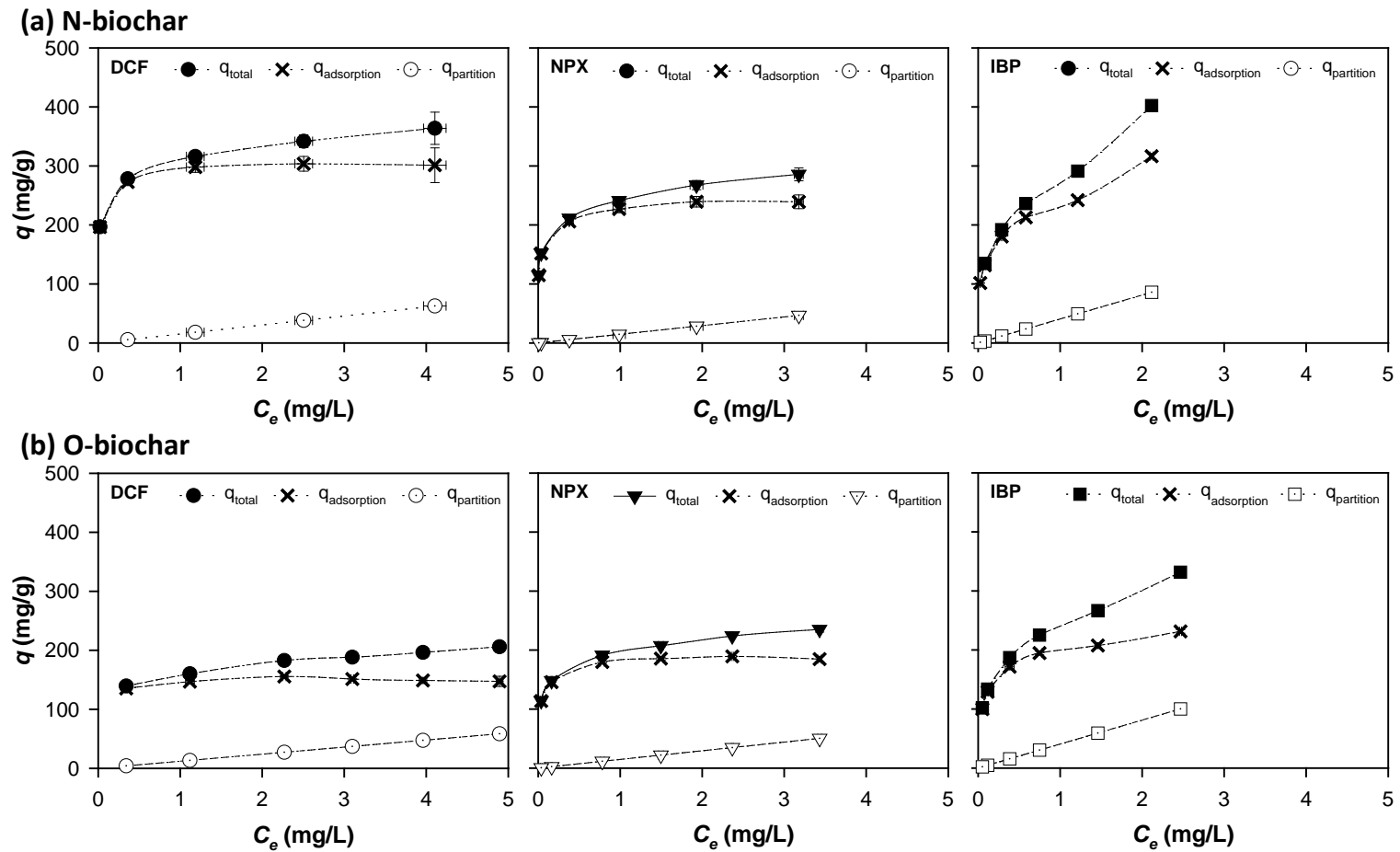
**Figure 6.6** Quantitative contributions of partition and adsorption to total sorption of NSAIDs onto (a) N-biochar and (b) O-biochar ( $q_{total} = q_{adsorption} + q_{partition}$; $q_{total} = q_{max} + K_p C_e$: $q_{max}$ is the maximum adsorption capacity (mg/g); $K_p$ is the partition coefficient; and $C_e$ is the solute equilibrium concentration (mg/L)).

**Table 6.8** Regression parameters of linear isotherms over high relative concentration range for adsorption of NSAIDs on biochars.

| Adsorbent | DCF | | NPX | | IBP | |
|---|---|---|---|---|---|---|
| | *Linear equation*[*] | $R^2$ | *Linear equation*[*] | $R^2$ | *Linear equation*[*] | $R^2$ |
| N-biochar | $q = 213.9\, C_e + 15.3$ | 0.980 | $q = 165.6\, C_e + 14.7$ | 0.981 | $q = 176.6\, C_e + 40.6$ | 0.987 |
| O-biochar | $q = 129.7\, C_e + 12.0$ | 0.981 | $q = 157.15\, C_e + 15.2$ | 0.982 | $q = 178.4\, C_e + 40.4$ | 0.987 |

[*] Linear isotherm over specific concentration range (i.e., $C_e$= 1.0-3.0) was regressed, and the slope and intercept on y-axis of the linear equation were used to calculate partition coefficient ($K_p$) and the maximum adsorption capacity ($q_A^{max}$, mg/g), respectively.

capacity. Because a given adsorbent has limited sorption sites, the higher binding energy between DCF and the biochars contributed to the occupation of the closed sector on the adsorbents and hindered hydrophobic interactions between IBP and the biochars. The cloud effect of the occupied DCF provided less opportunity for interaction between IBP and the aromatic fraction of the biochars, and the degree of this hindrance was greater for O-biochar due to its higher aromaticity compared to N-biochar. This shield of adsorption sites was a consequence of the strong interaction between the larger projected area of DCF and adsorption sites on the adsorbent, and IBP was more affected due to its smaller cross-sectional area with a lower binding energy. Moreover, the larger molecular size of DCF blocked the micro-pores, which were occupied preferentially by the smaller IBP molecules. The adsorption capacity of IBP then decreased sharply in the presence of DCF, with 58% and 62% reductions observed on N- and O-biochars, respectively. The higher hydrophobicity did not prevent the reduction in adsorption due to the lower binding energy and pore blockage in the competitive adsorption system, and similar results were obtained (Pelekani and Snoeyink 1999; Sander and Pignatello 2005).

The similar cosolute effects for NPX to DCF and DCF to NPX adsorption were examined due to their analogous dominant adsorption mechanisms; i.e., hydrophobic interactions such as π-π EDA interactions and polar interactions, which resulted in adsorption capacity of N-biochar and O-biochar as 35% and 27% in the presence of IBP, 38% and 27% in the presence of DCF, respectively, compared to the value of its single adsorption capacity. The greater hydrophobic interactions and higher polarity and π-energy of DCF indicated its considerable adsorption affinity toward the aromatic fraction of the adsorbent, resulting in the same tendency for the overall single-solute system.

122

A cosolute effect was observed between IBP and NPX; that is, IBP appeared to disrupt the adsorption of NPX. Compared to the adsorption capacity of NPX in the single-solute system, 84% and 93% of NPX were adsorbed onto the N- and O-biochars, respectively. The NPX also prevented IBP from occupying adsorption sites on the adsorbent, with only 20% and 18% of the IBP adsorbed onto N- and O-biochars, respectively, compared to the adsorption capacity of IBP in the single-solute system. The relatively weak binding energy between IBP and the biochars was increased dramatically in the presence of NPX as a cosolute, while the binding energy between NPX and the biochars was reduced, resulting in a lower overall binding energy in the competitive adsorption with IBP (Figure 6.4). Although a steep increase in the binding energy between IBP, and carbohydrate and carboxyl carbon on the adsorbent led to this energy reverse phenomenon, these non-aromatic interactions acted as a disruptor of other aromatic interactions, with a repulsive effect that mitigated the hydrophobic interaction (Miah, Iqbal, and Lai 2012). Therefore, the theoretical overall binding energy between IBP and biochars was higher than that for NPX. The lower binding energy between IBP and aromatic adsorbents enabled the adsorption sites to have greater affinity toward NPX on the aromatic sites, and this phenomenon was more marked with O-biochar due to its higher proportion of aryl and O-aryl fractions.

Another distinguishable feature of the cosolute effect was the enhancement of π-cloud overlap or π-π interaction due to the planar steric NPX, naphthalene (two benzene rings)-based structure, with the adsorbent (Bucheli and Gustafsson 2000; Cornelissen et al. 2004). This planarity effect was reliable in terms of the comparison between similar molecular sized compounds, and was verified by the additional driving force (π-π

123

interaction) between planar solutes (phenanthrene, benzo (a) anthracene) and graphene structured char rather than a compound containing one benzene ring (phenol, 2,2-methyllene-bis) with nonspecific Van der Waals interactions (Wang, Sato, and Xing 2006; Sander and Pignatello 2005). Hydrogen containing functional groups on the biochar, increased the number of competitive deprotonated IBP and NPX in neutral water conditions (neutral pH), acting as a H-donor and H-acceptor, presumably, leading to the small proportion of hydrogen bonding. The adsorption by hydrogen bonding was more pronounced between IBP and biochar due to relatively high hydrogen favorable property, and higher value of binding energy between hydrogen containing functional groups and IBP supported this distinction (Figure 6.4 (c)). Moreover, the higher polarity of NPX enhanced its affinity toward the adsorbent when excess water was present due to the partial deionization of the molecules at pH 7, with higher $pK_a$ values (Sander and Pignatello 2005). Unlike the competitive adsorption with DCF, the pore-blockage effect between the similar sized IBP and NPX molecules was negligible.

### 6.3.5. Tri-solute Adsorption.

The representation of tri-solute competitive adsorption was convoluted by the energy difference due to the complexity in configuration during the molecular modeling. However, the typical and dominant adsorption mechanisms in single- and bi-solute systems were considered to interpret the tri-solute system. The unchangeable physical properties of adsorbent for tri-solute adsorption played a crucial role to reveal the mechanisms rather than chemical reactions (binding energy, hydrophobic interaction, etc.). In contrast to the significant increase in the multi-solute adsorption predicted by Polanyi theory based on micropore filling without considering the flat surface adsorption (Manes

124

1998; Yang et al. 2006), the total amount of adsorbed solutes in the tri-solute system was increased slightly compared to the single- and bi-solute systems (Table 6.6). In the concept of monolayer adsorption, rather than multi-layer adsorption approach with a low concentration of each solute ($C_e/C_s < 1$), was ascribed to the relatively large surface area and pore volume of the biochars compared to other carbonaceous adsorbents. The adsorptions in the tri-solute system were similar but slightly lower than that of bi-solute system for both DCF or NPX, resulting in the range of adsorption capacities of as 53% to 65% of each single-solute system value, whereas adsorption for IBP in the tri-solute system achieved only 8% and 5% of the adsorption capacity of the single-solute system with N- and O-biochars, respectively. This was attributed to its lower competitive adsorption affinity. IBP in the tri-solute system was deprived of adsorption sites because they were occupied by DCF and NPX due to their higher binding energy with the adsorbent, higher polarity, and larger molecular size. The precarious and weaker affinity features of IBP toward the biochars in the presence of adsorptive competitors was caused by a repulsive effect between deprotonated IBP and the negatively charged adsorbent surfaces due to the occupation of deprotonated DCF and NPX (Figure. 6.7) (Shyadehi and Harding 1991; Behera, Oh, and Park 2012; Yangali-Quintanilla et al. 2009).

### 6.4. Conclusions

Biochar, a byproduct of biofuel, is an attractive material for adsorbing hydrophobic pharmaceuticals in terms of the reuse of waste materials that would otherwise be landfilled. Various analyses have been undertaken to better understand each property of the solutes and adsorbent and to evaluate their adsorption affinity and capacity, respectively. In particular, the characterization of biochars via NMR analysis has allowed the evaluation of

125
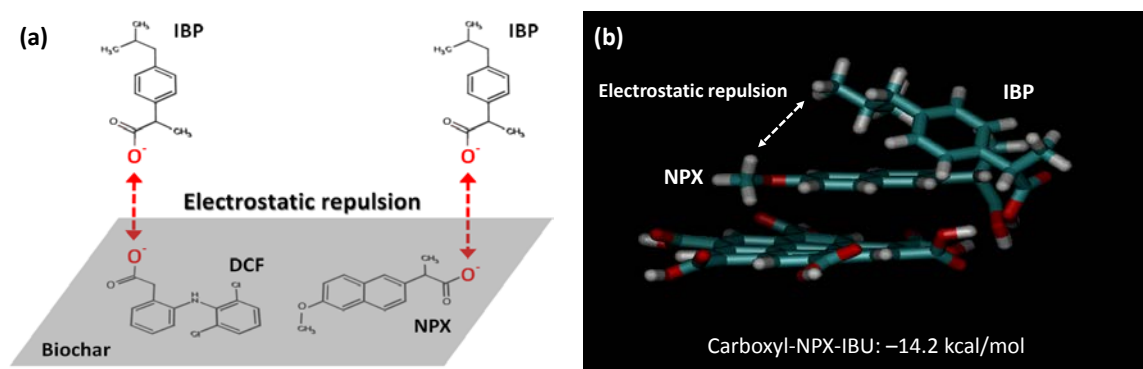
**Figure 6.7** Schematics of (a) electrostatic repulsion between protonated IBP and DCF and/or NPX in the competitive adsorption on the biochar, and (b) optimum condition of competitive adsorption of NPX in the presence of IBP in terms of binding energy model data fitting with carboxyl based biochar.

their structure and properties, while molecular modeling has revealed the intensity of binding energy between adsorption media. Molecular modeling of solutes and adsorbents has enhanced our understanding of binding energy with consideration of both the conformation and polarity of adsorbents and the physicochemical properties of NSAIDs. This new method enabled the investigation of specific hydrophobic interactions, which are dominant in the pharmaceutical adsorption system. To perform more accurate and reliable interpretations, further studies should apply not only multi-layer adsorption but also consider a number of cases of competitive adsorption under various water matrices. Finally, the fundamental fate of selected micro-pollutants and an understanding of the adsorption system on biochars will contribute to not only the improvement of the removal efficiency of adsorbents, but also prevent exposure to harmful chemicals under more complex environmental conditions.

**Acknowledgment**

126

# CHAPTER 7

## OVERALL CONCLUSIONS AND FUTURE RECOMMENDATIONS

Overall, this study evaluated the adsorption ability of various types of adsorbent such as activated carbon, carbon nanotubes, chitosan, and biochars for hexavalent chromium, pharmaceuticals, and EDCs removal. Physicochemical properties of both adsorbates and adsorbents were characterized for further understanding about each adsorption activity as well as molecular modeling analysis.

**Water purification for micro-pollutants**

Activated carbons have been most widely used for water treatment. However, sometimes high costs of manufactured adsorbents disrupt an engineer's decision to use it; their higher removal efficiency is not neglected. On other hand, biochar, which used to be regarded as a byproduct and waste from bio-oil production, is applied as a promising adsorbent in the water treatment filed. More developed activated biochar enables its adsorption capacity to increase by suitable removal of various aquatic contaminants. The higher property of biochar and usage of byproduct will replace coal-based activated carbons.

Differences from carbonaceous adsorbent, chitosan is biodegradable, and various functional groups are constituted. This property enables chitosan to adsorb ionic contaminants like heavy metals easily. If heavy metal adsorption on chitosan is

127

determined as more or similar to any other effective adsorbent, bio degradable and disposable characteristics can be considered as an environment-friendly adsorbent in this field.

**Broad understanding about characterization of adsorbent by NMR**

The application of NMR well known to the public is for medical diagnosis and research setting with using magnetic resonance imaging and microscopy, respectively. $^{13}$C NMR, one of NMR methods, is applied to identify carbon atoms in an organic compound rather than any other analytical techniques. Therefore, this revelation of organic molecules allows better understanding about carbonaceous adsorbent including activated carbon and biochar. This developed technique can encourage the elucidation of adsorption mechanisms between adsorbent and contaminants.

**Challenging to reveal the adsorption activity through binding energy between adsorbate and adsorbent by molecular modeling**

Investigation of structural property of adsorbent provides better understanding about the adsorption activity between pharmaceutical and biochar. Interactions between simplified coronene based structure of each functionalized biochars, analyzed by NMR, and each NSAIDs were determined in specific aromaticity, polarity, and configuration of each structure of biochar as well as hydrophobicity and dissolvability of chemicals. On the basis of this binding energy calculation, adsorption of single- and multi-adsorption system was able to distinguish even abstruseness and complexity in the analysis. Although this attempt of application of binding energy into analysis in the field of adsorption work still required more specific conditions to achieve the better understanding; however, result in

128

this approach in adsorption of NSADs onto biochar may strengthen the basis in adsorption study.

**Multi-applicability to other fields of science and engineering**

The similar physicochemical characteristics to activated carbons enable biochar to be used as an adsorbent for water treatment. Understanding of adsorption mechanism can be applied to any surface science field such as membrane, and filtration. These composited biochar techniques can synergize positive effects for mirco-pollutants' removal. In addition, knowledgeable sorption mechanisms between biochar and micro-pollutants can be broadened into an in-depth understanding of biomass surface science and contaminant cleaning, and this customized hydrophobic interaction can develop soil amendment.

# REFERENCES

Agrawal, A., Kumar, V., Pandey, B. D. 2006. Remediation options for the treatment of electroplating and leather tanning effenent contaning chromium: a Review. *Mineral Processing & Extractive Metallurgy Review* 27 (2): 99-130.

Ahmadpour, A., and D. Do. 1996. The preparation of active carbons from coal by chemical and physical activation. *Carbon* 34 (4): 471-479.

Ahmaruzzaman, M. 2009. Role of fly ash in the removal of organic pollutants from wastewater. *Energy & Fuels* 23 (3): 1494-1511.

Alkan, M., Ö. Demirbaş, and M. Doğan. 2007. Adsorption kinetics and thermodynamics of an anionic dye onto sepiolite. *Microporous and Mesoporous Materials* 101 (3): 388-396.

Álvarez-Ayuso, E., A. García-Sánchez, and X. Querol. 2007. Adsorption of Cr(VI) from synthetic solutions and electroplating wastewaters on amorphous aluminium oxide. *Journal of Hazardous Materials* 142 (1–2): 191-198.

Anupam, K., S. Dutta, C. Bhattacharjee, and S. Datta. 2011. Adsorptive removal of chromium (VI) from aqueous solution over powdered activated carbon: Optimisation through response surface methodology. *Chemical Engineering Journal* 173 (1): 135-143.

Aydin, Y. A., and N. D. Aksoy. 2009. Adsorption of chromium on chitosan: Optimization, kinetics and thermodynamics. *Chemical Engineering Journal* 151: 188-194.

Azargohar, R., and A. Dalai. 2006. Biochar as a precursor of activated carbon. *Applied biochemistry and biotechnology* 131 (1-3): 762-773.

Babbar, N. 2003. *Regulation and function of spermidine/spermine N¹ acetyl transferase (SSAT) in colon carcinogenesis*. University of Arizona Press.

Babel, S., and T. A. Kurniawan. 2004. Cr(VI) removal from synthetic wastewater using coconut shell charcoal and commercial activated carbon modified with oxidizing agents and/or chitosan. *Chemosphere* 54 (7): 951-967.

Baccile, N., G. Laurent, F. Babonneau, F. Fayon, M. M. Titirici, and M. Antonetti. 2009. Structural characterization of hydrothermal carbon spheres by advanced solidstate

MAS $^{13}$C NMR investigations. *Journal of Physics and Chemistry*. 113: 9644-9654.
Balasubramanian, K., and M. Burghard. 2005. Chemically functionalized carbon nanotubes. *Small* 1 (2): 180-192.

Balavoine, F., P. Schultz, C. Richard, V. Mallouh, T. W. Ebbesen, and C. Mioskowski. 1999. Helical crystallization of proteins on carbon nanotubes: a first step towards the development of new biosensors. *Angewandte Chemie International Edition* 38 (13/14): 1912-1915.

Basu, K. K., Chakraborty, S. 1989. Effluent treatment in leather processing industries. Indian *Journal of Environment Prouection* 9: 904-908.

Becke, A., C. F. Matta, and R. J. Boyd. 2007. *The quantum theory of atoms in molecules: from solid state to DNA and drug design*: John Wiley & Sons.

Behera, S., S. Oh, and H. Park. 2012. Sorptive removal of ibuprofen from water using selected soil minerals and activated carbon. *International Journal of Environmental Science and Technology* 9 (1): 85-94.

Beneitez, P., and S. Ayllon. 1987. Extraction studies on the system between bis(2-ethylhexyl) phosphoric acid and chromium(III) in several aqueous solutions. *Solvent Extraction and Ion Exchange* 5 (4): 597-609.

Benotti, M. J., R. A. Trenholm, B. J. Vanderford, J. C. Holady, B. D. Stanford, and S. A. Snyder. 2008a. Pharmaceuticals and endocrine disrupting compounds in U.S. drinking water. *Environmental Science & Technology* 43 (3): 597-603.

Bilotta, J., J. A. Barnett, L. Hancock, and S. Saszik. 2004. Ethanol exposure alters zebrafish development: a novel model of fetal alcohol syndrome. *Neurotoxicology and Teratology* 26 (6): 737-743.

Boateng, L. K., J. Heo, R. V. J. Flora, Y.-G. Park, and Y. Yoon. 2013. Molecular level simulation of the adsorption of bisphenol A and 17α-ethinyl estradiol onto carbon nanomaterials. *Separation and Purification Technology*. 116: 471-478.

Boddu, V. M., K. Abburi, J. L. Talbott, and E. D. Smith. 2003. Removal of hexavalent chromium from wastewater using a new composite chitosan biosorbent. *Environmental Science & Technology* 37 (19): 4449-4456.

Braida, W. J., J. J. Pignatello, Y. Lu, P. I. Ravikovitch, A. V. Neimark, and B. Xing. 2003. Sorption hysteresis of benzene in charcoal particles. *Environmental Science & Technology* 37 (2): 409-417.

Bucheli, T. D., and Ö. Gustafsson. 2000. Quantification of the soot-water distribution coefficient of PAHs provides mechanistic basis for enhanced sorption observations. *Environmental Science & Technology* 34 (24): 5144-5151.

Budarin, V., J. H. Clark, J. J. Hardy, R. Luque, K. Milkowski, S. J. Tavener, and A. J. Wilson. 2006. Starbons: New starch-derived mesoporous carbonaceous materials with tunable properties. *Angewandte Chemie* 118 (23): 3866-3870.

Cao, X., K. S. Ro, M. Chappell, Y. Li, and J. Mao. 2011. Chemical structures of swinemanure chars produced under different carbonization conditions investigated by advanced solid-state 13C nuclear magnetic resonance (NMR) spectroscopy. *Energy and Fuels* 25: 388-397.

Cerulli, J., D. W. Grabe, I. Gauthier, M. Malone, and M. D. McGoldrick. 1998. Chromium picolinate toxicity. *Annals of Pharmacotherapy* 32 (4): 428-431.

Chakarova-Käck, S. D., E. Schröder, B. I. Lundqvist, and D. C. Langreth. 2006. Application of van der Waals density functional to an extended system: Adsorption of benzene and naphthalene on graphite. *Physical Review Letters* 96 (14): 146107-1-146107-4.

CheapTubes. 2012. Multi walled nanotubes-MWNTs. The source for Mingle Walled Nanotubes-MWNTs.

ChemAxon. http://www.chemicalize.org.

Chen, B., D. Zhou, and L. Zhu. 2008. Transitional adsorption and partition of nonpolar and polar aromatic contaminants by biochars of pine needles with different pyrolytic temperatures. *Environmental Science & Technology* 42 (14): 5137-5143.

Chen, W., L. Duan, and D. Zhu. 2007. Adsorption of polar and nonpolar organic chemicals to carbon nanotubes. *Environmental Science & Technology* 41 (24): 8295-8300.

Chen, Y., and G. Gu. 2005. Preliminary studies on continuous chromium(VI) biological removal from wastewater by anaerobicâ€'aerobic activated sludge process. *Bioresource Technology* 96 (15): 1713-1721.

Chen, Z., B. Chen, D. Zhou, and W. Chen. 2012. Bisolute sorption and thermodynamic behavior of organic pollutants to biomass-derived biochars at two pyrolytic temperatures. *Environmental Science & Technology* 46 (22): 12476-12483.

Cho, H.-H., B. A. Smith, J. D. Wnuk, D. H. Fairbrother, and W. P. Ball. 2008. Influence of surface oxides on the adsorption of naphthalene onto multiwalled carbon nanotubes. *Environmental Science & Technology* 42 (8): 2899-2905.

Chun, Y., G. Sheng, C. T. Chiou, and B. Xing. 2004. Compositions and sorptive properties of crop residue-derived chars. *Environmental Science & Technology* 38 (17): 4649-4655.

Cimino, G., A. Passerini, and G. Toscano. 2000. Removal of toxic cations and Cr(VI) from aqueous solution by hazelnut shell. *Water Research* 34 (11): 2955-2962.

Cioslowski, J. 1988. Total π-electron energy in the "variable β" Hückel method. *International Journal of Quantum Chemistry* 34 (5): 417-421.

Cleuvers, M. 2004. Mixture toxicity of the anti-inflammatory drugs diclofenac, ibuprofen, naproxen, and acetylsalicylic acid. *Ecotoxicology and Environmental Safety* 59 (3): 309-315.

Comerton, A. M., R. C. Andrews, and D. M. Bagley. 2009. Practical overview of analytical methods for endocrine-disrupting compounds, pharmaceuticals and personal care products in water and wastewater. *Philosophical Transactions of the Royal Society A: Mathematical, Physical and Engineering Sciences* 367 (1904): 3923-3939.

Cornelissen, G., M. Elmquist, I. Groth, and Ö. Gustafsson. 2004. Effect of sorbate Planarity on environmental black carbon sorption. *Environmental Science & Technology* 38 (13): 3574-3580.

Cortés-Arriagada, D., L. Sanhueza, and M. Santander-Nelli. 2013. Modeling the physisorption of bisphenol A on graphene and graphene oxide. *Journal of Molecular Modeingl* 19: 3569–3580.

Debnath, S., and U. C. Ghosh. 2008. Kinetics, isotherm and thermodynamics for Cr(III) and Cr(VI) adsorption from aqueous solutions by crystalline hydrous titanium oxide. *The Journal of Chemical Thermodynamics* 40 (1): 67-77.

Dela Rosa, L., M. Pruski, D. Lang, B. Gerstein, and P. Solomon. 1992. Characterization of the Argonne premium coals by using hydrogen-1 and carbon-13 NMR and FT-IR spectroscopies. *Energy & Fuels* 6 (4): 460-468.

Dennington, R. I., T. Keith, J. Millam, K. Eppinnett, W. L. Hovell, and R. Gilliland. 2003. *GaussView, V3.0 Semichem Inc.*: Shawnee Mission, KS.

Dobrowolski, R., and M. Otto. 2010. Study of chromium(VI) adsorption onto modified activated carbons with respect to analytical application. *Adsorption* 16 (4): 279-286.

Dong, X., L. Q. Ma, and Y. Li. 2011. Characteristics and mechanisms of hexavalent chromium removal by biochar from sugar beet tailing. *Journal of Hazardous Materials* 190 (1–3): 909-915.

Drnevich, R. F., G. W. Fenner, H. Kobayashi, and L. E. Bool III. 2006. *Production enhancement for a reactor*: Google Patents.

Durban, S. A., and D. J. Brown. 1939. The Chromate–Chromic Electrode Potential. The *Journal of Physical Chemistry* 43 (4): 491-493.

EPA. 1990. *Environmental pollution control alternatives*. E.P. Agency, Cincinnati, US.

133

Feng, L., E. D. van Hullebusch, M. A. Rodrigo, G. Esposito, and M. A. Oturan. 2013. Removal of residual anti-inflammatory and analgesic pharmaceuticals from aqueous systems by electrochemical advanced oxidation processes. A review. *Chemical Engineering Journal* 228 (0): 944-964.

Fernandes, D. M., A. A. W. Hechenleitner, and E. A. G. Pineda. 2006. Kinetic study of the thermal decomposition of poly(vinyl alcohol)/kraft lignin derivative blends. *Thermochimica Acta* 441 (1): 101-109.

Fernandes, M. B., J. O. Skjemstad, B. B. Johnson, J. D. Wells, and P. Brooks. 2003. Characterization of carbonaceous combustion residues. I. Morphological, elemental and spectroscopic features. *Chemosphere* 51 (8): 785-795.

Flora, J. F. R., X. Lu, L. Li, J. R. V. Flora, and N. D. Berge. 2013. The effects of alkalinity and acidity of process water and hydrochar washing on the adsorption of atrazine on hydrothermally produced hydrochar. *Chemosphere* 93: 1989–1996.

Formuzis, A. 2013. *State "Clean Up" plan could leave 24 million Californians exposed to Potent carcinogen*. Environmental Working Group.

Fraser, B. G., M. D. Pritzker, and R. L. Legge. 1994. Development of liquid membrane pertraction for the removal and recovery of chromium from aqueous effluents. *Separation Science and Technology* 29 (16): 2097-2116.

Fukai, R. 1967. Valency state of chromium in seawater. *Nature* 213 (5079): 901.

Gorell, J., C. Johnson, B. Rybicki, E. Peterson, G. Kortsha, G. Brown, and R. Richardson. 1997. Occupational exposures to metals as risk factors for Parkinson's disease. *Neurology* 48 (3): 650-658.

Gotovac, S., L. Song, H. Kanoh, and K. Kaneko. 2007. Assembly structure control of single wall carbon nanotubes with liquid phase naphthalene adsorption. Colloids and Surfaces A: *Physicochemical and Engineering Aspects* 300 (1): 117-121.

Graber, E., A. Sorek, L. Tsechansky, and N. Atzmon. 2007. Competitive uptake of trichloroethene and 1, 1, 1-trichloroethane by Eucalyptus camaldulensis seedlings and wood. *Environmental Science & Technology* 41 (19): 6704-6710.

Greenwood, N. N., and A. Earnshaw. 1998. *Chemistry of the Elements* (2nd Edition): Elsevier.

Grimme, S., S. Ehrlich, and L. Goerigk. 2011. Effect of the damping function in dispersion corrected density functional theory. *Journal of computational chemistry*. 32: 1456-1465.

Gupta, V. K., S. Agarwal, and T. A. Saleh. 2011. Chromium removal by combining the magnetic properties of iron oxide with adsorption properties of carbon nanotubes. *Water Research* 45 (6): 2207-2212.

134

Gurgel, L. V. A., J. C. Perin de Melo, J. C. de Lena, and L. F. Gil. 2009. Adsorption of chromium (VI) ion from aqueous solution by succinylated mercerized cellulose functionalized with quaternary ammonium groups. *Bioresource Technology* 100 (13): 3214-3220.

Gustafsson, Ö., T. D. Bucheli, Z. Kukulska, M. Andersson, C. Largeau, J. N. Rouzaud, C. M. Reddy, and T. I. Eglinton. 2001. Evaluation of a protocol for the quantification of black carbon in sediments. *Global Biogeochemical Cycles* 15 (4): 881-890.

Halling-Sørensen, B., S. Nors Nielsen, P. Lanzky, F. Ingerslev, H. Holten Lützhøft, and S. Jørgensen. 1998. Occurrence, fate and effects of pharmaceutical substances in the environment-a review. *Chemosphere* 36 (2): 357-393.

Hameed, B., A. Ahmad, and N. Aziz. 2007. Isotherms, kinetics and thermodynamics of acid dye adsorption on activated palm ash. *Chemical Engineering Journal* 133 (1): 195-203.

Hoeger, B., B. Köllner, D. R. Dietrich, and B. Hitzfeld. 2005. Water-borne diclofenac affects kidney and gill integrity and selected immune parameters in brown trout (*Salmo trutta* f. *fario*). *Aquatic Toxicology* 75 (1): 53-64.

Hong, H.-j., H. Kim, K. Baek, and J.-W. Yang. 2008. Removal of arsenate, chromate and ferricyanide by cationic surfactant modified powdered activated carbon. *Desalination* 223 (1–3): 221-228.

Hu, J., C. Chen, X. Zhu, and X. Wang. 2009. Removal of chromium from aqueous solution by using oxidized multiwalled carbon nanotubes. *Journal of Hazardous Materials* 162 (2–3): 1542-1550.

Huang, C., S. Chen, and J. Ruhsing Pan. 2000. Optimal condition for modification of chitosan: a biopolymer for coagulation of colloidal particles. *Water Research* 34 (3): 1057-1062.

Hui Qiu, L. L., Bing-cai Pan, Qing-jian Zhang and Wei-ming Zhang, et al. 2009. Critical review in adsorption kinetic models. *Science A* 10 (5): 716-724.

Hunter, C. A., K. R. Lawson, J. Perkins, and C. J. Urch. 2001. Aromatic interactions. *Journal of the Chemical Society, Perkin Transactions* 2 (5): 651-669.

Hunter, C. A., and J. K. M. Sanders. 1990. The nature of .π-π interactions. *Journal of the American Chemical Society* 112 (14): 5525-5534.

Hyung, H., and J.-H. Kim. 2008. Natural organic matter (NOM) adsorption to multi-Walled carbon nanotubes: Effect of NOM characteristics and water quality parameters. *Environmental Science & Technology* 42 (12): 4416-4421.

IARC. 1989. Monograph on Chromium, *Nickel and Welding. In International Agency for Research on Cancer*. Lyon, France.

135

Iijima, S. 1991. Helical Microtubules of Graphitic Carbon. *Nature* 354 (6348): 56-58.

Ilium, L. 1998. Chitosan and its use as a pharmaceutical excipient. *Pharmaceutical Research* 15 (9): 1326-1331.

Jacukowicz-Sobala, I. 2009. New methods for removal of chromium from wastewater. *Przemysl Chemiczny* 88 (1): 51-60.

Ji, L., F. Liu, Z. Xu, S. Zheng, and D. Zhu. 2010. Adsorption of pharmaceutical antibiotics on template-synthesized ordered micro- and meso-porous carbons. *Environmental Science & Technology* 44 (8): 3116-3122.

Ji, L., Y. Shao, Z. Xu, S. Zheng, and D. Zhu. 2010. Adsorption of monoaromatic compounds and pharmaceutical antibiotics on carbon nanotubes activated by KOH etching. *Environmental Science & Technology* 44 (16): 6429-6436.

Joseph, L., Q. Zaib, I. A. Khan, N. D. Berge, Y. G. Park, N. B. Saleh, and Y. Yoon. 2011. Removal of bisphenol A and 17α-ethinyl estradiol from landfill leachate using single-walled carbon nanotubes. *Water Research* 45 (13): 4056-4068.

Jung, C., J. Heo, J. Han, N. Her, S.-J. Lee, J. Oh, J. Ryu, and Y. Yoon. 2013. Hexavalent chromium removal by various adsorbents: Powdered activated carbon, chitosan, and single/multi-walled carbon nanotubes. *Separation and Purification Technology* 106: 63-71.

Jung, C., J. Park, K. H. Lim, S. Park, J. Heo, N. Her, J. Oh, S. Yun, and Y. Yoon. 2013. Adsorption of selected endocrine disrupting compounds and pharmaceuticals on activated biochars. *Journal of Hazardous Materials* 263: 702-710.

Kandah, M. I., and J. L. Meunier. 2007. Removal of nickel ions from water by multi-walled carbon nanotubes. *Journal of Hazardous Materials* 146 (1-2): 283-288.

Karthikeyan, S., and P. Mahalingam. 2013. *Syntheses and Applications of Carbon Nanotubes and Their Composites. Chapter 11. Carbon nanotubes from unconventional resources: Part A: Entangled multi-walled carbon nanotubes and Part B: Vertically-aligned carbon nanotubes*. INTECH: 241-256.

Kastner, J., J. M. Carr, T. W. Keal, W. Thiel, A. Wander, and P. Sherwood. 2009. DL-FIND: an open-source geometry optimizer for atomistic simulations. *Journal of Physics and Chemistry A* 113: 11856–11865.

Khezami, L., and R. Capart. 2005. Removal of chromium(VI) from aqueous solution by activated carbons: Kinetic and equilibrium studies. *Journal of Hazardous Materials* 123 (1–3): 223-231.

Kilduff, J. E., T. Karanfil, Y.-P. Chin, and W. J. Weber Jr. 1996. Adsorption of natural organic polyelectrolytes by activated carbon: A size-exclusion chromatography study. *Environmental Science & Technology* 30 (4): 1336-1343.

136

Kiran Kumar, A., and S. Venkata Mohan. 2012. Removal of natural and synthetic endocrine disrupting estrogens by multi-walled carbon nanotubes (MWCNT) as adsorbent: Kinetic and mechanistic evaluation. *Separation and Purification Technology* 87 (0): 22-30.

Ko, J. A., H. J. Park, S. J. Hwang, J. B. Park, and J. S. Lee. 2002. Preparation and characterization of chitosan microparticles intended for controlled drug delivery. *International Journal of Pharmaceutics* 249 (1–2): 165-174.

Kolpin, D. W., E. T. Furlong, M. T. Meyer, E. M. Thurman, S. D. Zaugg, L. B. Barber, and H. T. Buxton. 2002. Pharmaceuticals, hormones, and other organic Wastewater contaminants in U.S. streams, 1999−2000: *A National Reconnaissance. Environmental Science & Technology* 36 (6): 1202-1211.

Konradt Moraes, L. C., R. Bergamasco, C. G. Tavares, D. Hennig, and M. Carvalho Bongiovani. 2008. GPE 2007-Utilization of the coagulation diagram in the evaluation of the natural organic matter (NOM) removal for obtaining potable water. *International Journal of Chemical Reactor Engineering* 6 (1): 1-11.

Kotaś, J., and Z. Stasicka. 2000. Chromium occurrence in the environment and methods of its speciation. *Environmental Pollution* 107 (3): 263-283.

Kromhout, D., E. B. Bosschieter, and C. d. L. Coulander. 1985. The inverse relation between fish consumption and 20-year mortality from coronary heart disease. *New England Journal of Medicine* 312 (19): 1205-1209.

Kümmerer, K. 2004. *Pharmaceuticals in the environment: sources, fate, effects and risks*: Springer Verlag.

Küsgens, P., M. Rose, I. Senkovska, H. Fröde, A. Henschel, S. Siegle, and S. Kaskel. 2009. Characterization of metal-organic frameworks by water adsorption. microporous and mesoporous *Materials* 120 (3): 325-330.

Kyzas, G. Z., M. Kostoglou, and N. K. Lazaridis. 2009. Copper and chromium(VI) removal by chitosan derivatives: Equilibrium and kinetic studies. *Chemical Engineering Journal* 152 (2-3): 440-448.

Laird, D. A., R. C. Brown, J. E. Amonette, and J. Lehmann. 2009. Review of the pyrolysis platform for coproducing bio-oil and biochar. Biofuels, *Bioproducts and Biorefining* 3 (5): 547-562.

Lee, S. M., S. C. Lee, J. H. Jung, and H. J. Kim. 2005. Pore characterization of multi-walled carbon nanotubes modified by KOH. *Chemical Physics Letters* 416 (4–6): 251-255.

Leyva-Ramos, R., A. Jacobo-Azuara, P. E. Diaz-Flores, R. M. Guerrero-Coronado, J. Mendoza-Barron, and M. S. Berber-Mendoza. 2008. Adsorption of chromium(VI)

from an aqueous solution on a surfactant-modified zeolite. Colloids and Surfaces A: *Physicochemical and Engineering Aspects* 330 (1): 35-41.

Li, W., X. Gong, X. Li, D. Zhang, and H. Gong. 2012. Removal of Cr(VI) from low-temperature micro-polluted surface water by tannic acid immobilized powdered activated carbon. *Bioresource Technology* 113 (0): 106-113.

Liu, Y.-X., D.-X. Yuan, J.-M. Yan, Q.-L. Li, and T. Ouyang. 2011. Electrochemical removal of chromium from aqueous solutions using electrodes of stainless steel nets coated with single wall carbon nanotubes. *Journal of Hazardous Materials* 186 (1): 473-480.

Ludlow, D. K., R. Jain, and C. Adams. 2007. *Characterization of powdered activated carbon using gaseous-and aqueous-phase indices*. Paper read at The 2007 Annual Meeting.

Lv, X., J. Xu, G. Jiang, and X. Xu. 2011. Removal of chromium(VI) from wastewater by nanoscale zero-valent iron particles supported on multiwalled carbon nanotubes. *Chemosphere* 85 (7): 1204-1209.

Manes, M. 1998. Activated carbon adsorption fundamentals. *Encyclopedia of environmental analysis and remediation* 1: 26-68.

Mao, C., J. Lu, Q. Xu, S.-J. Chen, J. Ke, F.-X. Han, and H.-K. Yan. 1999. FTIR study of hydrogen bonding of stearic acid with ethanol, dimethyl sulfoxide, and acetonitrile in supercritical $CO_2$. *Chinese Journal of Chemistry* 17 (3): 223-230.

Martinez, C. R., and B. L. Iverson. 2012. Rethinking the term "pi-stacking". *Chemical Science* 3 (7): 2191-2201.

Mehinto, A. C., E. M. Hill, and C. R. Tyler. 2010. Uptake and biological effects of environmentally relevant concentrations of the nonsteroidal anti-inflammatory pharmaceutical diclofenac in rainbow trout (*Oncorhynchus mykiss*). *Environmental Science & Technology* 44 (6): 2176-2182.

Mehring, M. 1976. *High resolution NMR in solids*: Springer.

Miah, M., Z. Iqbal, and E. P. Lai. 2012. Rapid CE-UV evaluation of polypyrrole-coated magnetic nanoparticles for selective binding of endocrine disrupting compounds and pharmaceuticals by aromatic interactions. *Analytical Methods* 4 (9): 2866-2878.

Michael Hawthorne, T. R. 2010. *High levels of chromium found in Chicago-area tap water*. Chicago Tribune.

Mittal, A., L. Krishnan, and V. K. Gupta. 2005. Removal and recovery of malachite green from wastewater using an agricultural waste material, de-oiled soya. *Separation and Purification Technology* 43 (2): 125-133.

138

Molinari, R., F. Pirillo, V. Loddo, and L. Palmisano. 2006. Heterogeneous photocatalytic degradation of pharmaceuticals in water by using polycrystalline $TiO_2$ and a nanofiltration membrane reactor. *Catalysis Today* 118 (1): 205-213.

Morisset, P., J. W. Oswald, C. R. Draper, R. Pinner, and R. A. Ehrhardt. 1955. Chromium plating. *Journal of The Electrochemical Society* 102 (6): 143C-144C.

Muataz Ali Atieh, O. Y. B., Bassam S. Tawabini, et al. 2010. Removal of chromium (III) from water by using modified and nonmodified carbon nanotubes. *Journal of Nanomaterials* 2010 (1): 1-9.

Nakagawa, K., A. Namba, S. R. Mukai, H. Tamon, P. Ariyadejwanich, and W. Tanthapanichakoon. 2004. Adsorption of phenol and reactive dye from aqueous solution on activated carbons derived from solid wastes. *Water Research* 38 (7): 1791-1798.

Neurock, M. 2002. *Applications: catalysis. In applying molecular and materials modeling*, 107-147: Springer.

Nguyen, T. H., H. H. Cho, L. Dianne, and W. P. Ball. 2007. Evidence for a pore-filling mechanism in the adsorption of aromatic hydrocarbons to a natural wood char. *Environmental Science & Technology* 41 (4): 1212-1217.

Ni, J., J. J. Pignatello, and B. Xing. 2011. Adsorption of aromatic carboxylate ions to black carbon (biochar) is accompanied by proton exchange with water. *Environmental Science & Technology* 45 (21): 9240-9248.

Novak, J. M., I. Lima, B. Xing, J. W. Gaskin, C. Steiner, K. Das, M. Ahmedna, D. Rehrah, D. W. Watts, and W. J. Busscher. 2009. Characterization of designer biochar produced at different temperatures and their effects on a loamy sand. *Annals of Environmental Science* 3 (1): 195-206.

Novotny, E. H., M. H. Hayes, and T. J. Bonagamba. 2006. Characterisation of black carbon-rich samples by $^{13}C$ solid-state nuclear magnetic resonance. *Naturwissenschaften* 93 (9): 447-450.

Nowotny, N., B. Epp, C. von Sonntag, and H. Fahlenkamp. 2007. Quantification and modeling of the elimination behavior of ecologically problematic wastewater micropollutants by adsorption on powdered and granulated activated carbon. *Environmental Science & Technology* 41 (6): 2050-2055.

Oleszczuk, P., B. Pan, and B. Xing. 2009. Adsorption and desorption of oxytetracycline and carbamazepine by multiwalled carbon nanotubes. *Environmental Science & Technology* 43 (24): 9167-9173.

Owlad, M., M. Aroua, W. Daud, and S. Baroutian. 2009. Removal of hexavalent chromium-contaminated water and wastewater: A review. *Water, Air, & Soil Pollution* 200 (1): 59-77.

Oze, C., D. K. Bird, and S. Fendorf. 2007. Genesis of hexavalent chromium from natural sources in soil and groundwater. *Proceedings of the National Academy of Sciences of the United States of America* 104 (16): 6544-6549.

Packer, J. L., J. J. Werner, D. E. Latch, K. McNeill, and W. A. Arnold. 2003. Photochemical fate of pharmaceuticals in the environment: naproxen, diclofenac, clofibric acid, and ibuprofen. *Aquatic Sciences* 65 (4): 342-351.

Padhye, L. P., H. Yao, F. T. Kung'u, and C.-H. Huang. 2014. Year-long evaluation on the occurrence and fate of pharmaceuticals, personal care products, and endocrine disrupting chemicals in an urban drinking water treatment plant. *Water Research* 51 (0): 266-276.

Pan, B., and B. Xing. 2008. Adsorption mechanisms of organic chemicals on carbon nanotubes. *Environmental Science & Technology* 42 (24): 9005-9013.

Pandey, S., and S. B. Mishra. 2011. Organic–inorganic hybrid of chitosan/organoclay bionanocomposites for hexavalent chromium uptake. *Journal of Colloid and Interface Science* 361 (2): 509-520.

Park, J., J. Meng, K. H. Lim, O. J. Rojas, and S. Park. 2013. Transformation of lignocellulosic biomass during torrefaction. *Journal of Analytical and Applied Pyrolysis* 100: 199-206.

Patterson, J. W. 1985. *Industrial wastewater treatment technology*, Second edition. Butterworth.

Pelekani, C., and V. L. Snoeyink. 1999. Competitive adsorption in natural water: role of activated carbon pore size. *Water Research* 33 (5): 1209-1219.

Pillay, K., E. M. Cukrowska, and N. J. Coville. 2009. Multi-walled carbon nanotubes as adsorbents for the removal of parts per billion levels of hexavalent chromium from aqueous solution. *Journal of Hazardous Materials* 166 (2-3): 1067-1075.

Pramod Kumar Heged, A. V. A., M G Manjunatha. 2010. Electrochemical and optical properties of a new donor–acceptor type conjugated polymer derived from 3,4–didodecyloxythiophene. *Bulletin of Materials Science* 33 (6): 677-682.

Pyrzynska, K., A. Stafiej, and M. Biesaga. 2007. Sorption behavior of acidic herbicides on carbon nanotubes. *Microchimica Acta* 159 (3): 293-298.

Rengaraj, S., S.-H. Moon, R. Sivabalan, B. Arabindoo, and V. Murugesan. 2002. Agricultural solid waste for the removal of organics: adsorption of phenol from water and wastewater by palm seed coat activated carbon. *Waste Management* 22 (5): 543-548.

Richardson, S. D. 2008. Environmental mass spectrometry: emerging contaminants and current issues. *Analytical chemistry* 80 (12): 4373-4402.

Rojas, G., J. Silva, J. A. Flores, A. l. Rodriguez, M. Ly, and H. Maldonado. 2005. Adsorption of chromium onto cross-linked chitosan. *Separation and Purification Technology* 44 (1): 31-36.

Ruas, C. B. G., C. d. S. Carvalho, H. S. S. de Araújo, E. L. G. Espíndola, and M. N. Fernandes. 2008. Oxidative stress biomarkers of exposure in the blood of cichlid species from a metal-contaminated river. *Ecotoxicology and Environmental Safety* 71 (1): 86-93.

Rudder, J. d., T. V. d. Wiele, W. Dhooge, F. Comhaire, and W. Verstraete. 2004. Advanced water treatment with manganese oxide for the removal of 17α-ethynylestradiol (EE2). *Water Research* 38 (1): 184-192.

Saleh, N. B., L. D. Pfefferle, and M. Elimelech. 2008. Aggregation kinetics of multiwalled carbon nanotubes in aquatic systems: Measurements and environmental implications. *Environmental Science & Technology* 42 (21): 7963-7969.

Salloum, D. S., and J. B. Schlenoff. 2004. Protein adsorption modalities on polyelectrolyte multilayers. *Biomacromolecules* 5 (3): 1089-1096.

Sander, M., and J. J. Pignatello. 2005. Characterization of charcoal adsorption sites for aromatic compounds: insights drawn from single-solute and bi-solute competitive experiments. *Environmental Science & Technology* 39 (6): 1606-1615.

SanJuan-Reyes, N., L. M. Gómez-Oliván, M. Galar-Martínez, P. Vieyra-Reyes, S. García-Medina, H. Islas-Flores, and N. Neri-Cruz. 2013. Effluent from an NSAID-manufacturing plant in Mexico induces oxidative stress on Cyprinus carpio. *Water, Air, & Soil Pollution* 224 (9): 1-14.

Sarin, V., and K. K. Pant. 2006. Removal of chromium from industrial waste by using eucalyptus bark. *Bioresource Technology* 97 (1): 15-20.

Sawhney, B. L., and K. W. Brown. 1989. *Reactions and movement of organic chemicals in soils.* Soil Science Society of America 148(5): 387.

Schaefer, J., E. Stejskal, and R. Buchdahl. 1977. Magic-angle $^{13}$C NMR analysis of motion in solid glassy polymers. *Macromolecules* 10 (2): 384-405.

Schoenborn, E. M. 1969. Mass transfer operations, American Institute of Chemical Engineers Journal 15 (1): 155-156.

Schwaiger, J., H. Ferling, U. Mallow, H. Wintermayr, and R. Negele. 2004. Toxic effects of the non-steroidal anti-inflammatory drug diclofenac: Part I: histopathological alterations and bioaccumulation in rainbow trout. *Aquatic Toxicology* 68 (2): 141-150.

Segner, H., J. M. Navas, C. Schäfers, and A. Wenzel. 2003. Potencies of estrogenic compounds in in vitro screening assays and in life cycle tests with zebrafish in vivo. *Ecotoxicology and Environmental Safety* 54 (3): 315-322.

Shaik, S., A. Shurki, D. Danovich, and P. C. Hiberty. 2001. A different story of π-delocalizations: The distortivity of π-electrons and its chemical manifestations. *Chemistry Review* 101: 1501-1539.

Shyadehi, A. Z., and J. J. Harding. 1991. Investigations of ibuprofen and paracetamol binding to lens proteins to explore their protective role against cataract. *Biochemical Pharmacology* 42 (11): 2077-2084.

Simpson, M. J., and P. G. Hatcher. 2004. Determination of black carbon in natural organic matter by chemical oxidation and solid-state $^{13}C$ nuclear magnetic resonance spectroscopy. *Organic Geochemistry* 35 (8): 923-935.

Song, J., and P. a. Peng. 2010. Characterization of black carbon materials by pyrolysis–gas chromatography–mass spectrometry. *Journal of Analytical and Applied Pyrolysis* 87 (1): 129-137.

Song, J., P. a. Peng, and W. Huang. 2002. Black carbon and kerogen in soils and sediments. 1. Quantification and characterization. *Environmental Science & Technology* 36 (18): 3960-3967.

Stumm, W., and J. J. Morgan. 1970. *Aquatic chemistry: an introduction emphasizing chemical equilibria in natural waters*. New York: Wiley-Interscience.

Sullivan, M. J., and G. E. Maciel. 1982. Structural resolution in the carbon-13 nuclear magnetic resonance spectrometric analysis of coal by cross polarization and magic-angle spinning. *Analytical chemistry* 54 (9): 1606-1615.

Sun, K., B. Gao, Z. Zhang, G. Zhang, Y. Zhao, and B. Xing. 2010. Sorption of atrazine and phenanthrene by organic matter fractions in soil and sediment. *Environmental Pollution* 158 (12): 3520-3526.

Sun, K., K. Ro, M. Guo, J. Novak, H. Mashayekhi, and B. Xing. 2011. Sorption of bisphenol A, 17α-ethinyl estradiol and phenanthrene on thermally and hydrothermally produced biochars. *Bioresource Technology* 102 (10): 5757-5763.

Tekely, P., D. Nicole, J. Brondeau, and J. Delpuech. 1986. Application of $^{13}C$ solid-state high-resolution NMR to the study of proton mobility: Separation of rigid and mobile components in coal structure. *The Journal of Physical Chemistry* 90 (22):5608-5611.

Ternes, T. A., A. Joss, and H. Siegrist. 2004. Scrutinizing pharmaceuticals and personal care products in wastewater treatment. *Environmental Science & Technology* 38 (20): 392-399.

Titirici, M.-M., A. Thomas, and M. Antonietti. 2007. Aminated hydrophilic ordered mesoporous carbons. *Journal of Materials Chemistry* 17 (32): 3412-3418.

Titirici, M. M., A. Thomas, S.-H. Yu, J.-O. Müller, and M. Antonietti. 2007. A direct synthesis of mesoporous carbons with bicontinuous pore morphology from crude plant material by hydrothermal carbonization. *Chemistry of Materials* 19 (17): 4205-4212.

Treadgold, J., Q.-T. Liu, J. A. Plant, and N. Voulvoulis. 2012. *Pollutants, Human Health and the Environment: A Risk Based Approach: Chapter 8. Pharmaceuticals and personal-care products*: 207-225.

Vaiopoulou, E., and P. Gikas. 2012. Effects of chromium on activated sludge and on the performance of wastewater treatment plants: A review. *Water Research* 46 (3): 549-570.

Vinke, P., M. Van der Eijk, M. Verbree, A. Voskamp, and H. Van Bekkum. 1994. Modification of the surfaces of a gasactivated carbon and a chemically activated carbon with nitric acid, hypochlorite, and ammonia. *Carbon* 32 (4): 675-686.

Wackett, L., M. Sadowsky, B. Martinez, and N. Shapir. 2002. Biodegradation of atrazine and related s-triazine compounds: from enzymes to field studies. *Applied Microbiology and Biotechnology* 58 (1): 39-45.

Wan Ngah, W., and M. Hanafiah. 2008. Removal of heavy metal ions from wastewater by chemically modified plant wastes as adsorbents: A review. *Bioresource Technology* 99 (10): 3935-3948.

Wang, H., L. Ho, D. M. Lewis, J. D. Brookes, and G. Newcombe. 2007. Discriminating and assessing adsorption and biodegradation removal mechanisms during granular activated carbon filtration of microcystin toxins. *Water Research* 41 (18): 4262-4270.

Wang, X., T. Sato, and B. Xing. 2006. Competitive sorption of pyrene on wood chars. *Environmental Science & Technology* 40 (10): 3267-3272.

Wawer, I., and S. Witkowski. 2001. Analysis of solid state ^{13}C NMR spectra of biologically active compounds. *Current Organic Chemistry* 5 (10): 987-999.

Wu, G., D. Rovnyak, and R. G. Griffin. 1996. Quantitative multiple-quantum magic-angle-spinning NMR spectroscopy of quadrupolar nuclei in solids. *Journal of the American Chemical Society* 118 (39): 9326-9332.

Xie, M., L. D. Nghiem, W. E. Price, and M. Elimelech. 2012. Comparison of the removal of hydrophobic trace organic contaminants by forward osmosis and reverse osmosis. *Water Research* 46 (8): 2683-2692.

Xing, B., J. J. Pignatello, and B. Gigliotti. 1996. Competitive sorption between atrazine and other organic compounds in soils and model sorbents. *Environmental Science & Technology* 30 (8): 2432-2440.

Xu, W., Q. Gao, Y. Xu, D. Wu, Y. Sun, W. Shen, and F. Deng. 2009. Controllable release of ibuprofen from size-adjustable and surface hydrophobic mesoporous silica spheres. *Powder Technology* 191 (1): 13-20.

Yang, K., X. Wang, L. Zhu, and B. Xing. 2006. Competitive sorption of pyrene, phenanthrene, and naphthalene on multiwalled carbon nanotubes. *Environmental Science & Technology* 40 (18): 5804-5810.

Yang, T. C., and R. R. Zall. 1984. Absorption of metals by natural polymers generated from seafood processing wastes. I*ndustrial & Engineering Chemistry Product Research and Development* 23 (1): 168-172.

Yangali-Quintanilla, V., A. Sadmani, M. McConville, M. Kennedy, and G. Amy. 2009. Rejection of pharmaceutically active compounds and endocrine disrupting compounds by clean and fouled nanofiltration membranes. *Water Research* 43 (9): 2349-2362.

Yao, C., Y. Shin, L.-Q. Wang, C. F. Windisch, W. D. Samuels, B. W. Arey, C. Wang, W. M. Risen, and G. J. Exarhos. 2007. Hydrothermal dehydration of aqueous fructose solutions in a closed system. *The Journal of Physical Chemistry C* 111 (42): 15141-15145.

Yoon, Y., J. Ryu, J. Oh, B.-G. Choi, and S. A. Snyder. 2010. Occurrence of endocrine disrupting compounds, pharmaceuticals, and personal care products in the Han River (Seoul, South Korea). *Science of the Total Environment* 408 (3): 636-643.

Zaib, Q., I. A. Khan, N. B. Saleh, J. R. Flora, Y.-G. Park, and Y. Yoon. 2012. Removal of bisphenol A and 17 β-Estradiol by single-walled carbon nanotubes in aqueous solution: Adsorption and molecular modeling. *Water, Air, & Soil Pollution* 223(6): 3281-3293.

Zhu, D., S. Hyun, J. J. Pignatello, and L. S. Lee. 2004. Evidence for π-π electron donor-acceptor interactions between π-donor aromatic compounds and π-acceptor sites in soil organic matter through pH effects on sorption. *Environmental Science & Technology* 38 (16): 4361-4368.

Zhu, D., and J. J. Pignatello. 2005. Characterization of aromatic compound sorptive interactions with black carbon (charcoal) assisted by graphite as a model. *Environmental Science & Technology* 39 (7): 2033-2041.

# APPENDIX A – PRINTABLE AUTHORSHIP LICENSE

**ELSEVIER LICENSE**
**TERMS AND CONDITIONS**

Mar 31, 2014

This is a License Agreement between Chanil Jung ("You") and Elsevier ("Elsevier") provided by Copyright Clearance Center ("CCC"). The license consists of your order details, the terms and conditions provided by Elsevier, and the payment terms and conditions.

**All payments must be made in full to CCC. For payment instructions, please see information listed at the bottom of this form.**

| | |
|---|---|
| Supplier | Elsevier Limited<br>The Boulevard,Langford Lane<br>Kidlington,Oxford,OX5 1GB,UK |
| Registered Company Number | 1982084 |
| Customer name | Chanil Jung |
| Customer address | 1007 Catawba Circle |
| | Columbia, SC 29201 |
| License number | 3359411427659 |
| License date | Mar 31, 2014 |
| Licensed content publisher | Elsevier |
| Licensed content publication | Separation and Purification Technology |
| Licensed content title | Hexavalent chromium removal by various adsorbents: Powdered activated carbon, chitosan, and single/multi-walled carbon nanotubes |
| Licensed content author | Chanil Jung,Jiyong Heo,Jonghun Han,Namguk Her,Sung-Jae Lee,Jeill Oh,Jaena Ryu,Yeomin Yoon |
| Licensed content date | 14 March 2013 |
| Licensed content volume number | 106 |
| Licensed content issue number | |
| Number of pages | 9 |
| Start Page | 63 |
| End Page | 71 |
| Type of Use | reuse in a thesis/dissertation |
| Intended publisher of new work | other |
| Portion | full article |
| Format | both print and electronic |

145

## ELSEVIER LICENSE
## TERMS AND CONDITIONS

Mar 31, 2014

This is a License Agreement between Chanil Jung ("You") and Elsevier ("Elsevier") provided by Copyright Clearance Center ("CCC"). The license consists of your order details, the terms and conditions provided by Elsevier, and the payment terms and conditions.

**All payments must be made in full to CCC. For payment instructions, please see information listed at the bottom of this form.**

| | |
|---|---|
| Supplier | Elsevier Limited<br>The Boulevard,Langford Lane<br>Kidlington,Oxford,OX5 1GB,UK |
| Registered Company Number | 1982084 |
| Customer name | Chanil Jung |
| Customer address | 1007 Catawba Circle |
| | Columbia, SC 29201 |
| License number | 3359411219169 |
| License date | Mar 31, 2014 |
| Licensed content publisher | Elsevier |
| Licensed content publication | Journal of Hazardous Materials |
| Licensed content title | Adsorption of selected endocrine disrupting compounds and pharmaceuticals on activated biochars |
| Licensed content author | Chanil Jung,Junyeong Park,Kwang Hun Lim,Sunkyu Park,Jiyong Heo,Namguk Her,Jeill Oh,Soyoung Yun,Yeomin Yoon |
| Licensed content date | 15 December 2013 |
| Licensed content volume number | 263 |
| Licensed content issue number | |
| Number of pages | 9 |
| Start Page | 702 |
| End Page | 710 |
| Type of Use | reuse in a thesis/dissertation |
| Portion | full article |
| Format | both print and electronic |
| Are you the author of this Elsevier article? | Yes |
| Will you be translating? | No |

146